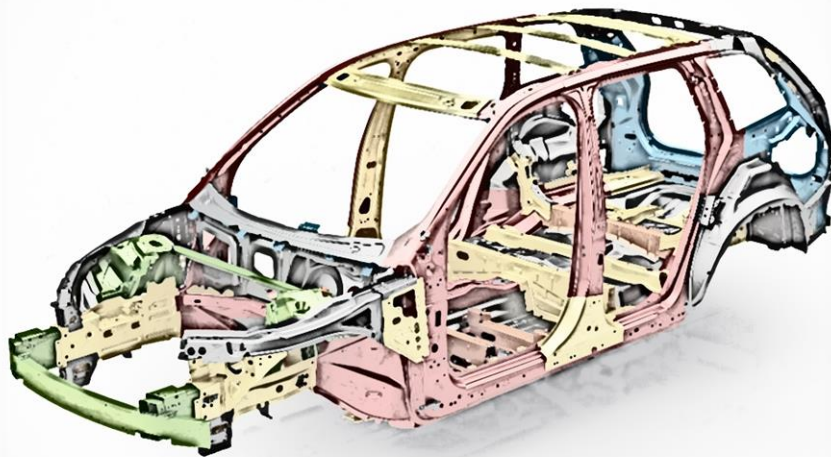




CHALMERS
UNIVERSITY OF TECHNOLOGY



TWB requirements in hot forming steels

Evaluation & Verification of the weld seam properties after hot forming

Master's Thesis in Materials Engineering

Nicklas Egger

Department of Industrial and Materials Science
CHALMERS UNIVERSITY OF TECHNOLOGY
Gothenburg, Sweden 2018

Tailor Welded Blank TWB

TWB requirements in hot forming steels

Evaluation & Verification of the weld seam properties after hot forming

Nicklas Egger

Diploma work in the Master's programme Materials Engineering



CHALMERS
UNIVERSITY OF TECHNOLOGY

Department of Industrial and Materials Science
CHALMERS UNIVERSITY OF TECHNOLOGY
Gothenburg, Sweden



Department of Painted Body & Closures.
Concept, Strategy & Advanced Engineering
VOLVO CAR CORPORATION
Gothenburg, Sweden

Performed at: Volvo Car Corporation/Chalmers University of Technology
SE-405 31 Gothenburg/SE-412 96 Gothenburg

Supervisor(s): Richard Johansson MSc. & Per Lindahl PhD.
Volvo Car Corporation
SE-405 31 Gothenburg

Examiner: Prof. Johan Ahlström
Department of Industrial and Materials Science
Chalmers University of Technology, SE-412 96 Gothenburg

TWB requirements in hot forming steels

Evaluation & Verification of the weld seam properties after hot forming

Nicklas Egger

© Nicklas Egger, 2018.

Diploma work in the Master's programme Materials Engineering

Department of Industrial and Materials Science

Chalmers University of Technology

SE-412 96 Gothenburg

Sweden

Telephone + 46 (0)31-772 1000

Cover:

Volvo XC90 body structure. The new XC90 has been made stronger by a more extensive use of hot-formed boron steel, which is the strongest type of steel presently used in the car body industry. The amount of hot formed steel is around 40 per cent of the total body weight

[Volvo Car Sverige AB, Newsroom]

Gothenburg, Sweden 2018

Abstract

In this thesis, the combination of two Al-Si coated hot forming steels were investigated for the most suitable process in terms of welding by Tailored Welded Blanks (TWB). The research aimed to establish the criterion for the proper material preparation and welding, as well as the establishment of the required joint and material properties both before and after hot forming. The Al-Si coating used on the hot forming steels have detrimental effects on the mechanical properties of the weld. A common method within the automotive industry, to avoid these effects, is to remove the coating prior to welding by laser ablation. In this research, four different laser welding processes regarding the ablation of the coating and the usage of filler wire were used to join the blanks together, and later analysed.

The two main welding processes investigated were: laser welding on partially ablated surfaces (called STD), and laser welding together with filler wire on coated surfaces (called FW). A relatively large literature survey was carried out on the subject. A series of 5 experiments were completed: a drop weight test on complete components; hardness profiling on the cross section of the weld; microstructural analysis on the cross section of the weld; analysis of the chemical composition in the cross section of the weld; tensile testing.

Segregated areas of ferrite and suspected intermetallic compounds were discovered in the fusion zone on the FW-welding process. The chemical composition of these segregated areas showed a relatively high constituent of aluminium. The tensile testing showed that the STD- and FW-welding process achieved similar or higher tensile strength than the parent material.

It was found that the FW-welding process resulted in equally or slightly better mechanical properties than the STD-welding process. The FW-welding process would require changes in the manufacturing chain of the body in white, while the STD-welding process would not. The addition of a filler wire in the laser welding would complicate and affect the robustness of an already complex welding process. Further studies and investigations are needed on larger sample series to verify these results and to clarify exactly what changes are necessary in the manufacturing chain for the FW-welding process. It was also found, that a tensile test together with a hardness profile over the cross section of the weld would be a good enough method to verify the weld properties after hot forming, for judgment of monotonic strength.

Keywords: Tailor Welded Blank, Laser welding, Filler wire, Al-Si coating, Laser ablation, 22MnB5

Acknowledgements

I would like to express my deep gratitude to Richard Johansson and Per Lindahl, my research supervisors, for their patient guidance, enthusiastic encouragement and useful critiques of this research work. I would also like to thank my examiner Professor Johan Ahlström for his assistance and support in keeping my progress on schedule. Also, special thanks to the staff at the department of manufacturing engineering and at the joining laboratory in Volvo Cars for always handling my requests as their top priority.

With the utmost respect for Mr Volvo a.k.a. Stefan, my “desk colleague”, thanks for the company and for always taking the side of the future of Swedish industry :)

Finally, I would like to express my deepest gratitude to Clara, my better half, for her unconditional encouragement and support during my studies.

Nicklas Egger, Göteborg, June 2018

Table of Contents

Table of Figures.....	XI
Table of Tables.....	XIII
List of acronyms and abbreviations	XIV
1 Introduction	1
1.1 Background	1
1.2 Aim	1
1.3 Limitations.....	2
1.4 Research questions	2
2 Theoretical Background	3
2.1 Tailored Blanks	7
2.1.1 Tailored Welded Blanks (TWB)	7
2.1.2 Patchwork Blanks (PB)	10
2.1.3 Tailored Rolled Blanks (TRB)	11
2.1.4 Tailored Heated Treated Blanks (THTB).....	12
2.2 Al-Si Coating	13
2.3 Laser Ablation.....	16
2.3.1 Full ablation.....	16
2.3.2 Partial ablation	17
2.4 Laser Welding.....	18
2.4.1 Heat Affected Zone HAZ.....	18
2.4.2 Laser welding and welding modes	20
2.4.3 Laser welding process parameters	21
2.4.4 Weld edge preparation	22
2.4.5 Laser welding imperfections	23
2.5 Verification after welding.....	25
2.5.1 Cup test and formability	25
2.6 Hot Forming	27
2.6.1 Hot forming steels.....	27
2.6.2 Hot forming process.....	31
2.6.3 Heat treatment/Heating	31
2.6.4 Known complications & challenges in the HF process.....	32
2.7 Verification after hot forming	33
2.8 Welding with filler wire & without ablation	34
2.8.1 Mechanical performance	34
2.8.2 Laser welding with filler wire	35
2.8.3 Production process and assembly	38
3 Experimental	39

3.1	Test specimens.....	40
3.2	Drop weight test.....	41
3.3	Hardness profile	43
3.4	Microstructure & Chemical analysis	44
3.4.1	Optical Microscopy	44
3.4.2	SEM/EDX Chemical Analysis.....	46
3.5	Tensile test	47
4	Results	49
4.1	Drop weight test.....	49
4.1.1	STD-welding process (No FW & Partial Ablation) X	52
4.1.2	FW-welding process (FW & No Ablation) X.....	52
4.1.3	STD2-welding process (No FW & Partial Ablation) Y	53
4.1.4	SC-welding process (FW & Partial Ablation) Y	53
4.1.5	Summary	54
4.2	Hardness profile	56
4.3	Microstructure & Chemical analysis	57
4.3.1	Optical Microscopy on B-Pillars	57
4.3.2	Optical Microscopy on Weld test coupon.....	58
4.3.3	SEM/EDX Chemical Analysis.....	59
4.4	Tensile test	61
4.4.1	B-pillars	61
4.4.2	Weld test coupons	64
4.4.3	Summary for B-pillars and Weld Test Coupons (WTC)	66
5	Discussion.....	67
6	Conclusion	71
7	Recommendations for actions and future work	73
8	References.....	74
	Acknowledgement of the sources	77
	Appendices	78
	Tensile test.....	78

Table of Figures

Figure 1. a) B-pillar, b) Front side member, c) Rear side member [1]	3
Figure 2. Side collision [1]	4
Figure 3. Design of the B-pillar (Courtesy of Ebbinger. H)	5
Figure 4. a) Front collision, b) Rear collision [1].....	5
Figure 5. Design of the front side member (Courtesy of Ebbinger.H)	6
Figure 6. Illustration of the TWB Process (based on [6])	7
Figure 7. Illustration of the TWC Process (based on [7])	9
Figure 8. Principle of Patchwork blank (based on [4]).....	10
Figure 9. Schematic view of an Al-Si phase diagram (based on [14])	13
Figure 10. Illustration of Al-Si coated HF-steel (based on [15]).....	14
Figure 11. Schematic view of a Fe-Al phase diagram (based on [16])	15
Figure 12. Schematic view of full ablation on Al-Si coated HF-steel (based on [15])	17
Figure 13. Schematic view of partial ablation on Al-Si coated HF-steel (Based on [15]).....	17
Figure 14. Square butt joint weld	18
Figure 15. Relationship between Fe-Fe ₃ C phase diagram and the microstructure in the HAZ of a plain-carbon steel [21]	19
Figure 16. a) Change in hardness as a function of recrystallization. b) Change in strength (hardness) as a function of recrystallization and grain growth of cold-worked materials. [21].....	20
Figure 17. Relationship between power density and weld mode (based on [25]).....	20
Figure 18. a) Conduction welding mode. b) Keyhole welding mode (based on [25]).....	21
Figure 19. Illustration of cutting defects on sheets and blanks (based on [28]).....	22
Figure 20. Cross section of a laser weld with different kinds of imperfections that could appear (based on [27]).....	23
Figure 21. Stretch forming/Equi-biaxial [31].....	26
Figure 22. Increase in proportion of HF-steel used in the BIW on Volvo models (based on [24])	27
Figure 23. Schematic illustration of the mechanical properties of 22MnB5 in different states compared to other steels (based on [32]).....	29
Figure 24. Illustration of a CCT diagram for quenching of austenitized steel (based on [32])	29
Figure 25. Direct Hot Forming process (based on [32])	31
Figure 26. Indirect hot forming process (based on [32])	31
Figure 27. Illustration of the hardness drop in the molten zone after hot-stamping of an Usibor 1500 TWB (conventional process) (based on [2])	34
Figure 28. Illustration of the white bands in the fusion zone, pointed out with arrows close to the fusion line and in the middle (based on [2]).....	35

Figure 29. a) Trailing feed, b) Leading feed (based on [45])	36
Figure 30. Illustration of different melt flow phenomena during laser welding; a) melt passing around the keyhole, b) Marangoni flow, c) drop ejection, d) humping, e) rear flow stagnation, f) inner eddies, g) flow downwards to the root, or flow underneath the keyhole [27]	37
Figure 31 Illustration of the falling weight test (courtesy of H. Ebbinger)	42
Figure 32. B-Pillar mounted in test Jig. a) Side view. b) View from left. c) View from right. d) View from right (b, c and d are relative to a)	42
Figure 33. a) 3D model of a B-pillar. b) Showing where the samples were cut out on the B-pillar.....	44
Figure 34. Weld Test Coupon.....	45
Figure 35. SEM/EDX Leo Ultra 55 & instrument data	46
Figure 36. Where tensile test samples were cut out from the B-Pillars	47
Figure 37. Dimensions of the B-pillar samples	48
Figure 38. Dimensions of the WTC samples	48
Figure 39. Overview of the test jig.....	50
Figure 40. a) Improvement after test run 1. b) Improvement after test run 2.....	50
Figure 41. Deformed B-Pillar with text and figures describing expressions used to explain locations	51
Figure 42. Crack in STD-welding process after drop weight test.	52
Figure 43. Crack in FW-welding process after drop weight test.	52
Figure 44. Appearance after drop weight test for the STD2-welding process. Red arrows to the left points at crack and crack indications.....	53
Figure 45. Appearance after drop weight test for the SC-welding process. Red arrows to the left points at cracks and crack indications	53
Figure 46. Impact point for STD (No FW & Partial ablation) and FW (FW & NO Ablation) welding process (B-Pillar X)	54
Figure 47. Impact point for STD2 (No FW & Partial ablation) and SC (FW & Partial Ablation) welding process (B-Pillar Y)	54
Figure 48. Line chart of hardness profile on (STD) No FW & Partial Ablation process	56
Figure 49. Line chart of hardness profile on (FW) FW & No Ablation process	56
Figure 50. Line chart of hardness profile on (WC) No FW & No Ablation process	56
Figure 51. Macrograph of the STD-welding process (No FW & Partial ablation)	57
Figure 52. Macrograph of the FW-welding process (FW & No ablation).....	57
Figure 53. Macrograph of the STD-welding process (No FW & Partial ablation)	58
Figure 54. Macrograph of the FW-welding process (FW & No ablation).....	58
Figure 55. Macrograph of the WC-welding process (No FW & No ablation).....	58
Figure 56. a) Macrograph of the laser weld cross section. b) BSE image of the dashed area in (a).....	59
Figure 57. Al content over measuring point LS 1-15.....	60

Figure 58. Si content over measuring point LS 1-15	60
Figure 59. Fe content over measuring point LS 1-15	60
Figure 60. Line chart showing force over displacement for the B-pillar samples. The red dashed area shows the nonlinear behaviour which is explained in the text above.	61
Figure 61. STD (No FW & Partial Ablation) X, sample 1 & 2 after tensile testing	62
Figure 62. FW (FW & No Ablation) X, sample 1 & 2 after tensile testing	62
Figure 63. STD2 (No FW & Partial Ablation) Y, sample 1 & 2 after tensile testing	62
Figure 64. SC (FW & Partial Ablation) Y, sample 1 & 2 after tensile testing	62
Figure 65. Bar chart showing Tensile strength for B-pillar samples.	63
Figure 66. Line chart showing force over displacement for weld test coupon samples. The red dashed area shows the nonlinear behaviour which is explained in the text above.	64
Figure 67. STD (No FW & Partial ablation), sample 1 to 3 after tensile testing.....	65
Figure 68. FW (FW & No ablation), sample 1 to 3 after tensile testing	65
Figure 69. WC (No FW & No ablation), sample 1 to 3 after tensile testing	65
Figure 70. Bar chart showing Tensile strength for weld test coupon samples	66

Table of Tables

Table 1. Volvo Cars definition of steel classes [24].....	28
Table 2. Chemical Composition of MBW 500 & 1500 [35]	28
Table 3. Chemical Composition of Ductibor 500 & Usibor 1500 [36]	28
Table 4. Chemical Composition of 22MnB5 [37]	28
Table 5. Material preparation, welding process and specimens	40
Table 6. Welding process & Type of specimen analysed by drop weight test.....	41
Table 7. Welding process & Type of specimen analysed by hardness profiling	43
Table 8. Welding process & Type of specimen analysed by optical microscope.....	45
Table 9. Welding process & Type of specimen analysed by optical microscope.....	45
Table 10. Welding process & Type of specimen analysed by tensile test	48
Table 11. Welding process & Type of specimen analysed by tensile test	48
Table 12. Results from the drop weight test	49

List of acronyms and abbreviations

BIW	Body in white
CE	Carbon equivalent
Ductile steel	Steels with a tensile strength around 500 MPa
FW	Filler wire
FW-welding	Welding process performed with No ablation & with filler wire
FZ	Fusion zone
HF	Hot forming
HAZ	Heat Affected Zone
IMC	Inter Metallic Compound
PB	Patchwork blank
RSW	Resistance spot welding
SC-welding	Welding process performed with Partial ablation & with Filler wire
SMP	Sample
STD & STD2-welding	Welding process performed with Partial ablation & No filler wire
THTB	Tailor heat treated blank
TRB	Tailor rolled blank
TWB	Tailor welded blank
VCC	Volvo Car Corporation
WTC	Weld Test Coupon
WC-welding	Welding process performed with No ablation & No filler wire

1 Introduction

Below follows a brief explanation about the background of this thesis and the questions at issue.

1.1 Background

Volvo Cars owned by Geely holding Group is a Swedish car manufacturer with production sites in Europe, Asia and North-America. Today the increased demand for lightweight solutions in the automotive industry challenges the current materials and processes. One currently available lightweight solution is Tailored Welded Blanks (TWB), where two blanks with either different thicknesses or properties are welded together and then formed into one final part. By using this technique it can lead to a:

- Reduction in weight
- Optimized material usage
- Increased technical performance
- Increased stiffness
- Better crashworthiness and energy absorption
- Shorter manufacturing process
- Reduction in number of parts needed to fulfil a demand

The right material is used in the right place to reduce weight and improve the properties. This process can currently be achieved by slightly different methods. Volvo Cars has a desire to clarify which production process performs the best, not only according to the properties of the Tailor Welded Blanks (TWB) but also how it affects the final assembly.

1.2 Aim

In this thesis the joining of two coated hot forming steels will be investigated for the most suitable process in terms of welding by Tailored Welded Blanks (TWB). The investigation targets to establish the criterion for the proper material preparation and welding as well as the establishment of the required joint and material properties both before and after hot forming.

1.3 Limitations

This work targets only to investigate:

- Tailor Welded Blanks (TWBs) (Benchmark could also include other techniques than below)
- Tailor Welded Blank (TWB) solutions for the B-pillar together with the rear and front side members.
- Practically only MBW 500 & Ductibor 500 vs MBW 1500 & Usibor 1500, with the same thicknesses (trials and investigation).
- Laser welding on Al-Si coated blanks.
- Three types of laser ablation (no, partial or full) with or without filler wire when laser welded.

1.4 Research questions

- Which are the challenges with the usage of filler wire? (Trade of process) (Chemical composition both in weld and in the filler wire used, Properties, shape, etc.)
- How will the usage of filler wire affect the hot forming process and the final assembly?
- Is the Verification of the joint after welding sufficient?
- How can the welded joint be verified after hot forming, without using a “full crash test”?

2 Theoretical Background

This theoretical background is structured to follow all manufacturing stages from blank to final component, but first follows a brief introduction about the car body components manufactured by the tailor welded blank technology covered in this thesis. The intention is to present the components and their purpose in the car body.

The car body components examined in this thesis:

- B-pillar (a)
 - Front side-member (b)
 - Rear side-member (c)
- (See figure below)

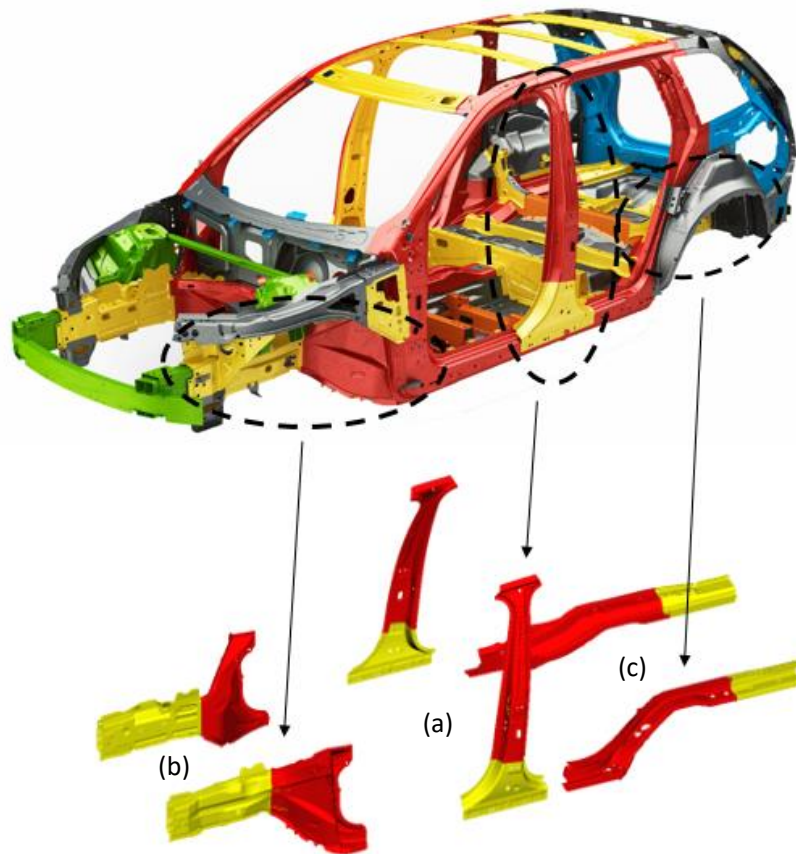


Figure 1. a) B-pillar, b) Front side member, c) Rear side member [1]

These three categories of components are all made from the Tailor welded blank (TWB) process, and subsequently hot formed (HF) into the final shape. Tailor welded blanks (TWBs) are at least two different blanks welded together in a butt joint configuration. The TWB technique will be explained more thoroughly in a separate sub-section 2.1.1, and this brief introduction is only intended to present the components and their purpose.

B-Pillar

The B-pillar and side-members are among the more important components of a car body with regard to the crashworthiness. The B-pillar is among the more complex car body components, mainly because the distance between the outer shell of the car body and the vehicle occupant is relatively short, which makes the possible deformation zone very short. Hence, the B-pillar has to be designed to deform (absorb kinetic energy) but at the same time allow minimal intrusion into the cabin, see Figure 2. As stated by [2], the B-pillar reinforcement has to satisfy the following requirements.

- To be able to transfer the crash loads to the vehicle lateral body structure
- To absorb as much kinetic energy as possible during the crash test, with minimal intrusions, at best localized at the passenger pelvis zone.



Figure 2. Side collision [1]

The car bodies developed around the Scalable Product Architecture (SPA) platform has today a B-pillar with a combined technology of both a Tailored Rolled Blank (TRB) and a Tailored Welded Blank (TWB), see Figure 3. Tailor Rolled Blanks (TRB) are blanks with a continuous thickness transition, and will be explained more thoroughly further ahead in sub-section 2.1.3.

As can be seen in Figure 3, the lower part of the B-pillar is made from 'ductile steel' and the upper part from boron steel (TRB). These two parts are welded together becoming a TWB and then subsequently Hot Formed (HF) into the final part.

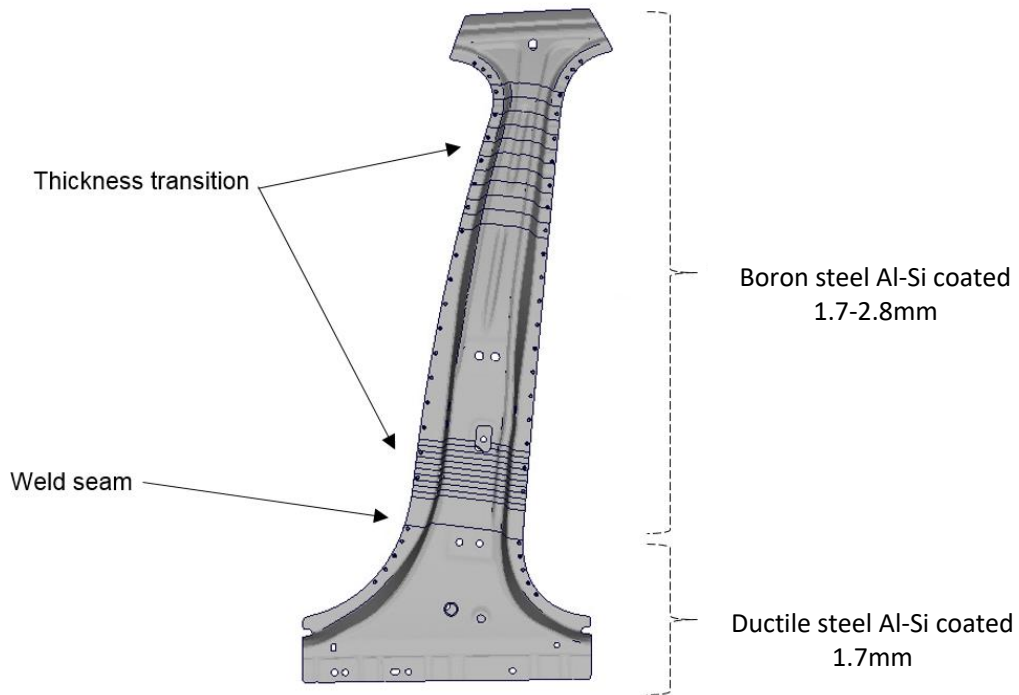


Figure 3. Design of the B-pillar (Courtesy of Ebbing. H)

The idea of having the more ductile steel in the lower part of the B-pillar is to control where the deformation takes place. The deformation should preferably occur in the pelvis area, where less vital organs of the vehicle occupant are situated, hence intrusion to the thorax area is prevented by using the stronger boron steel in the upper part.

Front Side member

Front and rear side members are also, as mentioned above, manufactured by the TWB technique. For the side-members the crashworthiness in a front and rear collision are of major concern. Illustrations of a front and rear collisions can be seen in Figure 4.

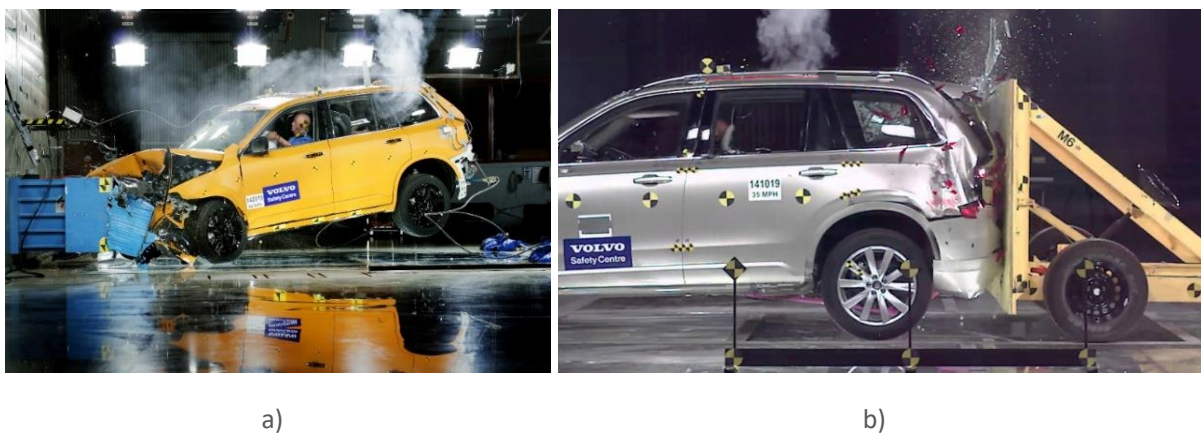


Figure 4. a) Front collision, b) Rear collision [1]

According to [3], the front and rear side members should be designed to efficiently absorb kinetic energy during a collision in order to secure occupants from the impact and penetration. The side members used on the SPA platform are designed to follow that statement. As illustrated in Figure 5 below, the frontmost part of the front side member is made from 'ductile steel' and the rearmost part from Boron steel. These two parts are welded together becoming a TWB and then subsequently Hot Formed (HF) into the final part. The idea of having the more ductile steel in the frontmost or rearmost part of the side-members is to control where the deformation takes place and to absorb kinetic energy during a collision. The purpose of the stronger and less deformable boron steel is to prevent intrusion in to the cabin.

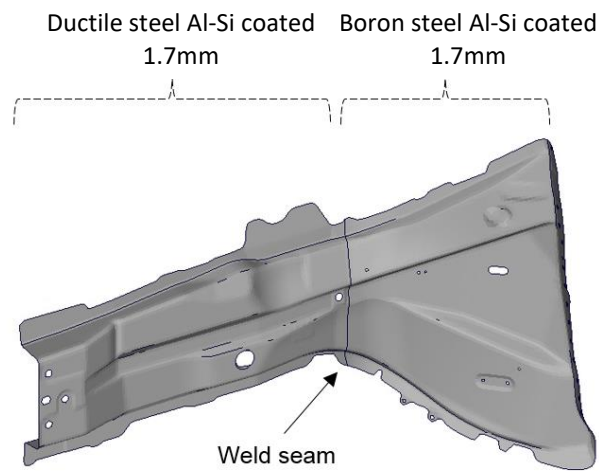


Figure 5. Design of the front side member (Courtesy of Ebbinger.H)

2.1 Tailored Blanks

Tailored blanks is the umbrella term for semi-finished parts which has tailored properties locally on the blank, these properties could relate to different materials, thicknesses or coatings etc. [4]. The main reasons for using tailored blanks is to reduce weight while maintaining or improving the mechanical properties in order to meet the increasing safety demands. Other reasons could also be to minimize the number of parts needed to fulfil a demand or to enhance the material utilization. A Tailored Blank can be achieved by a variety of methods: Tailor Welded Blanks (TWB), Patchwork Blanks (PB), Tailored Rolled Blanks (TRB) and Tailored Heat Treated Blanks (THTB). A brief explanation of these methods follows below. Tailor Welded Blank (TWB) is the type of tailored blank used for the components covered in this thesis.

2.1.1 Tailored Welded Blanks (TWB)

Volvo was first in Europe to introduce the Tailor Welded Blank technique in 1979 [4] [5]. TWBs consist of at least two single blanks of different thickness, grade, or coating that are welded together, (see Figure 6 below) and then formed into a final part through a forming process (hot or cooled). When large volumes are produced, laser welding is the more common welding technique to join the blanks together, other methods could be mash seam welding (resistance welding with a “pressurized wheel”), induction welding or friction stir welding (aluminium).

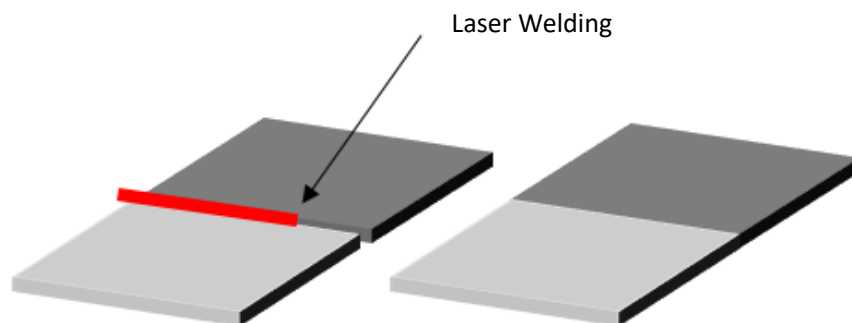


Figure 6. Illustration of the TWB Process (based on [6])

Laser welding is the more common welding technique because it produces a small heat affected zone (HAZ) and it is a relatively rapid process. Hence, the impact on the mechanical properties are minimized compared to other methods. According to [4], the major advantage of TWBs is the weight reduction, and the major disadvantage is the investment cost for the welding equipment and forming tools. The mechanical properties of a TWB is highly dependent on the properties of the weld since this is the area where the properties are changed due to the increase in temperature. The properties of the weld depends on many different parameters e.g. welding method, materials used, thickness ratio between the blanks, porosity, HAZ, microstructure and chemical composition etc. The mechanical properties like ductility and strength will therefore scatter more on TWB's compared to monolithic sheets [4]. The welding process

leads to a change in hardness, tensile yield strength (TYS) and ultimate tensile strength (UTS) but decreases the total elongation, depending on the carbon content [4]. The formability of TWBs can therefore be negatively affected by the welding operation.

2.1.1.1 Formability of TWBs

The swift cup test, the limiting dome height (LDH) test, and spherical punch stretch forming test could be used to analyse the formability after welding. The dominating parameters on the formability of TWBs are the thickness ratio and the orientation of the weld line to the loading direction [4]. It is said, in general, that the weld seam itself is not affecting the formability as much as the thickness transition. The effect of the thickness ratio was showed by milling a thickness gradient on a monolithic sheet that resembled a TWB with a thickness gradient. What was seen was that the larger the thickness ratio between the blanks, the lower the formability, due to the increase in non-uniform deformation. However, imperfections, inclusions and porosity in the weld line could also increase the non-uniform deformation [4].

2.1.1.2 Tailored Welded Coils (TWC)

Initially the laser capacity was the bottleneck operation in the TWB process, but the welding speed was improved when more powerful lasers became available, which made the material handling the new bottleneck [7]. To speed up the production process the TWB Company, which is a joint venture between Worthington steel and Wisco tailored blanks [8], started to elaborate on welding together the sheets instead of the blanks, so called Tailored Welded Coil (TWC). In this process, two or more coils are joined together along the coil edge, as illustrated in Figure 7. Individual steel sheets of different thickness, grade, and coating are joined in a laser butt-welding process [8]. The Tailored Welded Coil (TWC)

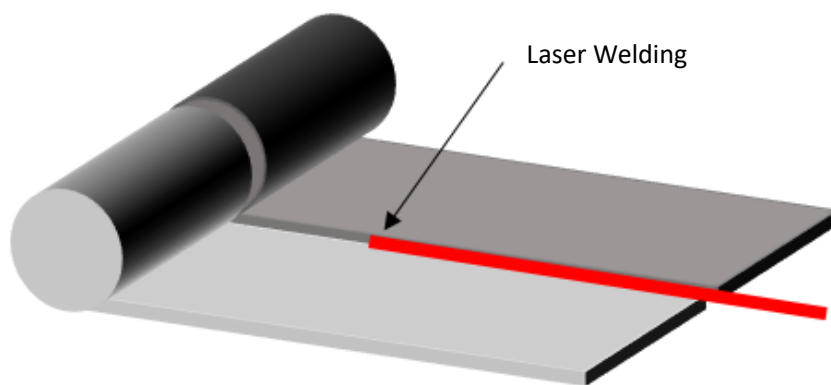


Figure 7. Illustration of the TWC Process (based on [7])

The TWC technique has the same pros and cons as the TWB when it comes to mechanical properties and formability, but it offers some advantages in the production process. According to [7], non-welding time is completely removed compared to the TWB process where individual blanks are welded separately, and the production process could in principle be spared from bottleneck operations. The production process could be much more streamlined and cost effective compared to the TWB technology [8]. However, the major disadvantage is that the material utilization could be decreased because nesting of the blanks could cause a great deal of material waste, especially on complex parts such as B-pillars.

2.1.2 Patchwork Blanks (PB)

The key idea of Patchwork Blanks (PB) is to partially reinforce the main blank by one or more smaller blanks [4], the principle of patchwork blank can be seen in Figure 8. There are many conventional methods within the automotive industry to reinforce certain areas with extra material, but what distinguishes Patchwork Blanks from the conventional methods is that the main blank and the reinforcing blank are joined before forming. Most commonly used joining techniques are laser welding in an overlap joint and spot welding. A combination of both techniques can also be used. Furthermore, both welding methods can also be used together with adhesives [4]. The advantages with PB are that only one forming tool is needed, it simplifies the assembly of the finished part, fitting accuracy is higher, very small areas can be reinforced and if adhesives are used vibration damping is increased. It is also relatively cheap compared to other techniques [4]. Disadvantages are that the weight reduction is not that significant, creating a stronger or more ductile area requires the addition of material, thus weight and volume increases. Crevice corrosion can occur if adhesives are not used, while the use of adhesives requires a well prepared surface.

In production mainly two techniques are used, one where the blanks are welded both before and after forming and one where the blanks are only welded before forming. The first technique is more “safe” while the other is more effective regarding production time. Patchwork blanks most often fail close to the border of the patch and the blank through a crack initiation caused by the sudden changes in stiffness. [4]. Common applications for PB in the car body are in the doors, floors, hinges, pillars, rails etc. [9].

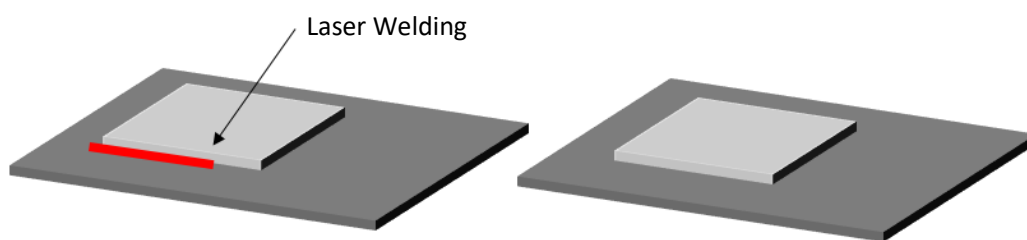


Figure 8. Principle of Patchwork blank (based on [4])

2.1.3 Tailored Rolled Blanks (TRB)

Tailor Rolled Blank (TRB) is a relatively novel and expanding technique to manufacture tailored blanks in high volumes. Compared to Patchwork Blanks (PB) and Tailor Welded Blanks (TWB), blanks are not joined. Instead the same material is used in the whole blank but rolled to different thicknesses, so where a stronger area is needed the sheet is thicker and vice versa with the less strong area. The transition between the thicker and thinner part is continuous which minimizes the stress-peak at the thickness variations. Most transitions between thicknesses are possible and the change between thick and thin can be made quite narrow [4]. Advantages with the TRB technology are that a better surface quality can be achieved since there is no weld seam. The number of transitions between thick and thin does not affect the production cost. Weight reduction is simple, thinner material can be used on less critical areas. Disadvantages are that the strain hardening effect in the sheet will vary due to the rolling process. This can cause challenges in the following forming step because the blank can have for example different material properties and spring back behaviour [4]. It is also difficult to utilize the sheet material effectively when cutting out the blanks due to the thickness variations. Localised energy absorption on certain areas (more ductility) are difficult if not impossible to achieve compared to Tailor Welded Blanks (TWB) and Tailored Heat Treated Blanks (THTB), where different materials and material microstructures ("soft zones") can be used, respectively. The sheets can be rolled in two different directions, longitudinal and latitudinal which are explained separately below. These two methods could also be combined and are then called 3D rolling.

Longitudinal

The flexible rolling process is used to achieve thickness variations in the longitudinal direction. It works just like conventional sheet rolling but with the addition of that the roll gap can be varied during the rolling process.

Lateral

Strip Profile Rolling process was developed to achieve thickness variation in the lateral direction on the sheets [4]. The process is relatively sensitive to how much the height is reduced per pass, if the height is reduced too much or and if too thin discs are used it can cause material flow in the longitudinal direction. This in turn can lead to flatness defects and small active plastic zones. To avoid this a number of rolling passes is needed [4]

2.1.4 Tailored Heated Treated Blanks (THTB)

The main characterization for this genre of process is that the blanks or sheets are heat treated to tailor their properties. The heat treatment process is controlled locally on the blank to alter the material properties. Tailored Heat Treated Blanks (THTB) can be achieved by many different methods, and company's providing tailored heat treating solutions often have their own twist on how the process is performed. In a conventional direct hot forming process the blanks are first austenitized at elevated temperature (uniformly heated) and then simultaneously formed and quenched into a fully martensitic microstructure (if hardenable). THTB resembles the conventional process but local areas are temperature controlled either by heating or cooling, so instead of quenching the whole part into martensite, only selected areas of the part is transformed into martensite [10]. According to [11], AP&T offers two solutions for THTB. The first, the blank is fully austenitized and then quenched with locally controlled cooling rates (differential cooling). Differential cooling is a more suitable method for Al-Si coated steels because the uniform coating properties are set from the uniform heating of the blank (further explained in section 2.2). In the second solution, the blanks are selectively heated on local areas (differential heating), where only specific areas are heated to austenitization T, and other areas are kept at room T before forming. By doing this the part can obtain tailored mechanical properties. For example, some areas on the part will obtain a martensitic microstructure with high TYS and hardness.

THTB is just like TRB a relatively novel process in large scale production. Advantages with THTBs are that the tailoring step is made in the hot stamping process, no pre-processing is necessary, like joining different materials. THTB is also a flexible process, multiple and very narrow areas can be tailored anywhere on the blank [11]. Material cost can be kept low since only one material is needed. Material utilization with regard to nesting becomes more efficient compared to other Tailored Blank (TB) techniques [11] [4].

2.2 Al-Si Coating

During hot forming, the blanks are austenitized and handled in an unprotected atmosphere. Without protection this will lead to high temperature oxidation and decarburization resulting in scaling on the substrate surface and lowering of the mechanical properties [12].

To avoid oxidation and decarburization, an aluminium silicon coating (trademark Alusi®) is applied on the steel blanks, not only to act as protection during heating but also as the basic corrosion protection on the finished part. Volvo Cars is currently using the coating Alusi® according to standard AS 150 (~25 µm thick (150 g/m² double sided)) on the steel supplied by both their suppliers ThyssenKrupp and ArcelorMittal. The coating has a near eutectic composition of 90wt% Al and 10wt% Si, see Figure 9 [13].

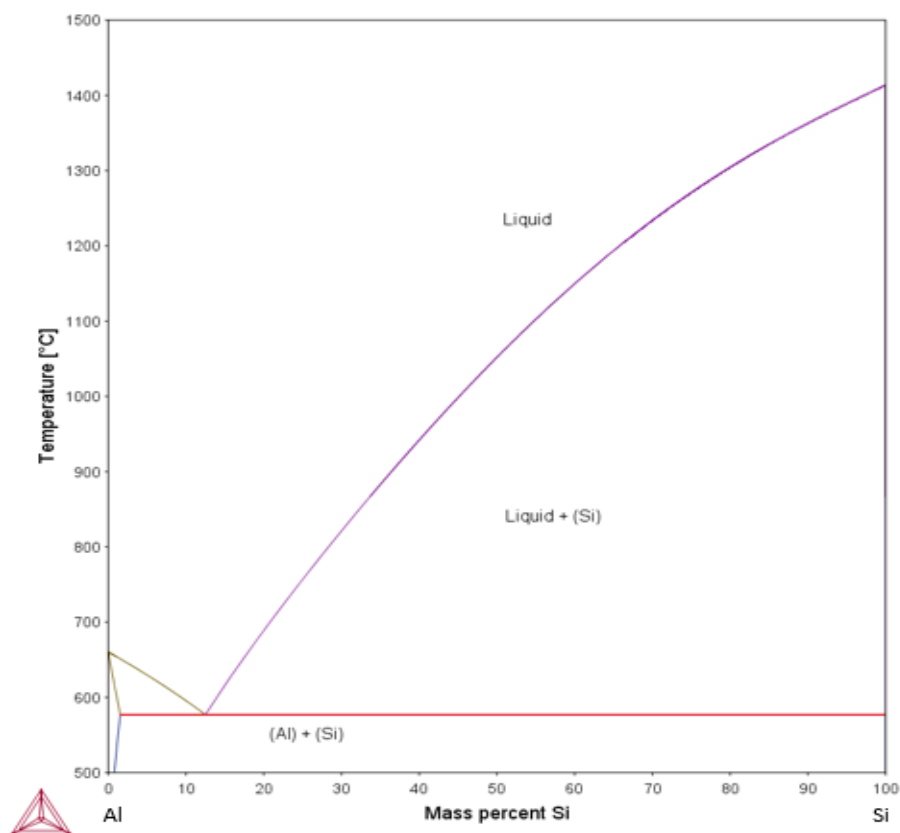


Figure 9. Schematic view of an Al-Si phase diagram (based on [14])

If comparing the Al-Si coating to the more traditionally coatings used in the automotive industry like zinc, the Al-Si has a much higher melting temperature, and is therefore much more suitable for the hot forming process. Zinc would both melt, evaporate and contaminate the forming tool.

The coating is applied through a hot dip aluminizing process, the temperature is typically between 650° and 700° [13]. During this process some diffusion occur between the substrate and the coating. Simplified it could be described as “two layers” are formed in the coating. The first is an intermediate layer consisting basically of an Al-Fe-Si intermetallic compound (IMC) closest to the substrate, due to the diffusion of Iron.

The second layer the “coating” has the primary composition of Al-Si, see Figure 10 below. The complete Al-Si coating is roughly 25 μm thick and the intermediate layer is roughly 5-10 μm thick. The intermediate layer has a higher fusion temperature and hardness than the top layer of the coating. Furthermore, the steel substrate has a higher fusion temperature than the intermediate layer, so

$$T_m^{Steel\ Substrate} > T_m^{Intermediate\ layer} > T_m^{Coating}.$$

These properties plays a significant role in a possible removal of the coating prior to welding, which is commonly performed via laser ablation which will be described in section 2.3.

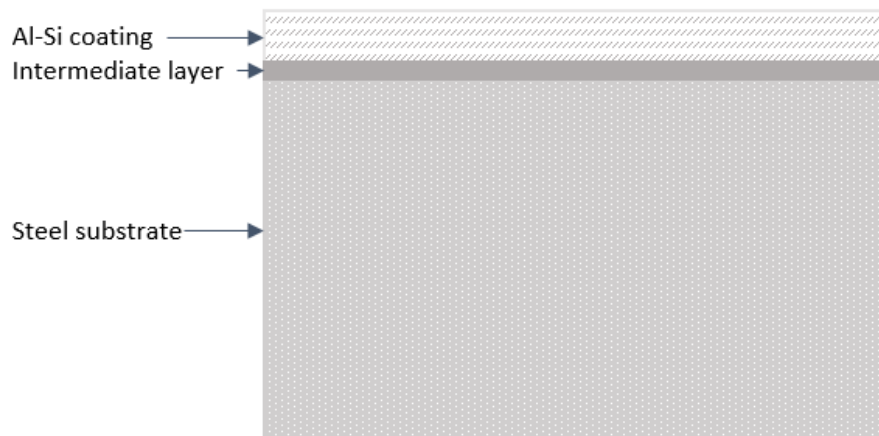


Figure 10. Illustration of Al-Si coated HF-steel (based on [15])

During austenitization in the hot forming process, the coating becomes highly adherent to the substrate. Also, the coating thickness increases due to time and temperature (atomic diffusion across interface) [13]. Multiple layers are formed in the coating both before and after hot-forming and this has been studied in several investigations involving Al-Si coating.

According to [13], Al_8Fe_2Si is formed in the “hot dip process”, and this diffusion is continued at the interface between the coating and steel substrate in the hot forming process (Iron diffuses into the coating). After further diffusion Al_8Fe_2Si is transformed into Al_5Fe_2 and precipitates of $Al_2Fe_3Si_3$. With an increasing heating time, Al_5Fe_2 transforms into $AlFe$, the transformation starts at the steel/coating interface and grows into to the coating [13]. The excellent corrosion resistance provided by the coating is due to the reaction between the atmosphere and the coating, forming aluminium oxide Al_2O_3 at the topmost part of the coating. A phase diagram of Fe-Al can be seen in Figure 11 below.

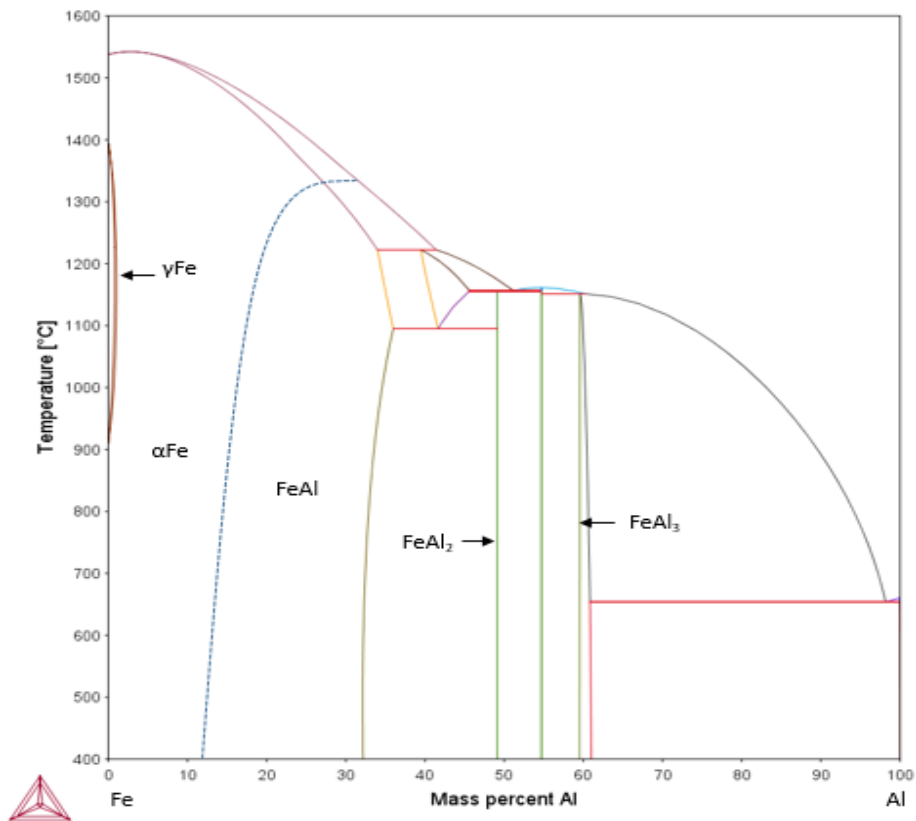


Figure 11. Schematic view of a Fe-Al phase diagram (based on [16])

On the contrary [17], reports that the Al_5Fe_2 and Al_3Fe exists already in the as received condition, i.e. after the hot dip process. Pursuant to [18], Al-Fe-Si IMCs exist in the coating only before austenitization, i.e. in the as-received condition. The Al-Fe-Si phases stops to exists during austenitization at 1173 K after 2 min soaking time, and after a soaking time of 6 min all the phases are converted into phases of types Al_5Fe_2 and $AlFe$. [18].

2.3 Laser Ablation

Fe-Al intermetallic phases and segregated areas of ferrite, also referred to as “white areas” or “white bands” in literature, could be created in the weld due to dilution of the Al-Si coating during laser welding. According to [19], the intermetallic phases possess low deformability and a low fracture toughness. It is also reported, that the weldability is decreased by the intermetallic phases and that the formation of them can be controlled in the heat treatment process by time and temperature. The mechanical properties of the weld could be reduced because of the formation of ferrite and intermetallic phases which would act as crack initiation sites and stress raisers. To avoid dilution of the Al-Si coating in the weld, the coating is today removed prior to welding, either completely or partially, referred to as *full ablation* and *partial ablation* respectively.

Ablation is defined as the removal of material from the surface of an object by vaporization, chipping, or other erosive processes [17]. Laser ablation as a method to remove Al-Si coating is chosen over other methods like mechanical removal because of its possibility to distinguish between the coating, intermediate layer and the steel substrate with high accuracy. The laser ablation process is controlled by parameters like wavelength, pulse duration, pulse energy, and energy density. With the correct parameters, the process can with high accuracy remove only the desired layers even if the surface is not completely even [17]. The partial and full ablation process will be more thoroughly described below.

2.3.1 Full ablation

When performing a laser full ablation, the Al-Si coating is completely removed, see Figure 12 below. The full ablation process is usually carried out in two runs, in the first run the laser is removing the primary Al-Si layer and in the second run the intermediate layer. The main advantage with using the full ablation process is that it completely eliminates the risk of polluting the weld. However in large volume production this could be a time consuming and expensive operation. The full ablation process will according to [17], also decrease the corrosion resistance significantly, partly due to the oxide layer created during hot forming (unprotected surface at elevated temperature). It is said that the possible oxide layers could cause the forthcoming layers of corrosive protective coatings not to adhere [17].

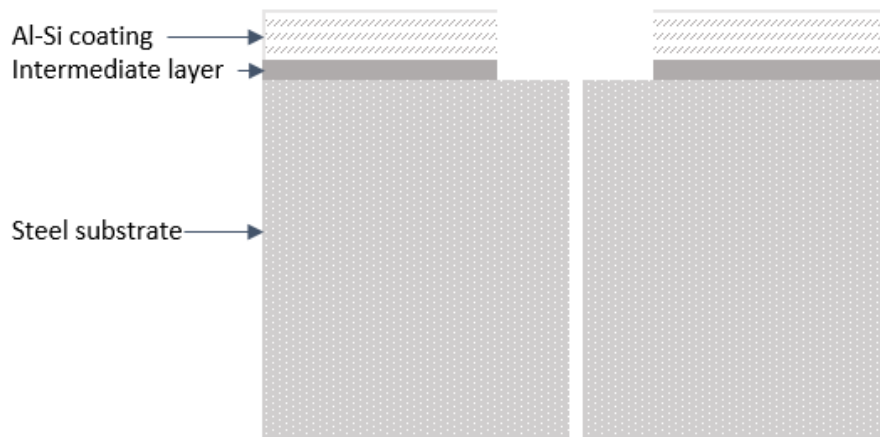


Figure 12. Schematic view of full ablation on Al-Si coated HF-steel (based on [15])

2.3.2 Partial ablation

ArcelorMittal has developed and patented a method to prepare the edges of the Al-Si coated blanks prior to welding, referred to as partial ablation. In this process the Al-Si coating is only partially removed leaving the intermediate layer on the blank, see Figure 13.

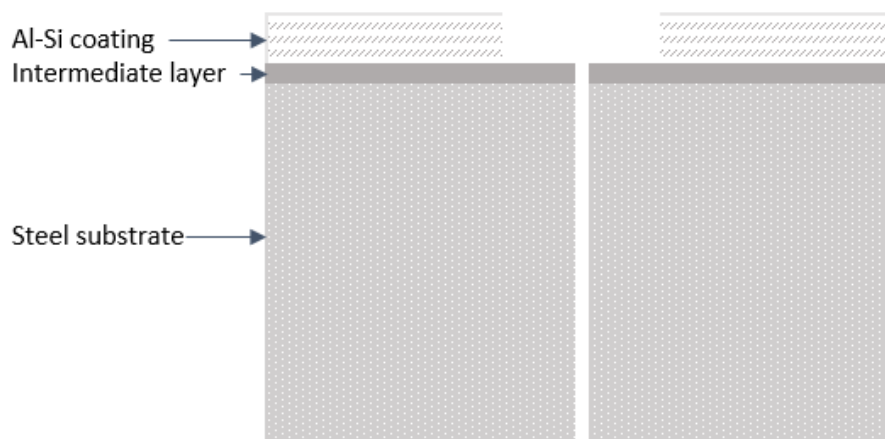


Figure 13. Schematic view of partial ablation on Al-Si coated HF-steel (Based on [15])

As described in section 2.2, the complete Al-Si coating is $\sim 30\mu\text{m}$ consisting of two “layers”, the Al-Si which is $20\text{-}25\mu\text{m}$ thick and the intermediate layer $5\text{-}10\mu\text{m}$ thick consisting of the Al-Fe-Si IMC. The intermediate layer has a higher hardness and higher fusion temperature than the Al-Si coating, it is therefore possible, with the correct process parameters to remove only the top part of the coating, without affecting the intermediate layer. The benefits with partially removing the coating are both a reduced process time compared to full ablation and a retained “good enough” surface corrosion protection without polluting the weld to a greater extent [17].

2.4 Laser Welding

Laser welding is a common welding method within the automotive industry, although the main joining method is still resistance spot welding (RSW). Laser welding are in some areas competing with RSW because a continuous weld seam can increase the robustness and stiffness of the part significantly [4]. When it comes to welding of TWB, RSW is however not an option since the blanks are joined, side by side, by a closed butt joint weld, see Figure 14 below. The main benefits with laser welding are that it produces a relatively small heat affected zone (HAZ) and narrow weld seam combined with a deep penetration.

The major parts of the laser welding process affecting the quality and mechanical properties of the weld will be explained in this section, but first follows a brief explanation of the heat affected zone (HAZ) to give a better understanding of how the welding affects the microstructure of the area surrounding the fusion zone.

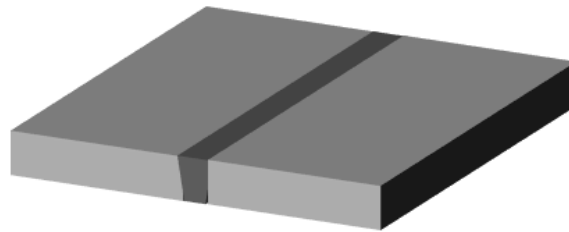


Figure 14. Square butt joint weld

2.4.1 Heat Affected Zone HAZ

The area from the fusion zone to the outermost zone of the HAZ will be explained according to Figure 15 below. The most middle part of the weld has been melted and mixed, this area of the weld is called the fusion zone (FZ). The microstructure and properties of the fusion zone (FZ) after welding will depend on the heat input, cooling rate and the “new” composition created by the fusion of different materials during welding. Depending on cooling rate and composition, the fusion zone (FZ) can obtain a microstructure of ferrite, perlite, bainite and martensite etc. in steels [20]. The area between the FZ and the unaffected base material experiences a change in microstructure and mechanical properties due to the affection of heat from the melted weld. This area is called the heat affected zone, also known as the HAZ [20].

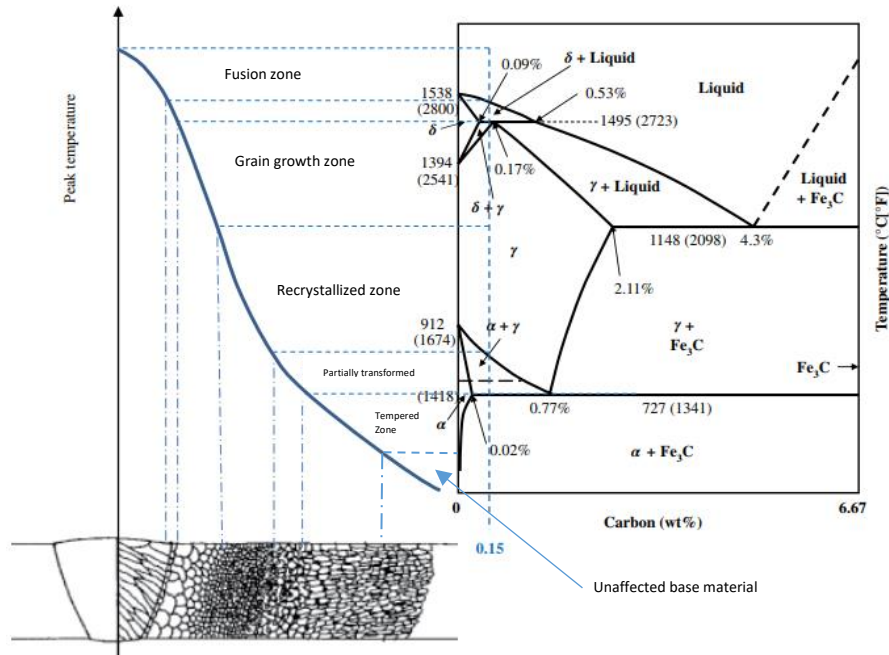


Figure 15. Relationship between Fe-Fe₃C phase diagram and the microstructure in the HAZ of a plain-carbon steel [21]

In the grain growth zone closest to the solidified weld, excessive grain growth occurs due to the high temperature change. Recrystallization zone, the temperature range initiates recrystallization and recovery of the grains. Widmanstätten ferrite is usually found in both the grain growth and recrystallization zone. Partial austenitization takes place in the partially transformed zone which is characterised by equiaxed grains “acicular ferrite”, due to the many nucleation sites. Depending on the cooling rate in these three zones, the austenite transforms to either ferrite, pearlite or martensite. Last is the tempered and unaffected zone, in the tempered zone formation of carbides embedded in ferrite could occur resulting in a reduction of hardness and strength. In the lower temperatures, in what is supposed to be the un-affected zone, diffusion of carbon and nitrogen to dislocations can occur, which can cause a brittle behaviour. (C&N locks dislocation movement).

According to [20], the metals most affected by the HAZ are cold-worked materials, because there is enough heat in this region to cause recrystallization and/or grain growth. Figure 16 a) below illustrates the effect on a cold worked low carbon steel. Cold worked steel sheets have higher energy in the system, recovery and recrystallization can therefore initiate at a lower temperature, thus a wider (HAZ). The same phenomena could be described with Figure 16 b), which shows how the microstructure of a cold worked steel is typically affected by time and temperature.

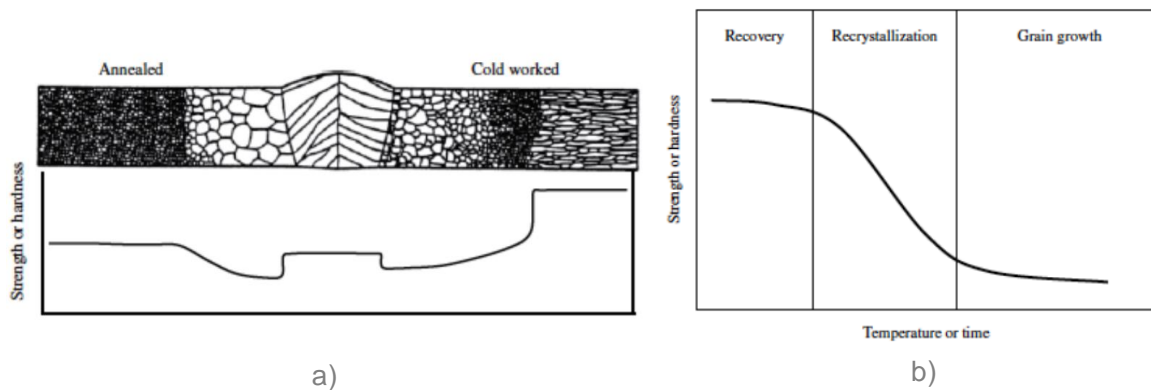


Figure 16. a) Change in hardness as a function of recrystallization. b) Change in strength (hardness) as a function of recrystallization and grain growth of cold-worked materials. [21]

2.4.2 Laser welding and welding modes

The most common type of laser used in the industry have been the CO₂-lasers. However, the usage of fibre laser, which belong to the group of so-called solid state lasers, is growing. Solid state lasers have a relatively short wave length 1 μm compared to ~10 μm [22] for CO₂-lasers, which increases the freedom of design. The solid state lasers are referred to as “bendable”, which simplifies the design, optics can be designed to fit its purpose more easily. Another benefit with solid state lasers over CO₂-lasers are that the efficiency is twice as good (creation of light) [23]. Keyhole and conduction welding are the two common types of heating modes to melt and fuse the material together and the main difference between the two is the power density at the weld spot, see Figure 17 [23] [24].

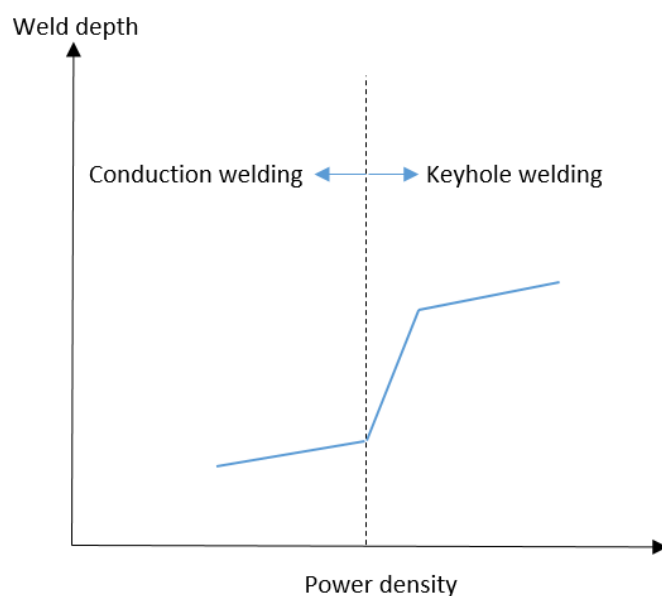


Figure 17. Relationship between power density and weld mode (based on [25])

In conduction welding, the power density is just enough to melt the top layer of the material and the weld penetration is achieved by the heat conducting down in the material. The weld is typically wide and shallow in this method.

The second mode, keyhole welding, is the most common method within the automotive industry and it is also the one used when welding TWBs. The power density is high enough to vaporize the metal. A thin cavity is formed and the metal gas escaping keeps the hole open, resembling a keyhole. This creates a deep and narrow weld [24]. The keyhole size is roughly the same as the laser beam diameter, and remains stable as long as a “process equilibrium” prevails. Several complex mechanisms are taking place in the keyhole and many of them are poorly understood. However, what is known is that the keyhole provides two main processing benefits. First is that it enables almost 100% absorption of the laser. Secondly, it acts as a conduit or light pipe, which deliver the laser energy efficiently in to the material. [26] [24] [22]. An illustration of the two modes can be seen in Figure 18 below.

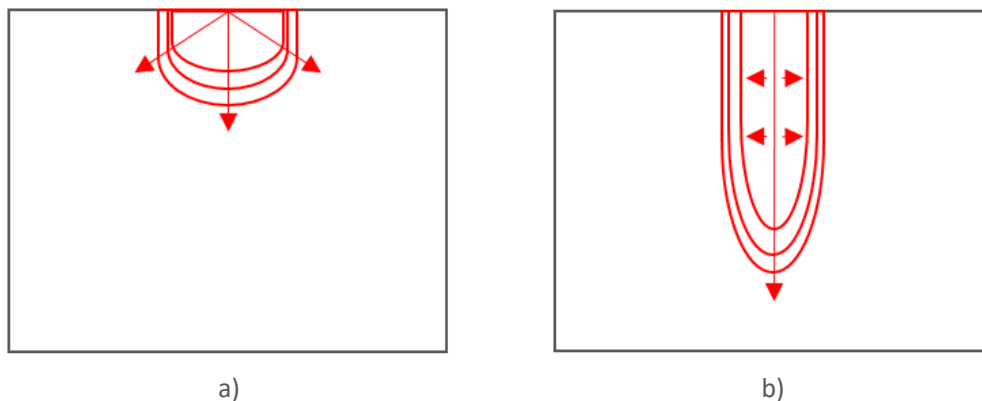


Figure 18. a) Conduction welding mode. b) Keyhole welding mode (based on [25])

2.4.3 Laser welding process parameters

One could say that the heat input is a measure of how well the laser power and welding speed are optimized. If the laser power is too high, the melted material will escape at the root of the weld [24], which is also called a root drop-out [27]. If the heat input is too low the result would be lack of penetration. The welding speed affects the weld pool, high speed gives a narrow weld pool and vice versa. Most laser welding sources within the automotive industry have today a maximum power around 4-10 kW [24].

Equation 1. Heat input (based on [24])

$$\text{Heat input } (Q) = \frac{\text{Laser power } (P)}{\text{Travel speed } (v)}$$

The focal height position of the laser beam in/on the sheet/blank affects the shape and penetration of the weld. According to [24], the keyhole in the workpiece is maintained when the generation of heat is

optimized, which on thin sheets most often occurs when the focus point is 1 mm below the surface (depending on spot size and focal length).

Process gases are used in laser welding to provide:

- An inert environment
- Suppress or re-direct the plasma
- Protect the optics

An inert environment protects the weld pool from getting contaminated. The laser beam can lose power and focus due to the occurrence of plasma. To remove the plasma a shielding gas can be used, often either as a high pressure cross flow jet or an air knife. Furthermore, a shielding gas can also re-direct the weld spray/spatter from damaging the optics. Most sheets/blanks within the automotive industry are commonly laser welded with only air as shielding gas. [24].

2.4.4 Weld edge preparation

The edges of the blanks play a significant role in how well the weld will perform [7]. The most common cutting method is cutting through shearing, the sheet metal is separated by applying a shearing force by two tools, one above and one below. The effect of using this technique is that the edges do not become completely straight. Cutting by shearing could result in a fracture angle, die roll and a small burr at the edges [28], see Figure 19 below.

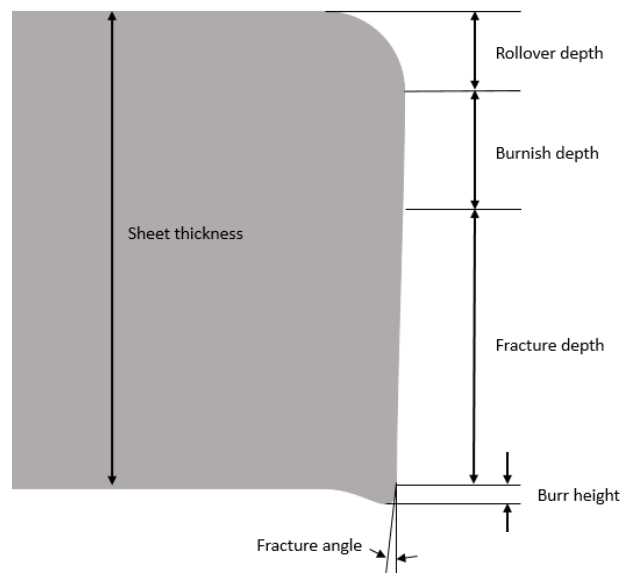


Figure 19. Illustration of cutting defects on sheets and blanks (based on [28])

How severe the defects becomes depends on how well tuned the cutting equipment is e.g. how precise the guidance for the cutting knives are [7]. When positioning the blanks prior to welding side by side, the shearing defects could have a big impact on the outcome and performance of the weld seam. According to

[7], the generally accepted requirement is a gap less than 0.1 mm anywhere between the blanks. Hence, if the gap is above 0,1mm the irregularities can for example cause insufficient material in the weld seam, resulting in an area reduction, different chemical composition, cracks and pores etc. [7].

2.4.5 Laser welding imperfections

A brief description of the most common imperfections appearing during laser welding follows below.

The fracture behaviour of a weld depend on the weld shape (cross section), the metallurgy, and imperfections such as pores, cracks and cavities (Figure 20). As stated by [27], the quality of the weld is often determined by its mechanical properties through destructive testing, for example hemispherical punch testing and tensile testing. Cracks and porosity can act as crack initiation sites, which could result in a complete failure of the weld. Porosities are usually caused by instabilities in the keyhole and entrapped gas bubbles from vaporized oxides. Cavities can also later form from merging pores [24].

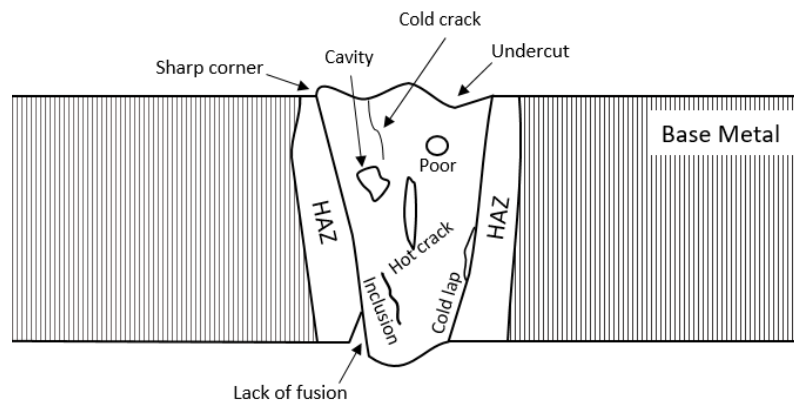


Figure 20. Cross section of a laser weld with different kinds of imperfections that could appear (based on [27])

Imperfections can generally be classified in two categories, outer and inner imperfections. Examples of outer imperfections are undercuts, shrinkages grooves and lack of penetration etc., while inner imperfections can be cracks and pores etc. [27]. The behavior and strength of the component are often determined by the outer imperfections, or in other words the shape of the weld. The penetration depth, or the area of the cross section, is the main strength criterion, while the geometrical imperfections such as undercuts or sharp corners can act as crack initiation sites and stress concentrators/raisers [27].

Among cracks, hot cracking is one of the most common phenomena that occurs in laser welding of thin sheet structures [24]. They are named hot cracking because they occur immediately after, or during the welding. The reason is that the liquid weld metal is insufficient to fill the spaces between the solidifying weld metal, which are opened by shrinkage strains [29]. Low melting eutectics are concentrated at the centre of the weld and the cracks usually appears longitudinal in the centreline, but they could take any orientation. To control hot cracking, the factors like weld metal composition, weld solidification pattern

and strain on the solidifying weld metal needs to be controlled [24]. According to [27], hot cracks can be suppressed or prevented by adding filler wire with a slightly different melting point.

Cold cracking or hydrogen cracking can occur either directly after welding or days later. They are formed partly because of the rapid cooling, which creates a martensitic microstructure. As stated by [27], rapid propagation of dislocations are corresponding to cold cracking. Other influencing factors prone to form cold cracking are the amount of diffusible hydrogen (hydrogen is trapped in the weld and creates internal stresses) and residual stresses. Materials with an increased amount of carbon are more likely to cold crack. Thicker materials are also more sensitive to cold cracking, since the cooling rate is higher. The material surrounding the weld will act as a heat sink resulting in the weld seam cooling down more rapidly [24]. To control cold cracking pre- and post- heat treatments can be used to control the martensite formation, e.g. pre-heating or post tempering of the welded piece. Filler material can be used to reduce the amount of diffusible hydrogen. The carbon equivalent (CE) (Equation 2) can be used to judge the risk of cracking, a high CE value often means an increased risk for cracking [24]. A fine grain size can also prevent the formation of cracks, or increase the resistance, the grain boundaries will redistribute strains and possibly block the propagation of cracks [27].

Equation 2. One commonly used equation for expressing the Carbon Equivalent (CE)

$$CE = \%C + \frac{\%Mn}{6} + \left(\frac{\%Cr + \%Mo + \%V}{5} \right) + \left(\frac{\%Cu + \%Ni}{15} \right)$$

2.5 Verification after welding

A destructive testing technique used after welding can verify the properties of the weld seam. The method used in this research is an Erichsen cupping test performed by the manufacturing companies according to a VCC standard, which is cross referencing to EN ISO 20482:2013. Below follows a brief explanation of the Erichsen test and the formability of thin metal sheets.

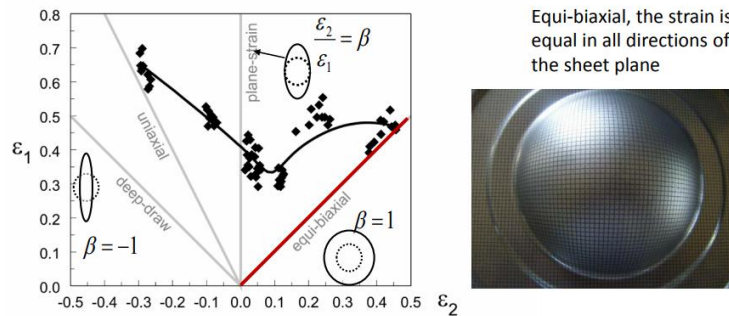
2.5.1 Cup test and formability

The Erichsen cupping test is used on the TWBs according to EN ISO 20482:2013 after welding to control the properties and quality of the weld seam. It is however also a measure of the formability of the blank. According to the standard (20482), the Erichsen test is used to evaluate the ability of metallic sheets to undergo plastic deformation in stretch forming (biaxial stretch forming or biaxial forming, see definition below). The blank is gripped by clamping devices and a spherical punch is pushed into the blank, forming it to a half sphere/dome. The test is finished either when a fracture starts to occur or at a certain dome height. In EN ISO 20482:2013 it is stated that the height is measured when a through crack appears. The blank should deform by elongation and uniform thinning (equi-biaxial, see Figure 21). When TWBs are tested, the weld seam is positioned over the centre of the spherical punch and the fracture is normally expected to happen outside of the weld. In the case of a TWB with the combination of a harder material joined with a softer material, the fracture is expected to appear in the softer material or across the weld seam, which is also what is considered as an approved weld. The fracture will most likely occur in or along the weld seam if the weld is weak or has a severe undercut. As reported by [20] a weld is considered good if the fracture occurs away from the HAZ and fusion zone on a low and mid-carbon steel. The Erichsen cupping index (IE) is the height the punch is pushed until fracture occurs, expressed in millimetres, and the measure of the formability is also known as the forming limit [30].

The judgment of the results from the Erichsen test according EN ISO 20482:2013 is listed in SS-EN ISO 10359:2015 from which EN ISO 20482:2013 is cross referenced. According to EN ISO 10359:2015, the weld seam is considered as OK if the crack appears across the weld or along outside of the weld. The weld is not accepted if the crack is considered to be in the weld or along the inside of the HAZ.

FLC: Formability related to strain states $\epsilon_1 + \epsilon_2 + \epsilon_3 = 0$

$$\beta = 1$$



Equi-biaxial, the strain is equal in all directions of the sheet plane

Figure 21. Stretch forming/Equi-biaxial [31]

Definition

Equi-biaxial state: The strain is equal in all directions of the sheet plane, thus no zero elongation strain state present. After a certain amount of strain, local necking will occur [31].

Several factors are affecting the formability of a material, such as mechanical properties, microstructure and thickness. How all factors and the combination of them affect the formability is not fully understood, and the definition is therefore quite vague, see definition below.

The formability of a TWB is often controlled by the formability of the weld seam. When two different materials are joined by welding, the most middle part of the weld has been melted and mixed, which is called the fusion zone (FZ). The final microstructure and properties of the FZ after welding will depend on the heat input, cooling rate and the “new” composition created by the fusion of different materials. Depending on cooling rate and composition, the FZ can obtain a microstructure of ferrite, pearlite, bainite and martensite (in steels). Depending on final microstructure the weld will obtain different forming properties [20].

Definition

What is formability?

The engineering/scientific approach: *The formability of a material is the amount of strain to which that material can be deformed (stretched) before fracture occurs.*

The industrial/practical approach: *A material shows good formability if it passes through the forming operations without presenting any problems.[31]*

2.6 Hot Forming

Hot forming refers to when a blank is heated and then sub-sequentially formed and quenched in the same tool. Hot forming can also be called hot stamping or press hardening. The term used in this thesis has and will only be hot forming, other denominations could however be seen in the figures. Hot formed parts has increased a lot the last years within the automotive industry, this due to the increasing demand for high strength and low weight. The Swedish company Plannja invented and patented the process in 1977 [32]. The SAAB 9000, introduced in 1984 was the first car with hot formed boron steel in the car body [33]. Today Volvo cars XC90 Body In White (BIW) contains 38% hot formed steel compared to only a few percentage on the V70 in year 2000, see Figure 22.

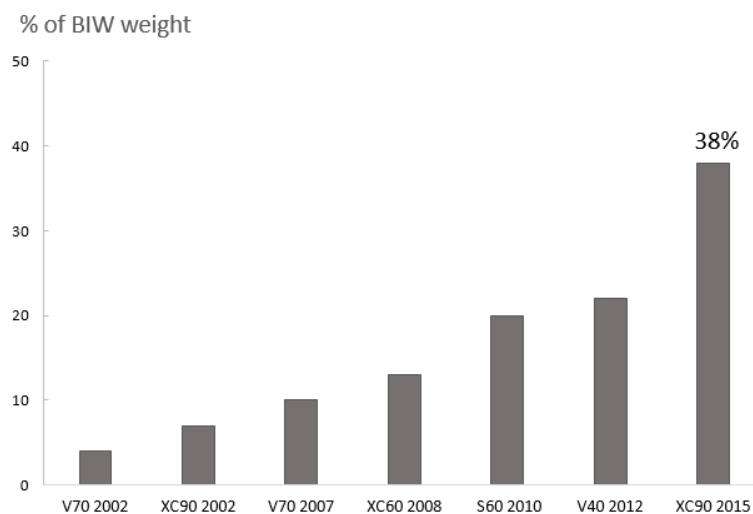


Figure 22. Increase in proportion of HF-steel used in the BIW on Volvo models (based on [24])

2.6.1 Hot forming steels

The demand for reduced vehicle weight and increased crashworthiness has been the driver for increasing the strength in car body components. By increasing the strength it becomes possible to decrease the thickness of the parts, which in turn leads to a weight reduction of the component [32]. This could sound like a win-win situation, the strength is increased and the weight is reduced. Nevertheless, the crash worthiness especially in the B-pillar also rely on having a more ductile zone to absorb energy during an impact. The B-pillar together with the front and rear side-members are therefore produced by joining an extra-high strength steel (EHSS) with an ultra-high strength steel (UHSS). The EHSS has a much lower tensile strength and higher ductility than the UHSS. The steel classifications used by Volvo cars can be seen Table 1 below. Classes from MS to EHSS are in 'as received condition' and the UHSS is defined for 'as in service condition' [32] [34].

Table 1. Volvo Cars definition of steel classes [24]

<i>Steel class</i>	<i>Abbreviation</i>	<i>Min yield strength [MPa]</i>
<i>Mild steel/forming grades</i>	MS	< 180
<i>High strength steel</i>	HSS	= 180 < 280
<i>Very high strength steel</i>	VHSS	= 280 < 380
<i>Extra high strength steel</i>	EHSS	= 380 < 800
<i>Ultra-high strength steel</i>	UHSS	= > 800

2.6.1.1 Ultra-high strength steels UHSS

The UHSS in the current components are boron steels from the substrate 22MnB5 supplied to Volvo Cars with the trade names Usibor 1500 and MBW 1500. In-house these materials are referred to as ‘1500 materials’, which is also the term used further on in this thesis when referring to either Usibor 1500, MBW 1500 or Boron steel. The compositions of the steel grades provided by the two companies are very similar to each other and the substrate 22MnB5, see Table 2, Table 3 and Table 4 below.

Table 2. Chemical Composition of MBW 500 & 1500 [35]

<i>Steel grade</i>	<i>C [%]</i>	<i>Si [%]</i>	<i>Mn [%]</i>	<i>P [%]</i>	<i>S [%]</i>	<i>Al [%]</i>	<i>Nb [%]</i>	<i>Ti [%]</i>	<i>Cr+Mo [%]</i>	<i>B [%]</i>
	<i>max.</i>	<i>max.</i>	<i>max.</i>	<i>max.</i>	<i>max.</i>	<i>max.</i>	<i>max.</i>	<i>max.</i>	<i>max.</i>	<i>max.</i>
<i>MBW 500</i>	0.10	0.35	1.00	0.030	0.025	0.015	0.10	0.15	-	0.005
<i>MBW 1500</i>	0.25	0.40	1.40	0.025	0.010	0.015	-	0.05	0.50	0.005

Table 3. Chemical Composition of Ductibor 500 & Usibor 1500 [36]

<i>Steel grade</i>	<i>C [%]</i>	<i>Mn [%]</i>	<i>Si [%]</i>	<i>B [%]</i>
	<i>max.</i>	<i>max.</i>	<i>max.</i>	<i>max.</i>
<i>Ductibor 500</i>	0.10	1.30	0.50	0.001
<i>Usibor 1500</i>	0.25	1.40	0.40	0.005

Table 4. Chemical Composition of 22MnB5 [37]

<i>Steel grade</i>	<i>C [%]</i>	<i>Si [%]</i>	<i>Mn [%]</i>	<i>P [%]</i>	<i>S [%]</i>	<i>Cr [%]</i>	<i>Mo [%]</i>	<i>B [%]</i>	<i>Ti [%]</i>	<i>A [%]</i>
<i>22MnB5</i>	0.20- 0.25	0.15- 0.50	1.00- 1.40	0.03 max	0.025 Max	0.10- 0.35	0.035 max	0.0015- 0.0050	0.03- 0.05	0.02- 0.06

Boron steel 22MnB5 is the most commonly used material in hot forming within the automotive industry. The formability of a boron steel or 1500 material increases when the steel is heated to austenitic

temperature because of a few factors: the flow stress decreases, the ductility increases, the spring back effect is reduced, and a lower forming pressure is needed (see Figure 23) [32]. A fully martensitic microstructure and tensile strengths around 1500 MPa are achieved after hot forming of 1500 material.

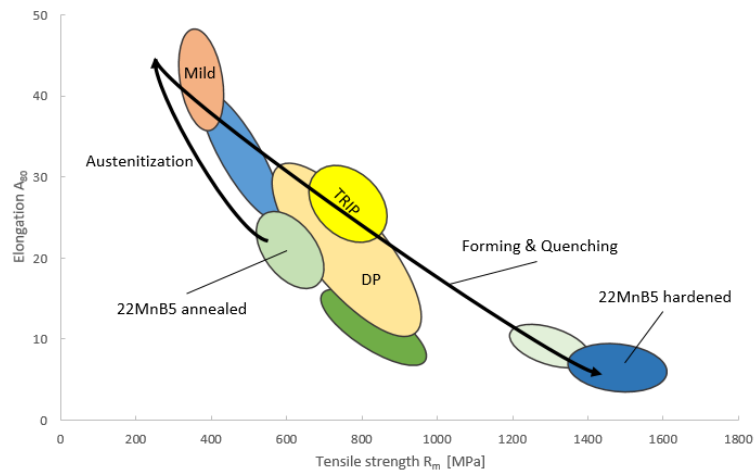


Figure 23. Schematic illustration of the mechanical properties of 22MnB5 in different states compared to other steels (based on [32])

To achieve a martensitic microstructure the material is first heated to an austenitic temperature and secondly cooled to below the martensite start temperature (M_s). The cooling rate from austenitic temperature to M_s temperature is critical and needs to exceed 25-30°K/s [24] to reach a fully martensitic microstructure, see Figure 24.

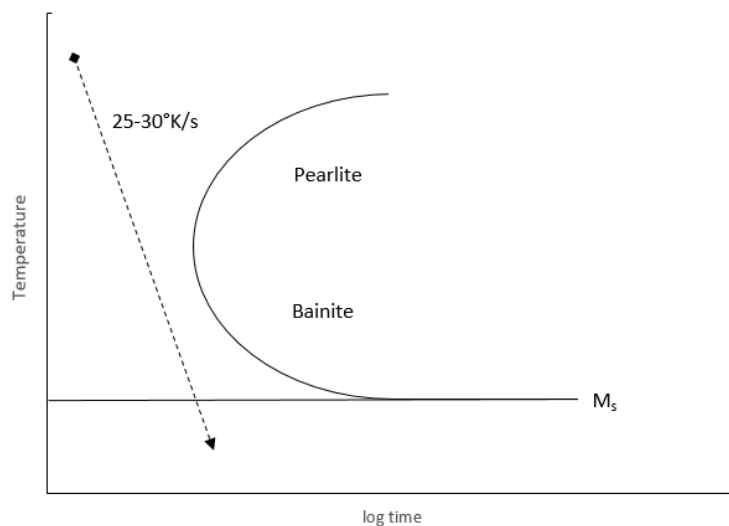


Figure 24. Illustration of a CCT diagram for quenching of austenitized steel (based on [32])

The effect of the alloying element Boron is that it “pushes away the ferrite and perlite nose” in the CCT diagram (Figure 24). The nucleation of ferrite and perlite at the grain boundaries (GB) are delayed, or in other words, the soluble boron is arranged around the austenite GB’s and retards the austenite to ferrite transformations by diffusion [38]. By delaying nucleation of ferrite more time is given to reach M_s , the critical cooling rate is decreased, thus the hardenability is enhanced. To achieve maximum hardenability

the quantity of boron should be 0.0003 to 0.0030% B [39]. If an excessive amount of boron is used or present the hardenability is lowered and the toughness is decreased. This is because the boron constituents becomes segregated around the austenite GB's, and leaves open spaces for ferrite nucleation [39]. The boron effect is quite beneficial in the hot forming process because it increases the window for reaching a full martensite transformation.

C is not only an interstitial enhancing the hardness it is also a strong austenite former/stabilizer together with Ni and Mn, where Mn also improves the hot ductility. Si and Cr increases the resistance to oxidation at higher temperature. Ti is a strong carbide former and prevents grain growth in the heat affected zone (HAZ) [40].

2.6.1.2 Extra high strength steel EHSS

For the more ductile areas of the current components Volvo cars are using a steel with an approximate tensile strength of 500 MPa, with the intention to absorb kinetic energy during a collision. According to the classification used by Volvo cars is the material classified as an extra-high strength steels (EHSS). In-house these materials are referred to as '500 materials', which is also the term used in this thesis when referring to the more ductile steel used in the current components.

When hot forming the 500 material no significant enhancement of the mechanical properties are achieved compared to the 'as received condition' [41]. The 500 material is not transformed into martensite during hot forming, because the carbon equivalent (CE) is very low and the amount of boron is close to zero. Thus, the critical cooling rate for this composition is not reached. The 500 material also has an addition of Nb, which is a ferrite stabilizer, meaning that it pushes the pearlite nose to the left in the CCT-diagram or in other words it facilitates ferrite nucleation at the austenite GBs. After heat treatment the microstructure consist of ferrite and carbon rich phases according to [41]. The study carried out by [41] could not define the carbon rich phases more specifically due to restrictions in the available equipment.

2.6.2 Hot forming process

The hot forming process most commonly consists of the four following steps:

- I. Heat treatment in furnace to austenitization temperature
- II. Transfer from furnace to hot forming tool
- III. Plastic hot forming
- IV. Quenching in the closed and cooled die

The hot forming process can be performed using two different methods, which are direct and indirect hot forming (HF). In the direct process, the blank is first fully austenitized and then simultaneously formed and quenched, see Figure 25 below. The TWBs hot formed at, and produced for, Volvo Cars, are manufactured by the direct hot forming process [32] [42].

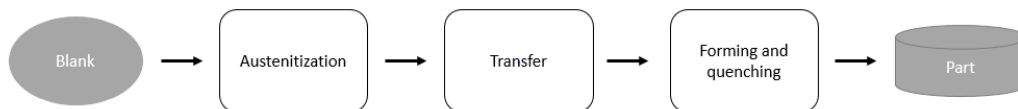


Figure 25. Direct Hot Forming process (based on [32])

The indirect process is similar to the direct process but it involves a pre-forming step before the sheet is fully austenitized see Figure 26. The pre-forming step increases the forming capabilities of the blank, thus more complex geometries can be obtained [32] [42].

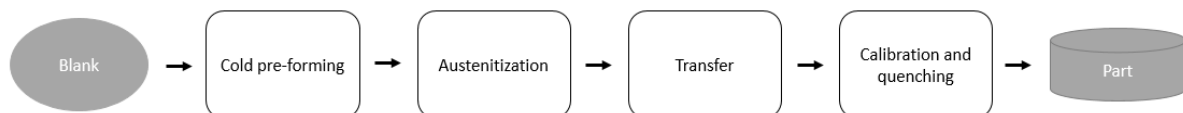


Figure 26. Indirect hot forming process (based on [32])

2.6.3 Heat treatment/Heating

The two most common ways to heat blanks prior to forming are either in a roller-hearth furnace or a multi-chamber furnace [33]. Lately the use of multi-chamber furnaces has increased considerably, mainly due to their compact design compared to the more space consuming roller-hearth furnaces. The disadvantage with multi-chamber furnaces is that the transfer time between the furnace and the forming is relatively long.

The increased demand for hot formed components has shed some light on the development of new heating solutions for the hot forming process. The new solutions currently under development are for example, resistance heating, induction heating, infrared heating and contact heating. Resistance heating is the most promising future alternative to multi-chamber and roller-hearth furnaces because it has a higher degree of

efficiency compared to the other methods [33]. The heating time is only a couple of seconds compared to a couple of minutes in a roller-hearth or multi-chamber furnace. No or very little oxidation is created on non-coated blanks because of the short heating time (2-10s). It also offers the possibility to perform partial heating. However, there is also a major disadvantage, and that is that the temperature is not uniformly distributed in non-rectangular sheets. There are however new methods currently under development for handling these issues [33].

2.6.4 Known complications & challenges in the HF process

A general challenge in the hot forming process is the risk for non-uniform cooling, which is often caused by the non-uniform contact between the blank and the tool during forming and quenching. For example, the bottom and the flange of a cup could have a low temperature, and the side wall a high temperature because of the insufficient contact with the tool, often caused by the possible thickness decrease in the side wall [33]. The differences in temperature can cause a difference in flow stress which in turn can affect the deformation behaviour. The insufficient contact between the tool and the workpiece can also affect the martensitic transformation. To completely reach below martensite start temperature (M_s), the workpiece is held in the die for about 10 s after forming. If the workpiece has only partial contact with the die during these 10s, the cooling speed will differ which could cause local areas not to fully transform into martensite. To minimize these problems the forming tool and holding force needs to be finely tuned and maintained [32].

To achieve a fully martensitic microstructure the material has to be quenched from an austenitic phase. Hence, there is a time slot for the transportation between the furnace and the forming tool. If the maximum time is exceeded the chance of reaching a fully martensitic transformation decreases significantly or completely. A rapid and well-tuned transportation between the furnace and the forming tool is therefore of utmost importance, and needs to be monitored to avoid a large temperature-drop [33].

2.7 Verification after hot forming

The verification of the TWB after hot forming is currently carried out according to a Volvo car standard (VCS 5730.4) which requires certain mechanical properties of the Al-Si coated steels. However, this standard is not including any specific demands on the mechanical properties of the weld. Since the B-pillars and side-members are hot formed components consisting of different Al-Si coated steels welded together, it has been difficult to implement complete requirements on such a component in a general standard. Volvo Cars therefore has a desire to supplement that standard with a mechanical test.

The only mechanical testing currently carried out on the B-pillars and side members to verify the mechanical properties of the weld is a full crash test (a complete car). To randomly crash a complete car when considered necessary to verify the mechanical properties of one component is of course extremely expensive. It is therefore wanted to implement requirements on the properties of the weld after hot forming, and to be able to mechanically test the component without having to perform a full crash test. There is today a standard including a mechanical testing of the weld to verify the weld properties after welding (section 2.5). However, the properties of the weld are modified after hot forming since the heat treatment is modifying the microstructure and distribution of the constituents in the weld. One could say that the requirements on an operation which has been verified is in need of a new verification due to a thermal refining process. On the other hand, the diffusion is at this low temperature and short soaking time, not that significant. One of the main goals in this thesis has been to find a solution on how such a verification could be performed.

2.8 Welding with filler wire & without ablation

One of the main objectives in this thesis is to investigate the mechanical performance of the weld without pre-preparing the blanks, i.e. removal of the Al-Si coating, and instead use a filler wire to dilute the coating in the weld. The filler wire is used in order to minimize, both in size and occurrence, the formation of ferrite and brittle IMCs. The possible impacts the usage of filler wire, without removal of the coating, could have on the: mechanical performance; welding process; assembly and HF process, will therefore be discussed here.

2.8.1 Mechanical performance

If the weld is performed with the addition of a filler wire and without removal of the coating, the quality of the weld seam could still be affected by the possible contamination of the coating which could alter the composition. Since little or no work has been reported about the usage of filler wire instead of performing the ablation process, this sub-section will focus on the work reported on when no precautions are taken prior to welding, thus without ablation and without filler wire. [2] and [43] studied the mechanical performance of TWBs made by Al-Si coated Usibor 1500 and 22MnB5, respectively. Where no precautions were taken prior to welding.

Pursuant to [2], the contamination of Al-Si coating in the fusion zone will lead to a modification of the transformation kinetics (CCT-diagram) for that specific area. The contaminated area then requires a higher critical cooling rate than the parent material, and higher than what is normally reached during quenching. This could lead to a microstructure of ferrite and bainite instead of martensite, with a hardness drop of -200 HV to ~300 HV (Usibor 1500). See Figure 27.

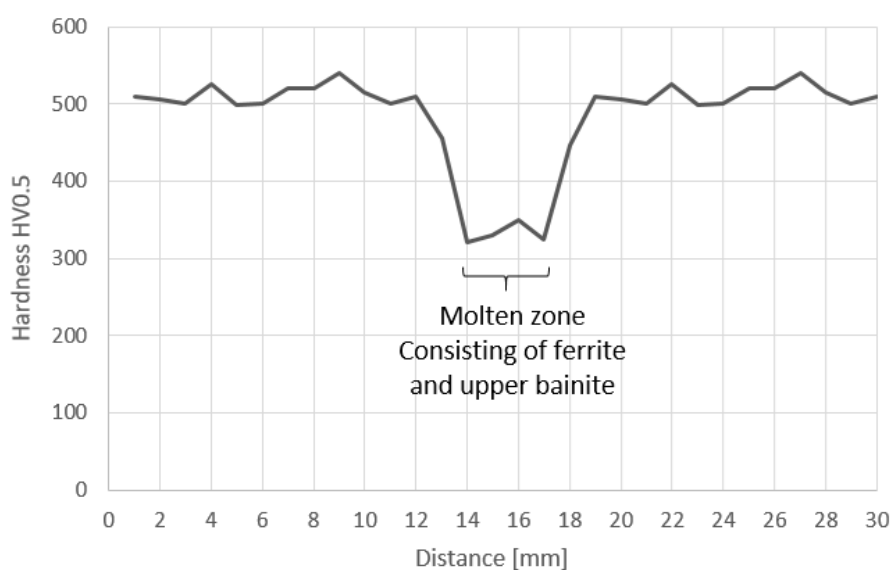


Figure 27. Illustration of the hardness drop in the molten zone after hot-stamping of an Usibor 1500 TWB (conventional process) (based on [2])

The differences in microstructure between the base-metal and the weld could increase the risk of strain localization during mechanical influence on the weld. Furthermore, both [2] and [44] confirmed that the components failed in the weld seam during tensile testing. Micrographic investigations showed that the failure occurred exactly on the intermetallic compounds (IMC) a.k.a. whitebands see Figure 28.

- A: Close to the surface of the weld aligned along Marangoni's flow lines. The Fe-Al-Si particles in this area are quite large with an elongated shape [2]
- B: The central part of the molten zone. The Fe-Al-Si particles are relatively small with an equiaxed shape. A fairly turbulent area – at the intersection of Marangoni's flow lines [2]

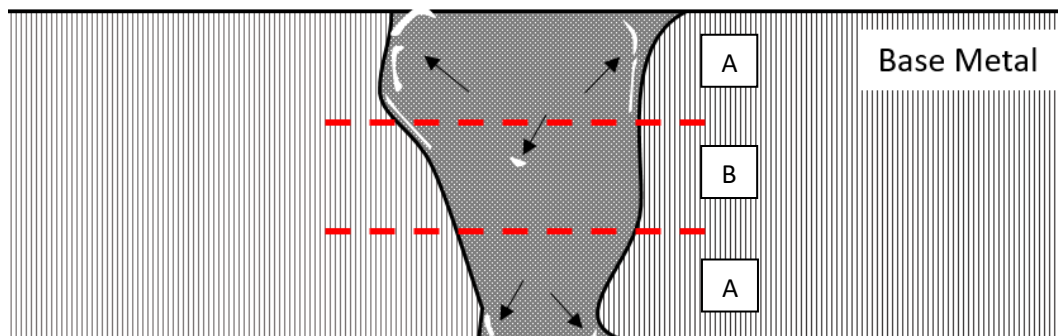


Figure 28. Illustration of the white bands in the fusion zone, pointed out with arrows close to the fusion line and in the middle (based on [2])

These two studies strongly indicates that the weld becomes the weakest link when two 1500 materials are welded together without removal of the coating. Even if this is the case when two 1500 materials are joined together, it does not necessarily say that it is also the case for the currently investigated components of this thesis, which have a material combination consisting of a 500 material joined with a 1500 material.

2.8.2 Laser welding with filler wire

Laser welding in its primary form is performed in a keyhole mode on a butt weld configuration without any gap between the blanks/sheets. If a filler material would be introduced to the welding, it could be either in the form of powder, wire or a profile. In line with [45], a filler material in the form of a wire is considered to be the least complex and most promising for laser welding. If a filler wire is added to the process, it becomes possible to: influence the metallurgical composition, lower the demands for edge misalignment and edge preparation, and to compensate for geometrical defects like weld concavity and undercuts [45].

The main purpose of using filler wire stated by [45] & [46] is to reduce the tight fit up requirements (geometrical edge misalignment). They report that the gap tolerance can be increased significantly compared to autogenous welding (welding where no additional filler material is used). However, to compensate for a varying gap between the blanks can lead to a much more complex welding process (weld seam tracking & wire feeding) and to difficulties in maintaining the mechanical properties along the weld

seam (the ratio of filler wire to base metal). Another purpose to use filler wire is to control the weld chemistry, it creates possibilities to modify not only the weld chemistry but also the mixing. It is however difficult to achieve a good mixing of the weld, because it is a relatively rapid process. Nonetheless, some investigations [45] have showed that depending on where the laser beam intersects with the filler wire will alter the mixing of the weld (Z-direction). Depending on in which angle and feeding position (trailing or leading, see Figure 29) the wire is feed by, the mixing, the symmetry of the weld, the reflection of the beam and behaviour of the plume could be affected [47]. These are just some of the phenomena occurring when filler wire is added to the laser welding process, a lot more are occurring and many of them are not yet fully understood. Laser welding with filler wire can offer a bigger versatility, but it also complicates the process [48] [45].

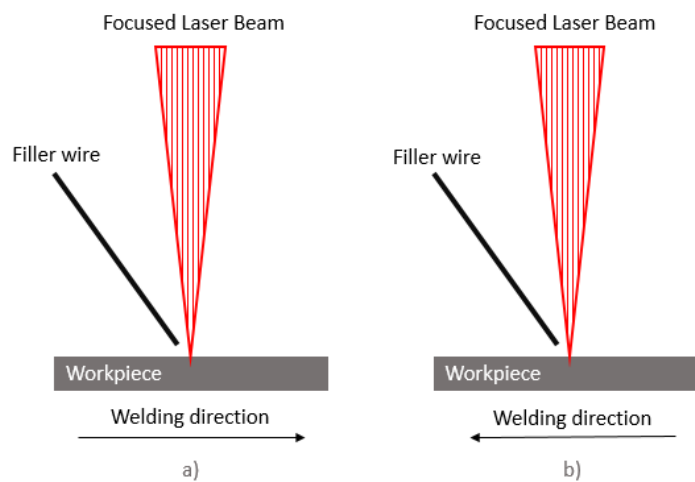


Figure 29. a) Trailing feed, b) Leading feed (based on [45])

2.8.2.1 Melt flow

In Figure 28 above, whitebands consisting of intermetallic compounds (IMCs) and ferrite can be seen in the corners and in the middle of the fusion zone, the cross section is from a laser welding performed without filler wire and without removal of the coating. The melt flow in a keyhole laser weld results from a lot of complex phenomena, yet the whitebands in the figure illustrates one quite common melt flow phenomenon known to appear in laser welding and arc welding, the Marangoni flow or effect [27].

As stated by [27], the Marangoni flow is driven by surface tension gradients. Surface tension is lowered in the middle due to the temperature difference towards the solid-liquid interface. This causes flows outwards towards the higher surface tension, the flow is redirected down when it hits the solidified wall (higher surface tension at solid-liquid boundary). The result of the Marangoni flow is not only the microstructural segregation in the corners and the middle but also the creation of eddies. Eddies are the second known phenomena, in which the melt flow is going upwards in the middle of the weld (Figure 30),

caused by the turbulence created by the redirected Marangoni flow. Depending on the welding speed, eddies can in turn cause humping, the higher the speed the more severe eddies, thus increasing the risk for humping. Humping is also a well-known weld defect in laser welding, and the upward flow can create solidified “waves” in the finished weld [27] [22], see Figure 30.

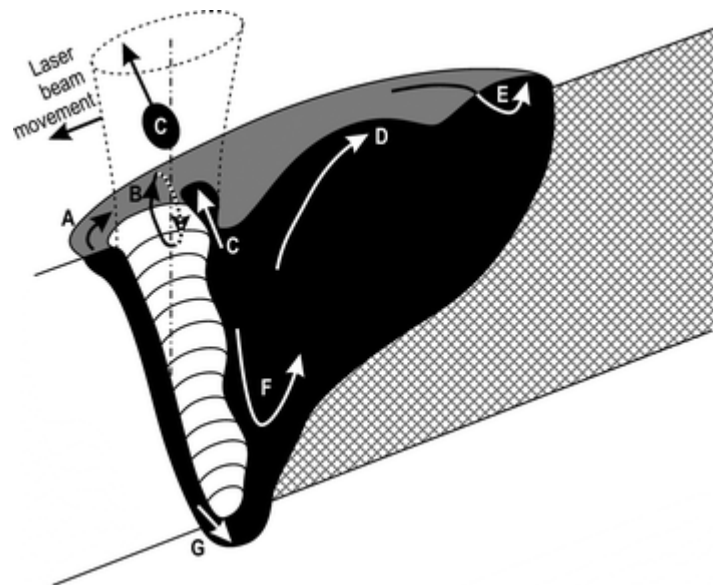


Figure 30. Illustration of different melt flow phenomena during laser welding; a) melt passing around the keyhole, b) Marangoni flow, c) drop ejection, d) humping, e) rear flow stagnation, f) inner eddies, g) flow downwards to the root, or flow underneath the keyhole [27]

2.8.3 Production process and assembly

The usage of filler wire in the welding process can cause a weld bead and a larger root drop-out on the weld seam (excessive material on top and bottom). The excessive material can in turn cause issues in the hot forming process and in the final assembly.

The hot forming process is currently performed in-house at Volvo Car Body Components (VCBC) for the European production sites, and by subcontractors supplying the Asian and North-American production sites. The major impact a weld bead would have on the hot forming process is in the forming tool. A groove might need to be milled out in the forming tool to facilitate a complete and accurate pressing of the blank.

The weld bead could also have a minor effect on the stack height deflection for the TWBs. The weld bead could and most likely would cause a deflection on the stacked TWBs. To get the deflection within limits the number of TWBs in a tray might need to be reduced, which in turn could lead to a more time consuming material handling.

The components presently produced by the TWB technology have mating surfaces when being assembled in the BIW. The excessive material on the weld seam caused by the filler wire could then affect the mating surfaces. If filler wire is to be implemented in the welding process the mating surfaces in the assembly needs to be reviewed and most likely re-designed. It becomes therefore very difficult to introduce TWBs manufactured with filler wire in the current production, so-called 'carry-back'. If filler wire is to be implemented in the welding process, the target is that the weld beads and root drop-out should be max 10 % of t_{nom} not to affect the design in a greater sense.

3 Experimental

In this chapter the Experimental procedure will be discussed, the intention is to provide and describe what and how it was carried out in order to be able to reproduce the results of this work.

Experiments and samples were only performed on, and taken from, B-pillars and Weld Test Coupons (WTC) in this thesis. Previous work has been performed on the side members by both Volvo Cars and the subcontractor Wisco Tailored blanks. The main working plan has been to analyse and compare the results produced in this research to the previous results. Most experiments carried out have therefore been experiments which could easily be compared with the previous work. The intention was also to evaluate the processes investigated as efficiently as possible, and to work out a solution of how the weld seam properties can be verified after hot forming.

3.1 Test specimens

Experiments and analyses were performed on both full sized components (B-Pillars) and Weld Test Coupons. The B-Pillars used were from two different types (different car models), here called X & Y. As pointed out in the introduction, the only material combination investigated in this thesis has been 500 material joined with 1500 material. Four different welding processes regarding material preparation and welding method were tested and analysed. These are described in the list below together with an acronym/code for every welding process, which is going to be used throughout the rest of the report, and be written together with an explanation of the process used on each version. The intention is to simplify the content for a better reading experience.

Laser welding with:

1. No FW & Partial Ablation ('Standard' (STD)) & ('Standard2' (STD2))
2. FW & Partial Ablation ('Special Case' (SC))
3. FW & No Ablation ('Filler Wire' (FW))
4. No FW & No Ablation ('Worst Case' (WC))

Process 1 is the so-called standard process, acronym STD, currently used in manufacturing sites in Europe. To broaden this survey the same welding process was also performed by a different subcontractor and added to the investigation, that process is called Standard 2 (STD2) to separate it from the first one. Process 2 is a process currently in use at the Asian manufacturing site. In this process, the filler wire is only added to compensate for the weld concavity and no weld bead should be created. The filler wire used is not alloyed to enhance the properties of the weld, and the acronym/code for it is Special Case (SC). Process 3, coded FW, is the new process suggested to replace the standard process. The chemical composition of the filler wire used in this process is today unknown, but it is most likely containing alloys to suppress ferrite formation in the fusion zone. This process also creates a weld bead. Process 4 was added with the intention to represent the worst case scenario, to answer how the mechanical properties would be affected if no precautions were taken prior to welding. The process is also therefore called Worst Case (WC). The Table 5 below provides an overview of which material preparation and welding methods, used, on what specimens.

Table 5. Material preparation, welding process and specimens

<i>Code/Acronym</i>	<i>Welding Process</i>	<i>Filler Wire</i>	<i>Laser Ablation</i>	<i>Weld Test Coupon</i>	<i>B-pillar</i>
<i>STD & STD2</i>	No FW & Part. Abl.	No	Partial	Yes	Yes
<i>SC</i>	FW & Part. Abl.	Yes	Partial	No	Yes
<i>FW</i>	FW & No Abl.	Yes	No	Yes	Yes
<i>WC</i>	No FW & No Abl.	No	No	Yes	No

3.2 Drop weight test

A drop weight test was carried out at Volvo Cars safety centre. The specimens tested were complete B-pillars with three different welding processes regarding material preparation and welding method, and they were:

1. No FW & Partial Ablation ('Standard' (STD & STD2))
2. FW & Partial Ablation ('Special Case' (SC))
3. FW & No Ablation ('Filler Wire' (FW))

The three different welding processes were divided into four sample groups, since the No FW & Partial Ablation process was represented as STD and STD2. Which welding process used on what component can be seen in Table 6.

Table 6. Welding process & Type of specimen analysed by drop weight test

<i>Code/Acronym</i>	<i>Welding process</i>	<i>Specimen</i>
<i>STD</i>	No FW & Partial Ablation	B-Pillar X
<i>FW</i>	FW & No Ablation	B-Pillar X
<i>STD2</i>	No FW & Partial Ablation	B-Pillar Y
<i>SC</i>	FW & Partial Ablation	B-Pillar Y

The complete B-pillars were mounted in a test jig and subjected to a falling body with a weight of 129 kg. The parts were positioned so the impact would occur directly at the weld seam, which was believed to give the maximal load on the weld seam. A typical B-pillar also consists of a body side inner and a body side outer. In this test, precautions were taken to minimize the risk of damaging the testing equipment, and to better mimic the complete design of the B-pillar by mounting the body side inner (spot-welded) on all the B-pillars. By mounting the body side inner, the total deformation was reduced, thus the risk of the B-pillar bending into the testing equipment was minimized.

A 3-D Illustration of the test jig with the B-Pillar mounted is seen in Figure 31. The bottom part of the B-pillar was bolted to the test jig and the top part was hanging freely (Cantilever) with the exceptions of two bars restricting the upper part from exaggerated bending during deformation.

The key idea was that the B-pillar in the drop test should have been subjected to an energy corresponding to the absorbed energy by the B-pillar in a side collision with a complete car. It was however shown that it was challenging to predict the energy absorbed by the B-pillar in a side collision. The main objective became instead to subject the weld seam to a load high enough to cause severe damage, and to compare the performances of the different welding processes.

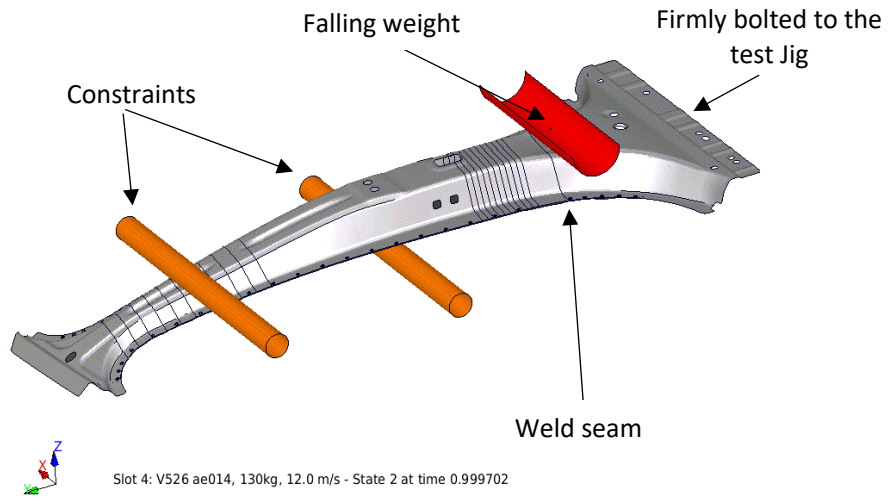
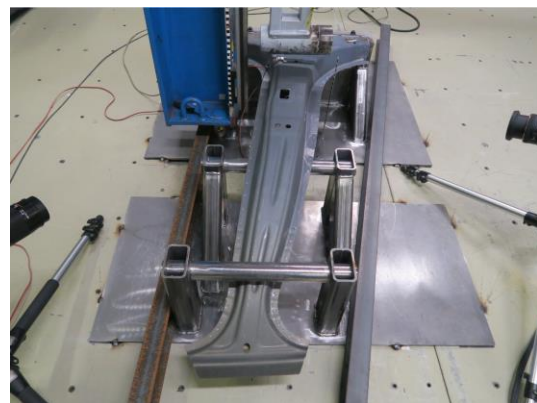


Figure 31 Illustration of the falling weight test (courtesy of H. Ebbing)

The test jig was custom built for the purpose by the department of manufacturing engineering (ME) at VCC. Figure 32 below shows the B-pillar mounted in the test Jig at Volvo safety centre.



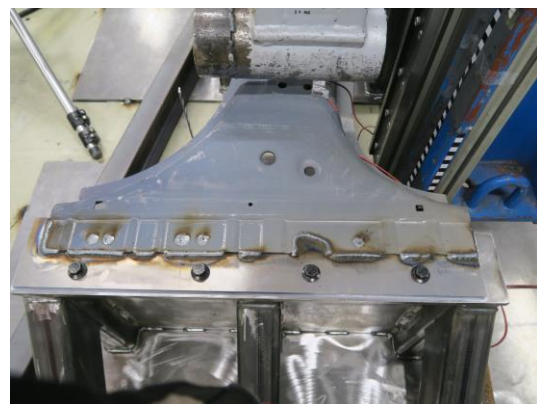
a)



b)



c)



d)

Figure 32. B-Pillar mounted in test Jig. a) Side view. b) View from left. c) View from right. d) View from right (b, c and d are relative to a)

3.3 Hardness profile

Hardness profiles were carried out on mounted and polished cross sections of the welds to evaluate if any differences in hardness could be seen between the different welding processes. Equipment used was a Zwick/Roell Indentec ZHV Vickers hardness indenter and the test load was 1 kgf. Hardness profiling was only carried out on weld test coupons (WTC) and the welding processes investigated can be seen in Table 7.

Table 7. Welding process & Type of specimen analysed by hardness profiling

<i>Code/Acronym</i>	<i>Welding process</i>	<i>Specimen</i>
<i>STD</i>	No FW & Partial Ablation	Weld test coupon
<i>FW</i>	FW & No Ablation	Weld test coupon
<i>WC</i>	No FW & No Ablation	Weld test coupon

3.4 Microstructure & Chemical analysis

In this section, the experimental setup concerning the microstructural and chemical analysis are presented and described.

3.4.1 Optical Microscopy

Macro examination of the weld cross section was performed with a magnification from 5X to 20X to get an overview of the microstructure in the weld. The analysis was carried out to investigate how the welding processes affected the microstructures in the welds. Location was the department of Industrial and Material Science (IMS) at Chalmers University of technology and the equipment used was a Leica DMRX Optical microscope. The samples were prepared, polished (1 μ m) and etched with 2% Nital solution. Specimens analysed were both from B-pillars and Weld Test Coupons (WTC), and will be described separately below.

B-Pillar

The material availability has been limited during this entire thesis. It was therefore decided to take samples from the deformed B-pillars after the drop weight test instead of using complete intact pillars for this analysis. The samples were cut out from the less affected area of the flange on the B-pillars, see Figure 33 below. The samples analysed are shown in Table 8.

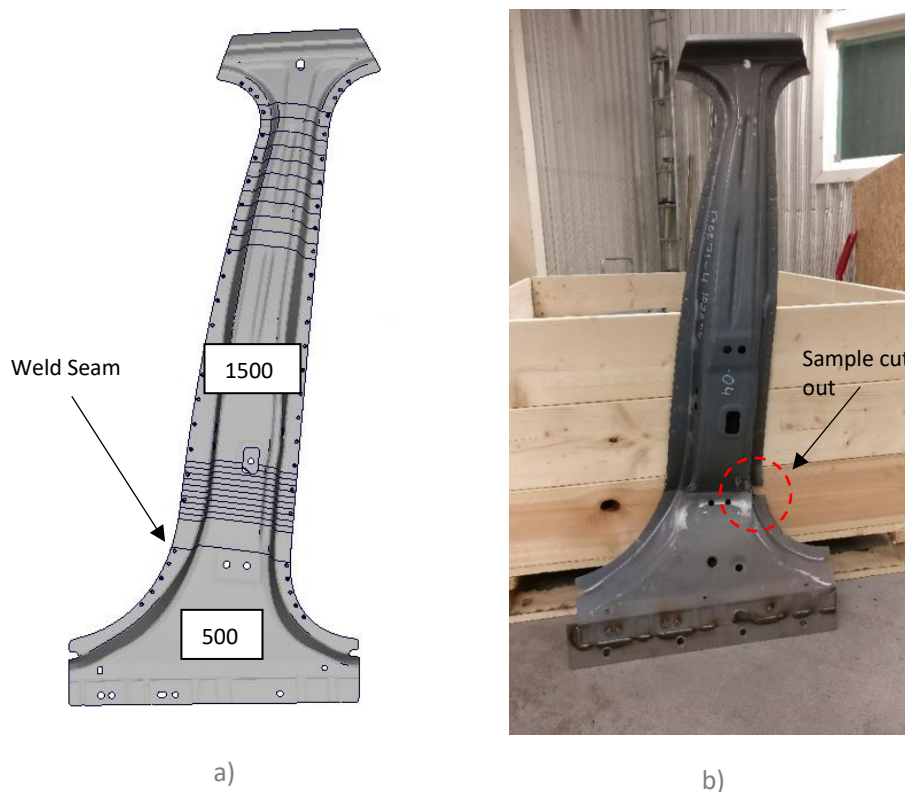


Figure 33. a) 3D model of a B-pillar. b) Showing where the samples were cut out on the B-pillar

Table 8. Welding process & Type of specimen analysed by optical microscope

<i>Code/Acronym</i>	<i>Welding process</i>	<i>Specimen</i>
<i>STD</i>	No FW & Partial Ablation	B-pillar X
<i>FW</i>	FW & No Ablation	B-pillar X
<i>STD2</i>	No FW & Partial Ablation	B-pillar Y
<i>SC</i>	FW & Partial Ablation	B-pillar Y

Weld test coupon

Cross sections were cut out from the weld test coupons, see Figure 34. The samples analysed are shown in Table 9.

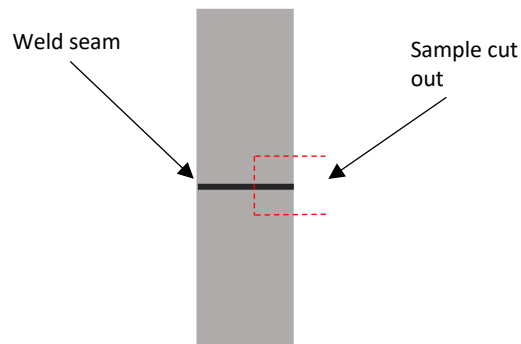


Figure 34. Weld Test Coupon

Table 9. Welding process & Type of specimen analysed by optical microscope

<i>Code/Acronym</i>	<i>Welding process</i>	<i>Specimen</i>
<i>STD</i>	No FW & Partial Ablation	Weld test coupon
<i>FW</i>	FW & No Ablation	Weld test coupon
<i>WC</i>	No FW & No Ablation	Weld test coupon

3.4.2 SEM/EDX Chemical Analysis.

A scanning electron microscope (SEM) was used to investigate the phases in the so-called whitebands of the weld. The intention was to separate/distinguish ferrite from intermetallic phases. An EDX analysis was also carried out to determine the chemical composition in the whitebands.

One sample, the FW-welding process (FW & No ablation) was analysed. The location was the department of Physics (Chalmers Material Analysis Laboratory) and equipment used was a SEM/EDX Leo Ultra 55. Electron source was a Field Emission Gun and the acceleration voltage was 30 kV. The instrument data can be seen below.



Instrument data:

- Spatial resolution:
 - 15 kV: 1.0 nm
 - 1 kV: 1.7 nm
 - 0.1 kV: 4.0 nm
- Operating voltage: 0.1 - 30 kV
- Probe current: 4 pA - 10 nA
- Field emission gun (FEG)
- Equipped with:
 - Oxford Inca EDX system
 - EBSD system
 - STEM detector

Figure 35. SEM/EDX Leo Ultra 55 & instrument data

3.5 Tensile test

Specimens from both the B-pillars and the Weld Test Coupons (WTC) were tensile tested. All samples were tested on a Zwick/Roell tensile testing machine, model Z050. The pre-load was 2 N and the test speed was 10mm/min on all samples.

B-Pillar

Two samples from each welding process were tested from the B-pillars. Laser cutting was used to cut out the samples, thus the two samples in each welding process were from the same B-pillar. Figure 36 below illustrates where the samples were cut out.

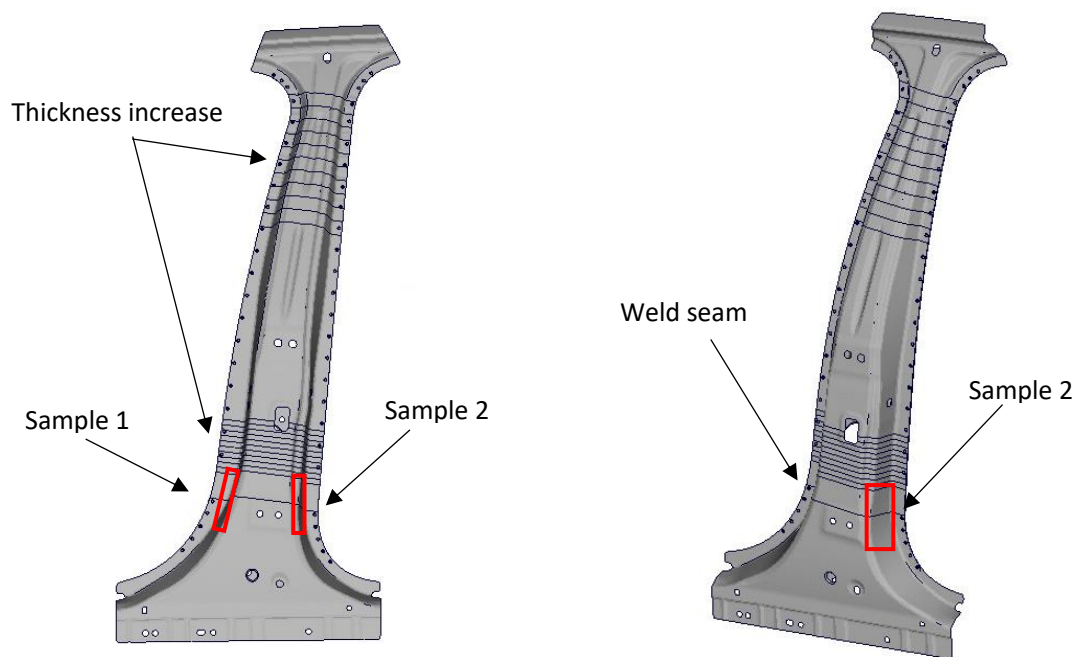


Figure 36. Where tensile test samples were cut out from the B-Pillars

The dimension of the samples were 108x48 mm. However, the wanted dimensions were 200x48 mm to enable a better gripping of the samples and to not risk reaching the maximum possible force available in the equipment. The geometry of the available components limited the possibilities to achieve more corresponding dimensions (Geometry and TRB thickness increase, see Figure 36). Also, the weld seam was not completely perpendicular to the pulling direction – the samples from the Y B-Pillars deviated more than the X B-pillar samples. The welding processes tested were according to Table 10 below.

Table 10. Welding process & Type of specimen analysed by tensile test

<i>Code/ Acronym</i>	<i>Welding process</i>	<i>Specimen</i>
STD	No FW & Partial Ablation	B-pillar X
FW	FW & No Ablation	B-pillar X
STD2	No FW & Partial Ablation	B-pillar Y
SC	FW & Partial Ablation	B-pillar Y

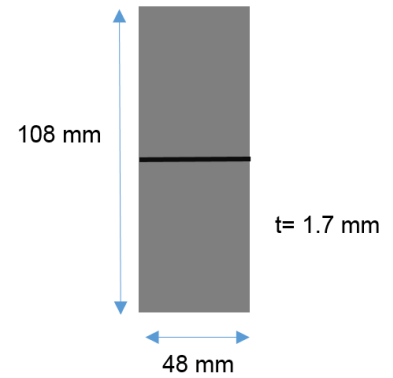


Figure 37. Dimensions of the B-pillar samples

Weld test coupon

The Weld Test Coupons were supplied by Wisco tailored blanks, and three coupons from each welding process were tensile tested. The dimensions were 150x48 mm, they were also completely flat and had the weld perpendicular to the pulling direction. Welding methods tested are shown in Table 11.

Table 11. Welding process & Type of specimen analysed by tensile test

<i>Code/ Acronym</i>	<i>Welding process</i>	<i>Specimen</i>
STD	No FW & Partial Ablation	Weld test coupon
FW	FW & No Ablation	Weld test coupon
WC	No FW & No Ablation	Weld test coupon

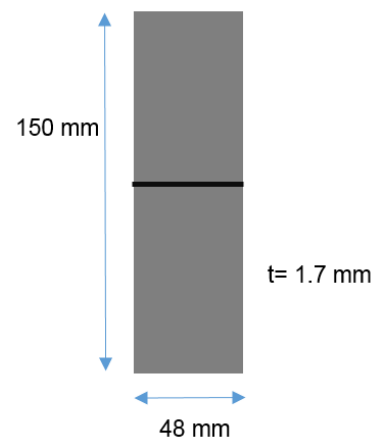


Figure 38. Dimensions of the WTC samples

4 Results

In the following chapter, the results from the experimental are presented.

4.1 Drop weight test

The B-pillar of type X welded according to the STD process (No FW & partial ablation) was considered as the reference in the test. The B-pillars used for the test were both taken from the right and left hand side (abbreviated LHS and RHS respectively). The results from the test are given in Table 12.

Table 12. Results from the drop weight test

Welding process:	Side	No. in drop-test	Velocity [m/s]	Crack	Comment
No FW & Part. ablation (X)	LHS	176271-01	10.18	Yes	Crack not in Weld or HAZ *
No FW & Part. ablation (X)	LHS	-02	10.16	No	*
No FW & Part. ablation (X)	LHS	-03	10.20	No	
No FW & Part. ablation (X)	LHS	-04	10.20	No	
No FW & Part. ablation (X)	LHS	-05	12.08	Yes	Crack not in Weld or HAZ
No FW & Part. ablation (X)	LHS	-06	12.07	Yes	Crack not in Weld or HAZ
FW & No ablation (X)	RHS	-07	10.22	Yes	Crack not in Weld or HAZ
FW & No ablation (X)	RHS	-08	10.29	Yes	Crack not in Weld or HAZ
FW & No ablation (X)	RHS	-09	10.31	Yes	Crack not in Weld or HAZ
FW & No ablation (X)	RHS	-10	10.27	Yes	Crack not in Weld or HAZ
FW & No ablation (X)	RHS	-11	12.10	Yes	Crack not in Weld or HAZ
FW & No ablation (X)	RHS	-12	12.14	Yes	Crack not in Weld or HAZ
No FW & Part. ablation (Y)	LHS	-13	12.14	No	
No FW & Part. ablation (Y)	LHS	-15	11.79	No	
No FW & Part. ablation (Y)	LHS	-17	12.02	Yes	Crack not in Weld or HAZ
No FW & Part. ablation (Y)	LHS	-19	12.11	Yes	Crack not in Weld or HAZ
FW & Part. ablation (Y)	LHS	-14	12.10	Yes	Crack not in Weld or HAZ
FW & Part. ablation (Y)	LHS	-16	12.08	Yes	Crack not in Weld or HAZ
FW & Part. ablation (Y)	LHS	-18	12.13	Yes	Crack not in Weld or HAZ
FW & Part. ablation (Y)	LHS	-20	12.13	Yes	Crack not in Weld or HAZ

* Complications during testing, see text.

It was discovered during the initiating tests that the drop weight pillar moved sideways during the impact. The drop weight pillar is normally fixed to the floor, but during these tests it was not possible to fixate the pillar in its normal position due to that the position was occupied by the test jig, see Figure 39.

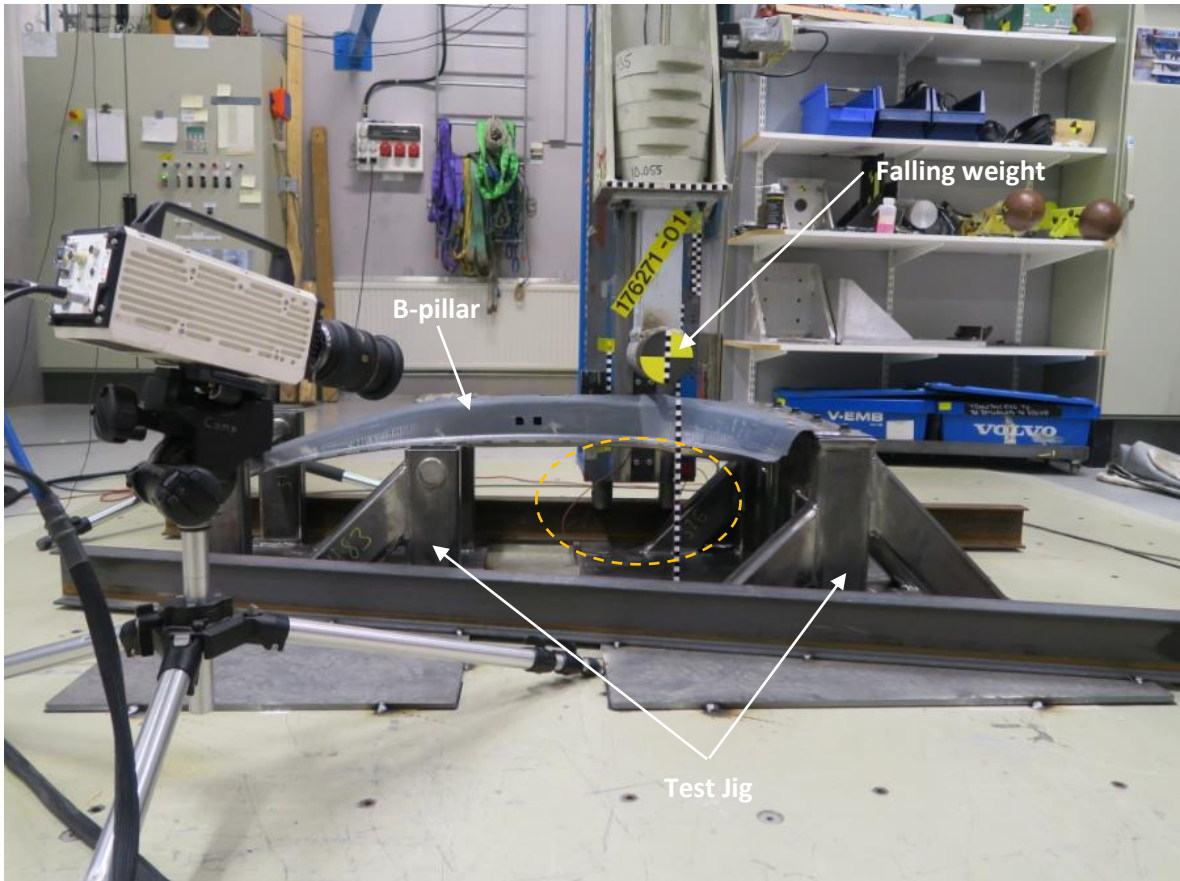
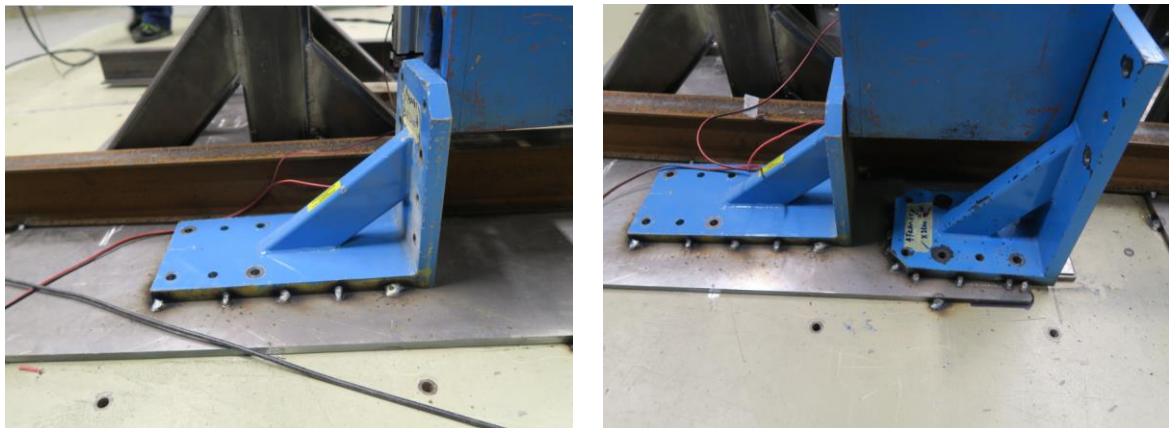


Figure 39. Overview of the test jig

Improvements were made both after the first and the second test run to fixate the position (see figures below). Hence, only test runs 3 to 20 are tested under the same conditions. The two variants of Y B-pillars were alternated, hence the odd and even test numbers for the two variants.



a)

b)

Figure 40. a) Improvement after test run 1. b) Improvement after test run 2

It can be seen in Table 12 that different velocities were applied on the falling weight within the tests in the two first groups, and that the same velocity was used on all the tests in latter groups. This limited the possibility to compare the results between the different welding processes since four out of six B-pillars in the two former groups were tested at 10 m/s, and none in the two latter groups.

Comments on each welding process follows below but first follows an explanation of expressions used in the text, see Figure 41

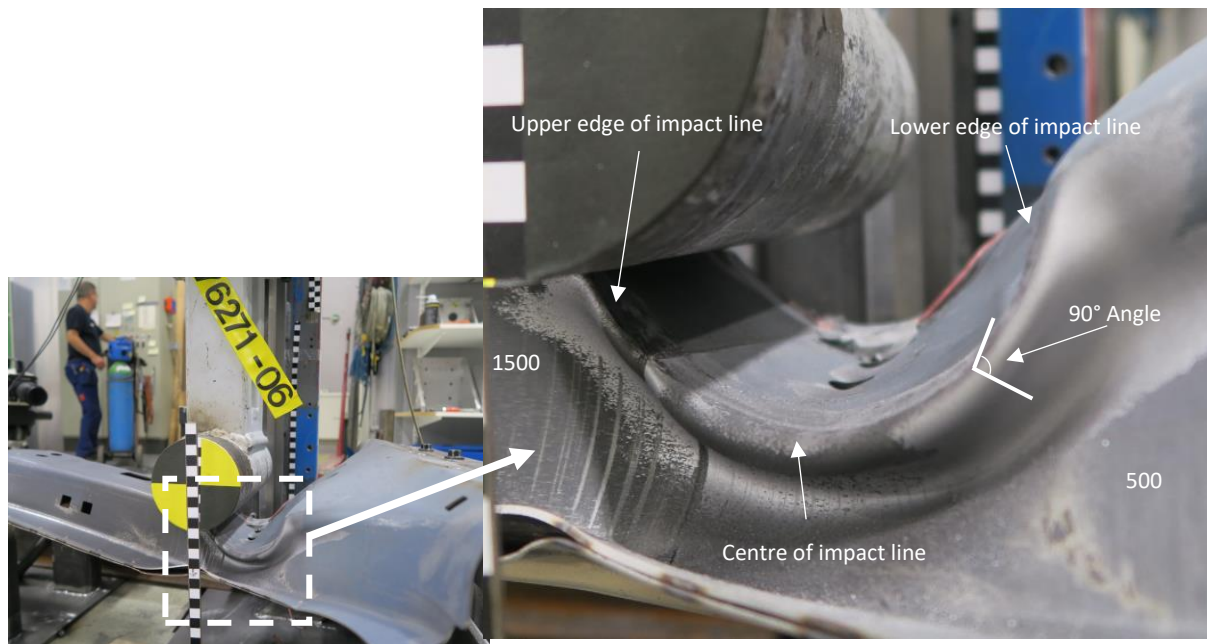


Figure 41. Deformed B-Pillar with text and figures describing expressions used to explain locations

Slightly different results can be seen for the B-pillars in the test. For most B-pillars a crack occurred either near, around or across the weld seam, but never along the weld seam. One representative sample from each welding process will be presented and commented separately below and summarized together further ahead.

4.1.1 STD-welding process (No FW & Partial Ablation) X

Cracks appeared in the 90° angle at the upper edge of the impact point, most likely due to shearing. Noticeable here is that the weld line and the centre of impact line are not coinciding, and this was the case for all samples from this process.

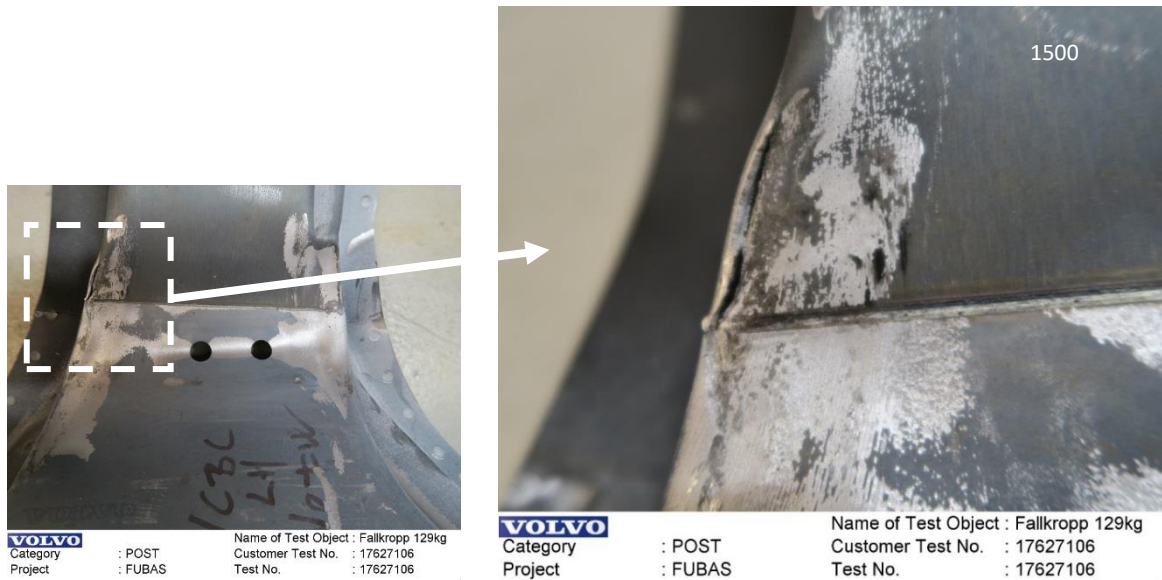


Figure 42. Crack in STD-welding process after drop weight test.

4.1.2 FW-welding process (FW & No Ablation) X

Similar appearance as the STD-welding process (No FW & Part. Ablation). Cracks appeared in the 90° angle at the upper edge of the impact line, most likely due to shearing. Noticeable here is that the weld line and the centre of the impact line is not coinciding, this was the case for all samples from this process.

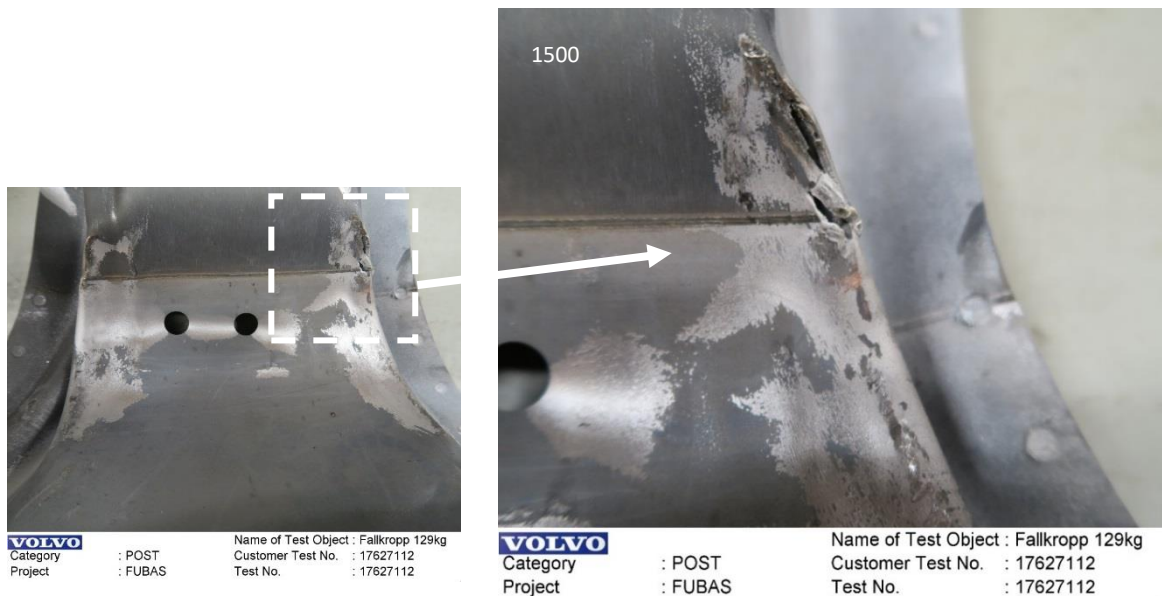


Figure 43. Crack in FW-welding process after drop weight test.

4.1.3 STD2-welding process (No FW & Partial Ablation) Y

No cracks appeared anywhere near the weld seam, see Figure 44. However indication of cracks appeared further up at the upper edge of the impact line in the 90° angle (left in Figure 44, red arrows).

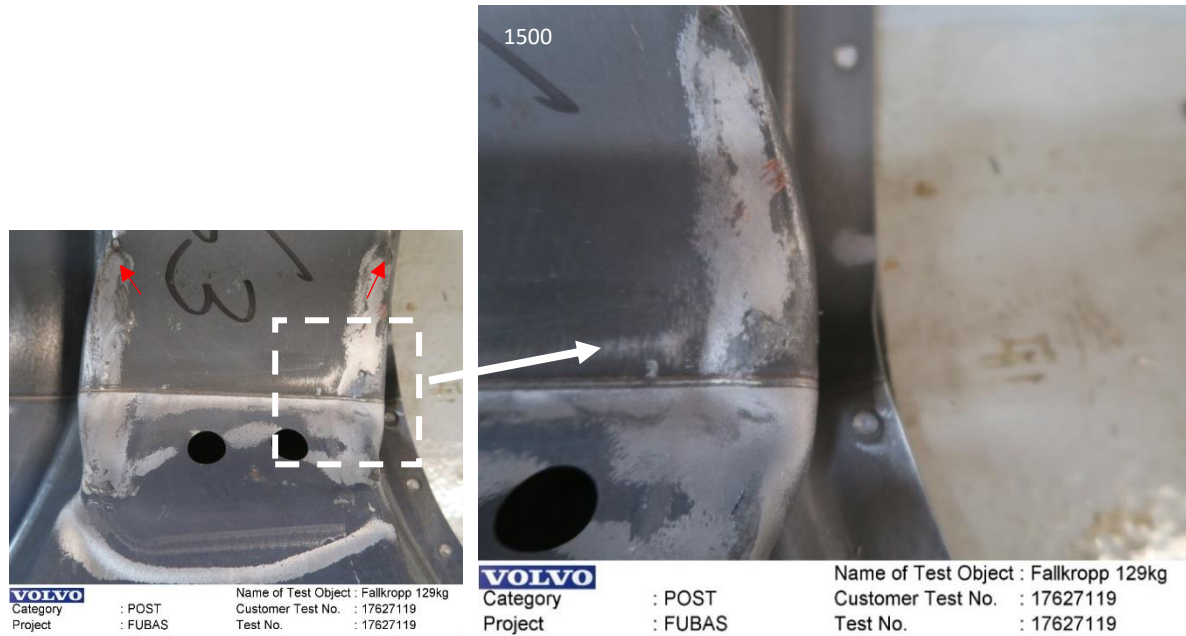


Figure 44. Appearance after drop weight test for the STD2-welding process. Red arrows to the left points at crack and crack indications

4.1.4 SC-welding process (FW & Partial Ablation) Y

No cracks appeared anywhere near the weld seam, see Figure 45. However indication of cracks appeared further up at the upper edge of the impact line in the 90° angle (left in Figure 45, red arrows).

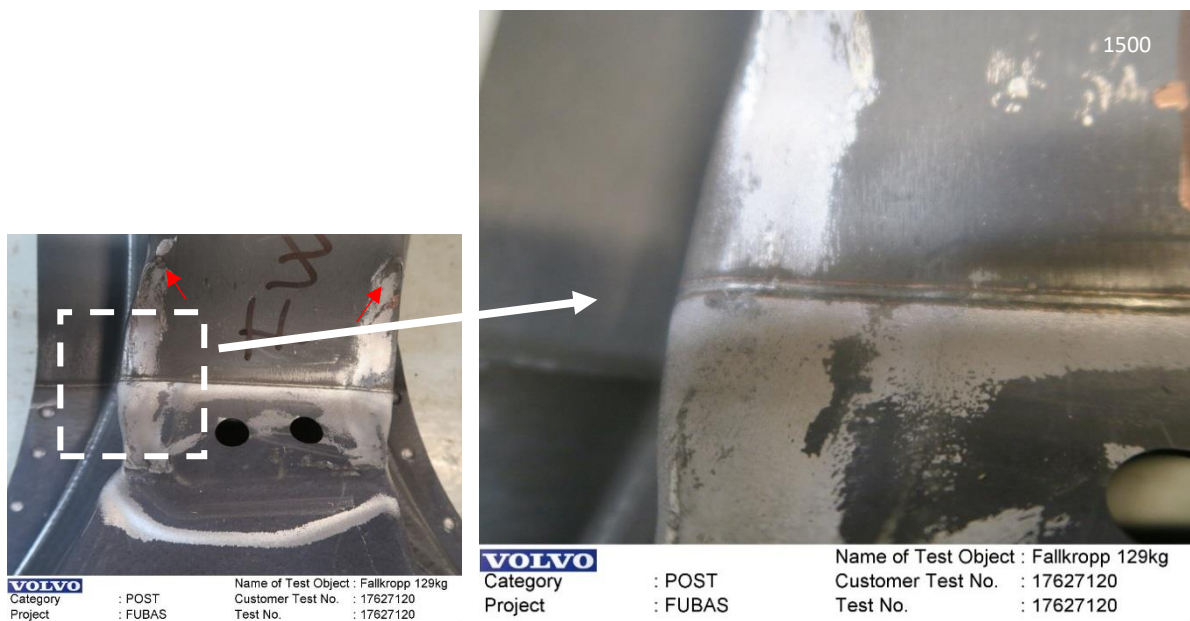


Figure 45. Appearance after drop weight test for the SC-welding process. Red arrows to the left points at cracks and crack indications

4.1.5 Summary

The cracks that appeared, did most likely not occur do to failure in the weld or HAZ. As can be seen in the figures below, the material is bulging quite significantly at the centre of the impact line in the 90° angle compared to the edge of the impact line. The cracks always occurred in the 1500 material at the upper edge of the impact line, independently of welding process.

The weld seam location relative to centre of the impact line was changing in-between the processes tested. The processes used on the X B-Pillars, the weld seam was always between the centre of the impact line and the edge of the impact line, see Figure 46. In the processes used on the Y B-pillars, the weld seam was always close to the centre of the impact line, see Figure 47. The major reason to this was that the test jig had to be rearranged in-between testing of the different processes. Both right and left hand side B-pillars were tested and also that the type of B-pillar (X & Y) among the processes differed.

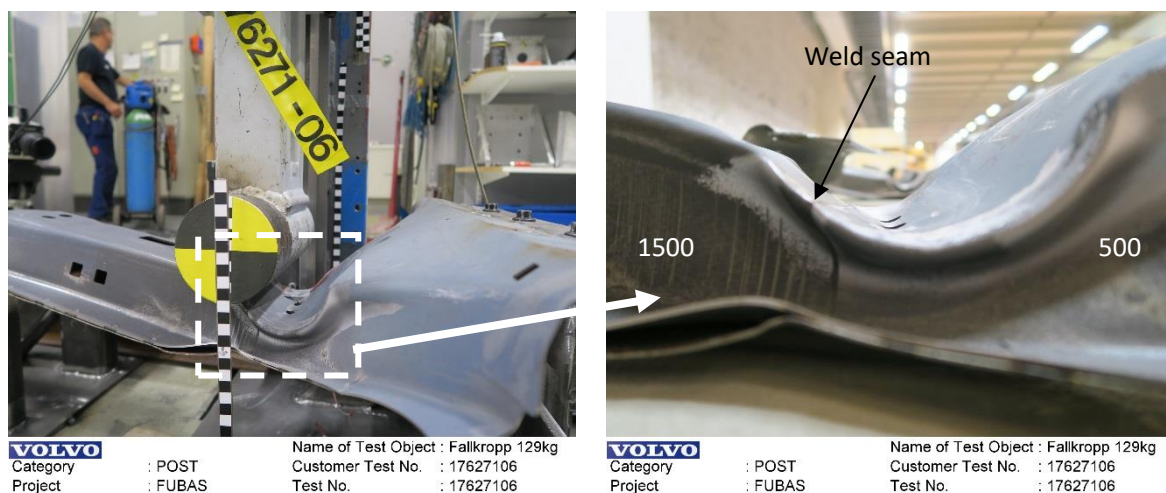


Figure 46. Impact point for STD (No FW & Partial ablation) and FW (FW & NO Ablation) welding process (B-Pillar X)

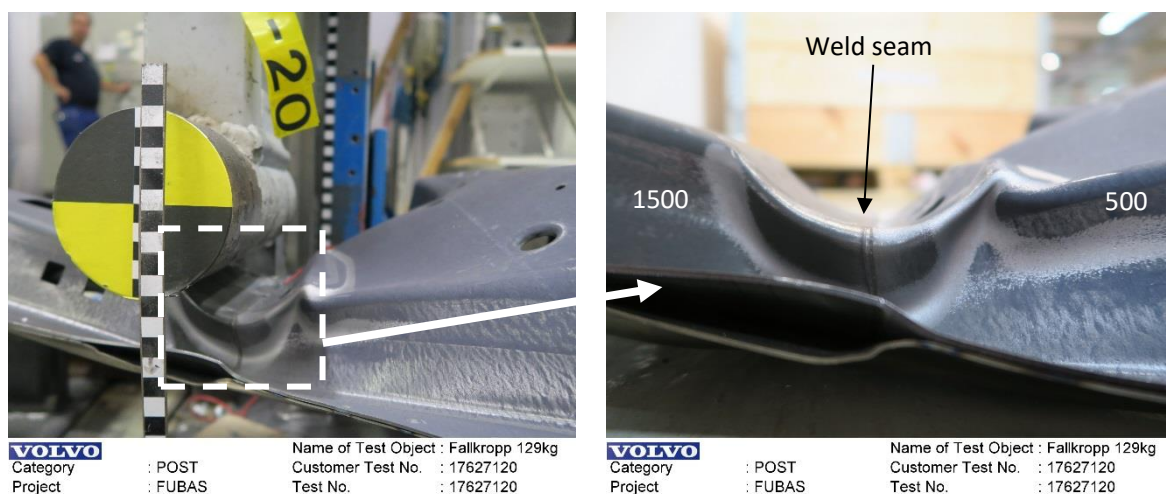


Figure 47. Impact point for STD2 (No FW & Partial ablation) and SC (FW & Partial Ablation) welding process (B-Pillar Y)

The steel sheet seems to bulge more in the centre of the impact than on edges regardless of where the weld seam was positioned relative to the centre of the impact line. The material also tended to crack in the upper edge of the impact point in the 1500 material. Since less bulging appeared here a possible reason could be that the material cracked because of a combination of higher tensile stresses and shearing. No tendency was seen that the material cracked due to failure in the weld or the HAZ.

4.2 Hardness profile

Hardness profiles were determined on Weld Test Coupons (WTC). The profiling was performed on the weld seam cross section on three samples from each process. The result can be seen in Figure 48, Figure 49 and Figure 50 to the right. The hardness tester used was equipped with a manual X-Y table without a grade scale. Hence, the starting position on the profiling and the distance between the indents were not fixed. This resulted in that the distances between indents became unknown. However, the profiles are starting in the 500 material (from the left in the charts) continuing over to the 1500 material (to the right in the charts). All samples independent of welding processes were shifting from ~200HV to ~500 HV. Only minor differences could be distinguished between the samples, STD-welding process (No FW & Partial Ablation) is increasing more rapidly in hardness over the fusion zone and the WC-welding process (No FW & No ablation) is increasing in hardness after the fusion zone, this could indicate that the weld seam for this process could be softer than the others. However the microstructure in the WC-welding process is expected to have a large segregation of ferrite distributed among martensite and the results could also indicate that only ferrite was encountered.

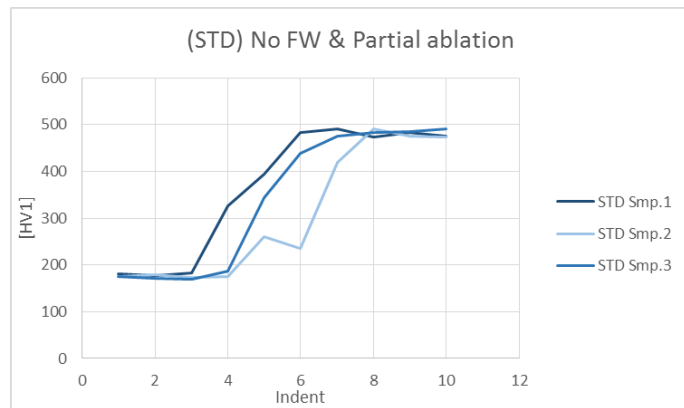


Figure 48. Line chart of hardness profile on (STD) No FW & Partial Ablation process

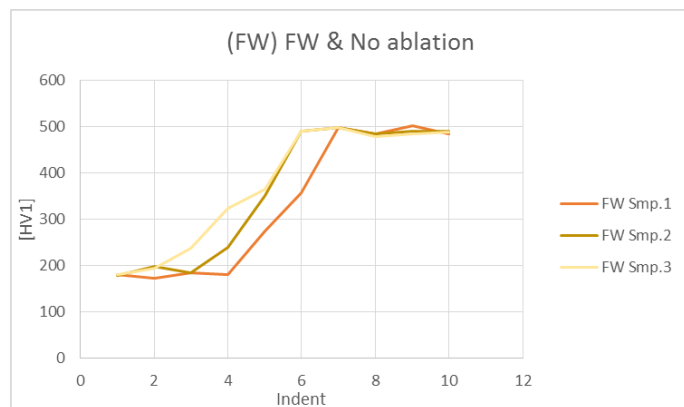


Figure 49. Line chart of hardness profile on (FW) FW & No Ablation process

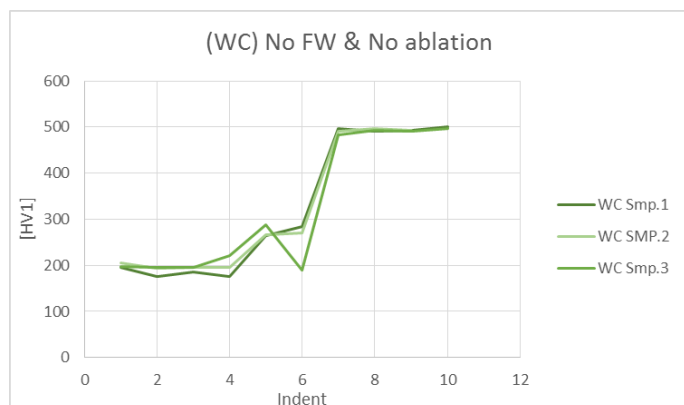


Figure 50. Line chart of hardness profile on (WC) No FW & No Ablation process

4.3 Microstructure & Chemical analysis

In this chapter the results from the optical microscopy and the SEM/EDS analysis are presented and discussed. The macro examinations were carried out on samples both from B-Pillars and Weld test coupons and are presented separately. Four to eight cross sections from each welding process were examined and the most representative and interesting graphs are shown here.

4.3.1 Optical Microscopy on B-Pillars

Below follows the results and comments from the macro examinations on the B-Pillars.

STD-welding process (No FW & Partial Ablation) X

The microstructure is changing from martensite to ferrite over the fusion zone with a relatively homogenous appearance.

FW-welding process (FW & No Ablation) X

The microstructure in the fusion zone had a slightly different appearance than the STD-welding process. The so-called whitebands can clearly be seen in the upper and lower right corners of the fusion zone, see Figure 52 below.



Figure 51. Macrograph of the STD-welding process (No FW & Partial ablation)



Figure 52. Macrograph of the FW-welding process (FW & No ablation)

STD2-welding (No FW & Part. Abl.) & SC-welding process (FW & Part. Abl.) Y

Both the STD2-welding process (No FW & Partial ablation) and SC-welding process (FW & Partial ablation) from the Y-variant showed similar appearance as the STD-welding process (No FW & Partial ablation) from the X variant. The microstructure is changing from martensite to ferrite over the fusion zone. When comparing FW-welding process (FW & No ablation) X variant to the SC-welding process (FW & Partial ablation) Y variant, the latter is showing a more homogeneous distributed microstructure. A possible reason to this appearance could be because no coating is diluted in to the weld, and that the filler wire used is likely not alloyed to stabilize austenite formation.

4.3.2 Optical Microscopy on Weld test coupon

STD-weld. process (No FW & Part. Abl.)

No significant differences could be seen in appearance when comparing the Weld test coupon samples to the B-pillar samples.

However, some decarburization on the edges outside the fusion zone were more prominent in these samples. The microstructure is otherwise changing from martensite to ferrite over the fusion zone with some segregation of ferrite in-between as been seen before, see Figure 53.



Figure 53. Macrograph of the STD-welding process (No FW & Partial ablation)

FW-welding process (FW & No abl.)

Just as the samples from the B-pillars with the same welding process, the microstructure is showing a more inhomogeneous distribution of ferrite and possible intermetallic compounds in the shape of whitebands in the fusion zone, compared to the STD-welding process (No FW & Partial ablation).



Figure 54. Macrograph of the FW-welding process (FW & No ablation)

WC-welding process (No FW & No Abl.)

The whitebands can clearly be seen in the Figure 55. The white areas of ferrite and possible intermetallic compounds are almost chaotically distributed in the microstructure.



Figure 55. Macrograph of the WC-welding process (No FW & No ablation)

4.3.3 SEM/EDX Chemical Analysis

A chemical analysis was performed on the FW-welding process (FW & No ablation). One sample was analysed and the intention was to establish the aluminium content in the whitebands (segregated areas of ferrite and possible IMCs). The area of interest, containing whitebands, which was analysed for its chemical composition can be seen in the macrograph of the cross section in Figure 56 (a) below.

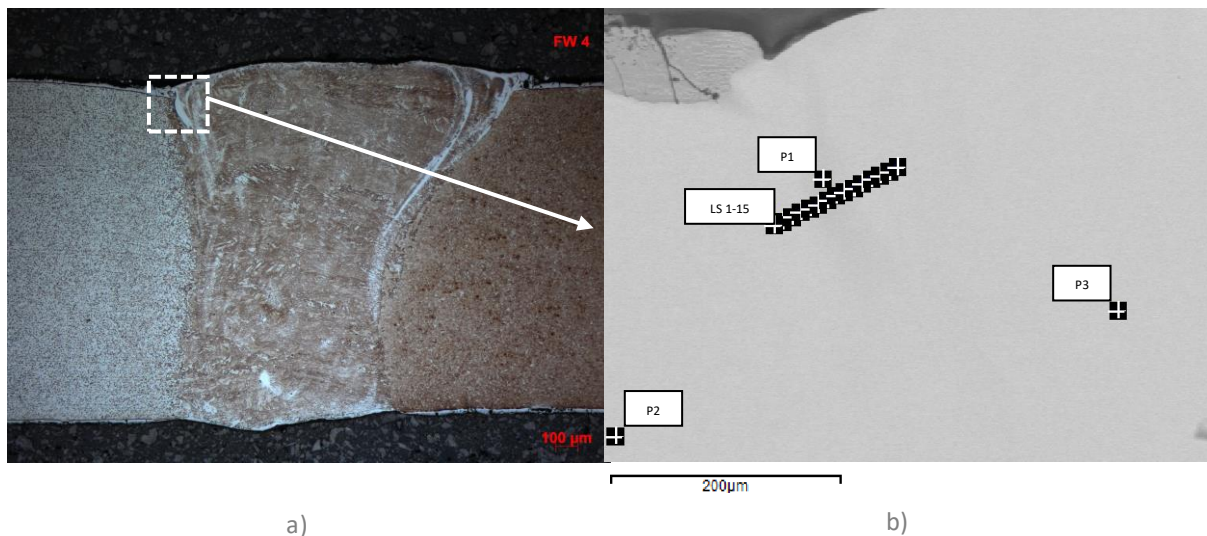


Figure 56. a) Macrograph of the laser weld cross section. b) BSE image of the dashed area in (a)

The sample analysed was only polished and not etched. Hence, the use of secondary electrons (SE) for imaging was not an option (no differences in topography). Imaging was instead carried out via backscattered electrons (BSE) and it was first believed that the two main microstructures ferrite and martensite would be distinguishable via BSE. However, this was not the case, initially no contrast was obtained but after several trials it became just possible to distinguish the whitebands from the upper left corner of the fusion zone, see Figure 56 (b) above.

Since obtaining contrast when imaging was almost impossible (for the layman) no effort was put into trying to distinguish any phases of intermetallic compounds. The possible reasons for not obtaining a higher contrast could be the relatively small differences in composition between the two phases and that the elements are relatively light. Three point analyses were carried out P1-3. Point 1 (P1) was performed in the slightly darker area believed to be in the whiteband. Point 2 (P2) and 3 (P3) was randomly chosen on the edges of the lighter areas in the image. Point 1, 2 and 3 showed an aluminium content of 9.89%, 0.82% and 0.13% respectively. The results strongly indicated that the slightly darker area most likely was the whiteband.

A line scan (LS) analysis was therefore carried out straight over the darker area, see Figure 56 (b) above. The results from the 15 points measured in the line scan analysis can be seen in the charts in: Figure 57, Figure 58 & Figure 59.

The accuracy of the results obtained from this analysis are affected by the resolution of the equipment, the technique is measuring a volume and the measurements could therefore be affected by the surrounding material. The results should therefore be taken as a good estimation rather than an exact number of the chemical composition. The line scan analysis showed that the aluminium and silicon content is peaking at point LS7 which is also coinciding with the centre of the slightly darker area in Figure 56 (b).

The analyses showed that the whitebands in the fusion zone was containing relatively high values of aluminium. However, to form IMCs the constituent of aluminium in composition with iron needs to exceed ~11.5wt% and the highest result during this analysis was 9.89wt%. Further work is needed. An EDX mapping is most likely a more suitable type of analysis to provide a better understanding of the element distribution.

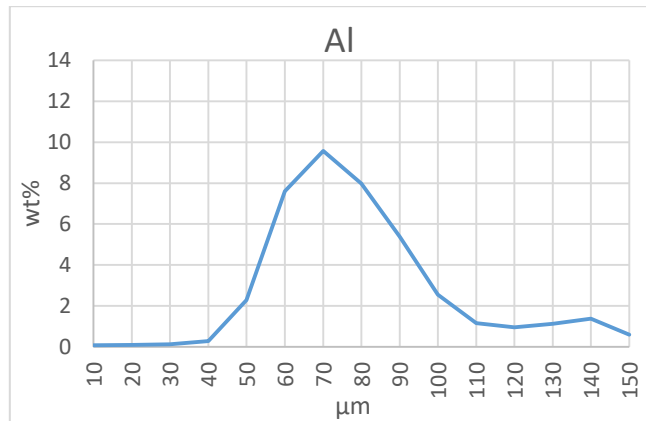


Figure 57. Al content over measuring point LS 1-15

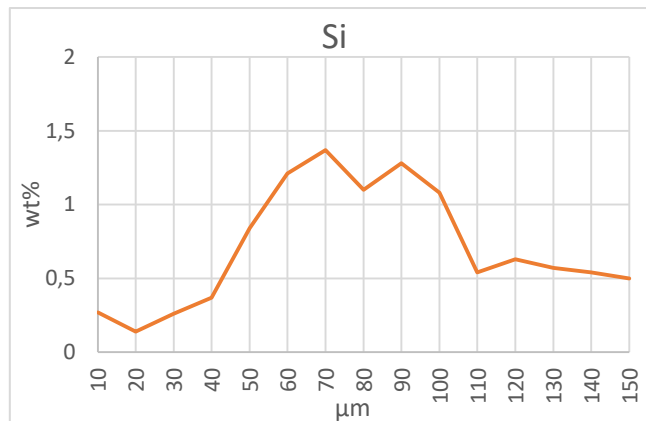


Figure 58. Si content over measuring point LS 1-15

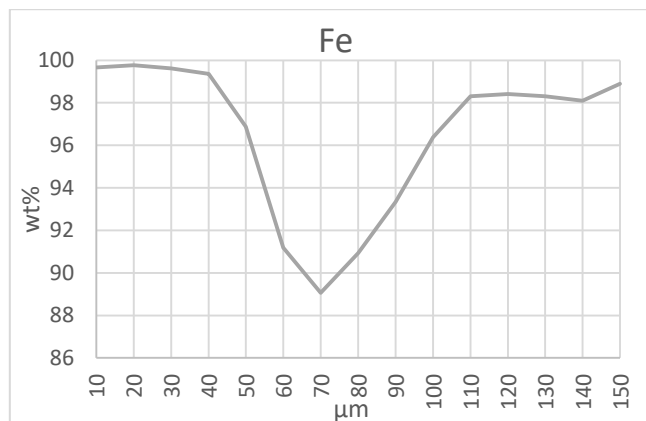


Figure 59. Fe content over measuring point LS 1-15

4.4 Tensile test

Here follows the results from the tensile testing carried out on samples both from B-Pillars and Weld test coupons, the results are presented separately and summarized together.

4.4.1 B-pillars

Complications was encountered during the tensile testing, which resulted in that material appears to have a nonlinear stress strain relationship, see dashed area in Figure 60. This is however not true and the reason to this appearance was mainly due to that the samples did not have the correct dimensions, as mentioned previously. This reduced the available gripping area between the clamping jaws and the sample which caused the samples to slip in the beginning of the test.

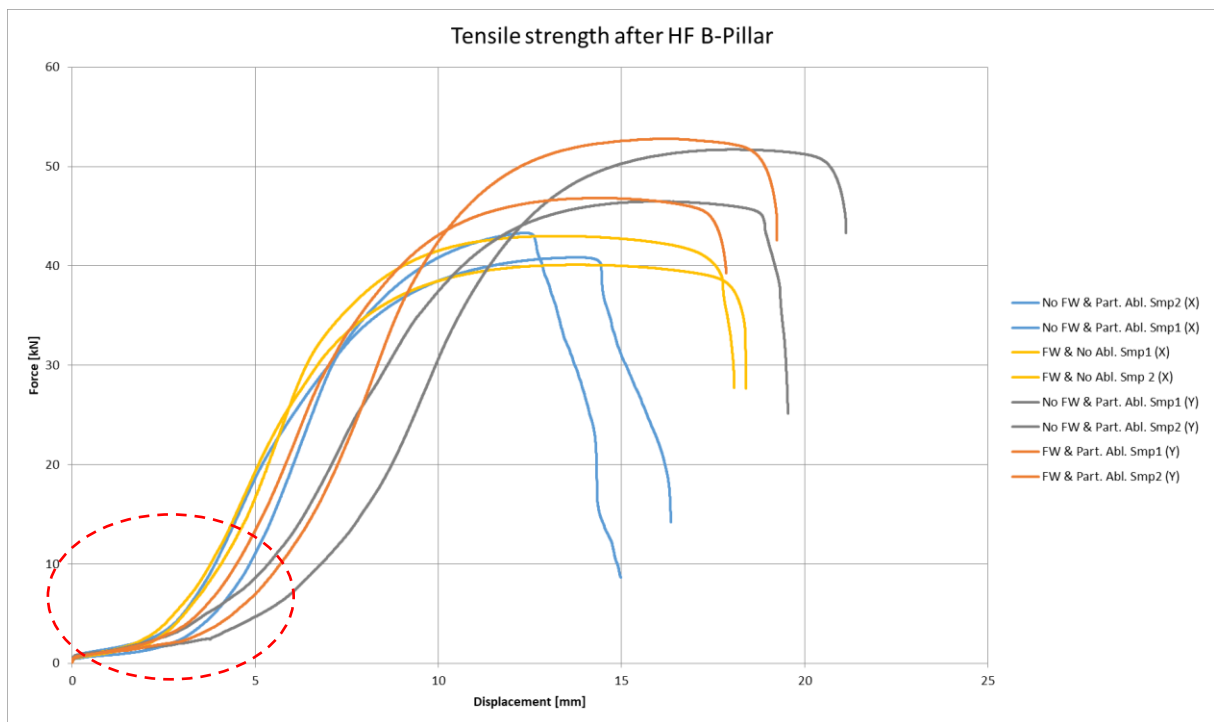


Figure 60. Line chart showing force over displacement for the B-pillar samples. The red dashed area shows the nonlinear behaviour which is explained in the text above.

Below follows comments on the appearance and the failure mode on each sample. Text with comments are separated for each welding process followed by a short summary.

STD-welding process (No FW & Partial Ablation) X

Sample 1 was considered to fail in the HAZ and sample 2 to fail in the softer parent material (500), see Figure 61.

FW-welding process (FW & No Ablation) X

Sample 1 & 2 failed in the softer parent material (500). The crack appeared for both samples in the gripping area of the clamping jaws. Possible crack initiations could be notches created by the clamping jaws, see Figure 62

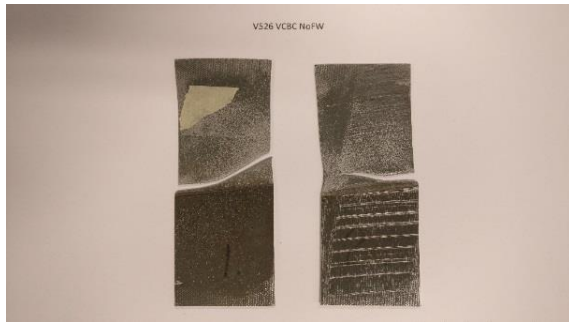


Figure 61. STD (No FW & Partial Ablation) X, sample 1 & 2 after tensile testing



Figure 62. FW (FW & No Ablation) X, sample 1 & 2 after tensile testing

STD2-welding process (No FW & Partial Ablation) Y

Sample 1 & 2 failed in the softer parent material (500). The crack appeared for both samples in the gripping area of the clamping jaws. However, the crack in sample 1 also propagated outside the gripping area. Possible crack initiations could be notches created by the clamping jaws, see Figure 63

SC-welding process (FW & Partial Ablation) Y

Sample 1 & 2 failed in the softer parent material (500). The crack appeared for both samples in the gripping area of the clamping jaws. Possible crack initiations could be notches created by the clamping jaws, see Figure 64



Figure 63. STD2 (No FW & Partial Ablation) Y, sample 1 & 2 after tensile testing

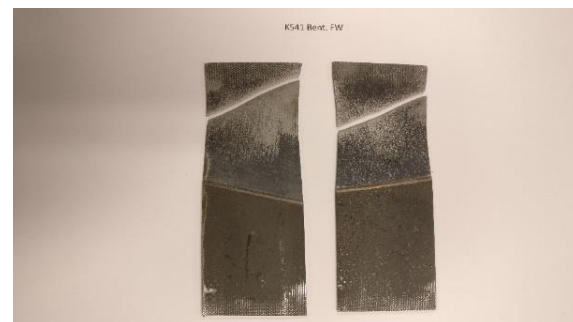


Figure 64. SC (FW & Partial Ablation) Y, sample 1 & 2 after tensile testing

The tensile strength for each sample can be seen in Figure 65 below. The nominal thickness of the blanks were used for calculations of the tensile strength, on all samples tested. The samples from the STD2-welding process (No FW & Partial ablation) and SC-welding process (FW & Partial ablation) performed slightly higher in tensile strength than the others. The higher results were caused by the slightly stronger 500 material used in these two processes compared to the other two STD & FW (different suppliers). The chemical composition in the two “different” 500 materials are in general equal but with some minor differences (see Table 2 & Table 3) in alloying content, which could affect the strength in the way that can be seen (Figure 65). Previous tests performed in the past has showed similar results. The strain is not taken into to consideration due to the complications encountered during testing, and that no extensometer was used. However, it can be seen in Figure 60 that the STD-welding process (No FW & Partial Ablation) shows a lower result in displacement compared to the other versions.

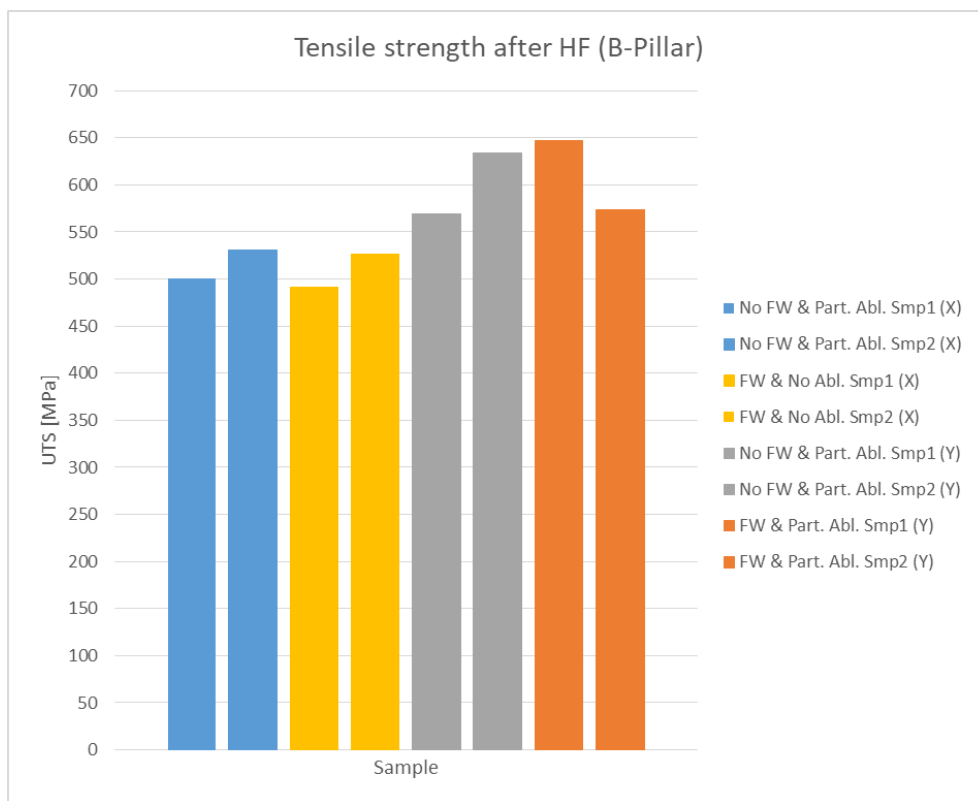


Figure 65. Bar chart showing Tensile strength for B-pillar samples.

4.4.2 Weld test coupons

The same complications was encountered during the tensile testing for the weld test coupon samples as for the B-pillar samples. This resulted in that the material also here appears to have a nonlinear stress strain relationship, see dashed area in Figure 66. The initial dimensions of the WTC samples was 150x48mm but it became necessary to cut them in half due to the slipping that occurred between the clamping jaws and the samples. The dimensions of the samples tested were instead 150x24mm.

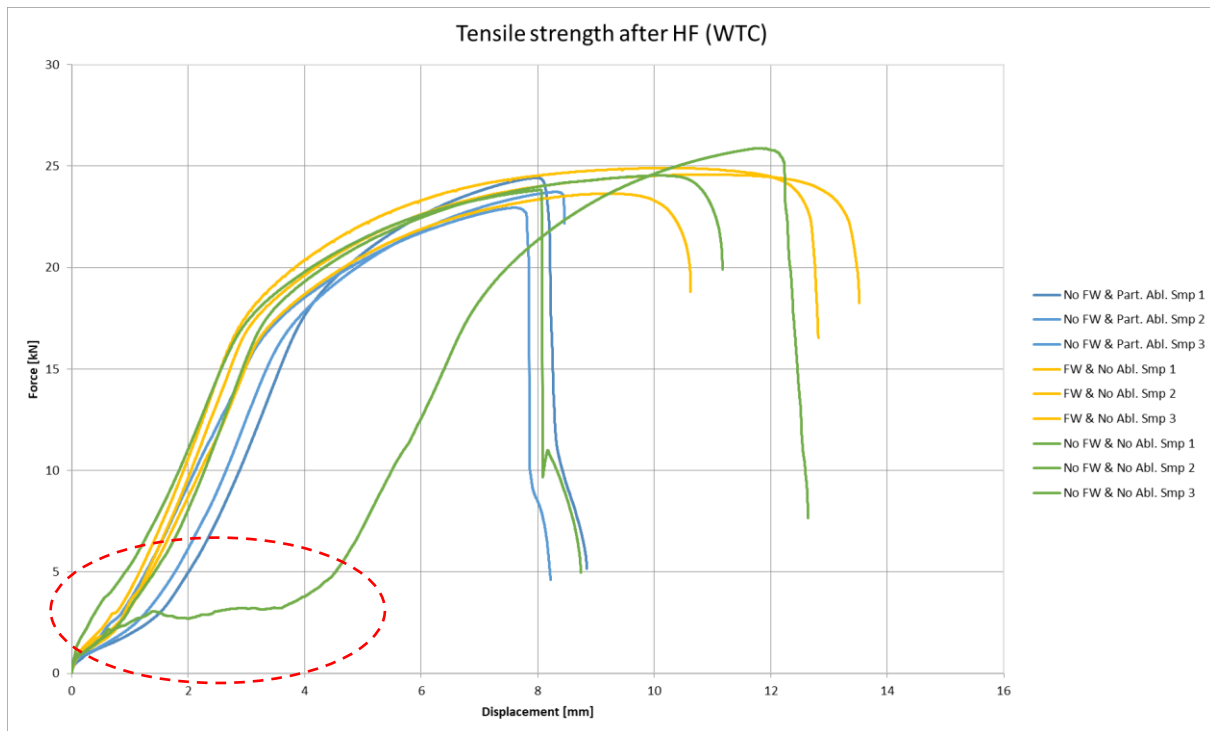


Figure 66. Line chart showing force over displacement for weld test coupon samples. The red dashed area shows the nonlinear behaviour which is explained in the text above.

Below follows comments on the appearance and the failure mode on each sample. Text with comments are separated for each process followed by a short summary.

STD-welding process (No FW & Partial ablation)

All three samples failed in the HAZ during testing, see Figure 67. Similarities can be seen with the results from the same welding process used on the B-pillar samples. On the B-pillar samples, only one sample failed in the HAZ and that sample belonged to the STD-welding process. A possible reason causing the failure to occur in the HAZ, could be the weld undercut present on all samples made with this process. The weld undercut is a stress raiser and the stress concentration factor is most likely high in this area.

FW-welding process (FW & No ablation)

All samples failed in the parent material. Sample 2 & 3 failed in the gripping area of the clamping jaws. Possible crack initiation could be the notches created by the clamping jaws, see Figure 68

WC-welding process (No FW & No Ablation)

As expected did all three samples fail in the HAZ, see Figure 69. The behaviour of failing in the HAZ has been reported in all studies found on the subject, where the same or a similar process and material has been used. The failure behaviour could be caused by the weld undercut, and the chaotically distributed microstructure, combined with large segregated areas of ferrite and possible IMCs on the fusion lines. Where the ductile to brittle transition between IMCs and ferrite or martensite and ferrite would act as a stress raiser together with the weld undercut.



Figure 67. STD (No FW & Partial ablation), sample 1 to 3 after tensile testing



Figure 68. FW (FW & No ablation), sample 1 to 3 after tensile testing

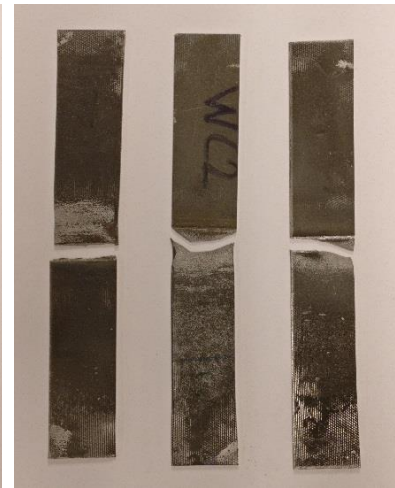


Figure 69. WC (No FW & No ablation), sample 1 to 3 after tensile testing

In Figure 70 below, the tensile strength for all WTC samples are presented. An interesting result is that WC-welding process (No FW & No Ablation) shows slightly higher results in tensile strength than the others. The strain has not been taken into consideration due to the complications encountered during testing, as mention earlier, and that no extensometer was used. Nonetheless, it can be seen in Figure 66 above that the FW-welding process (FW & No Ablation) shows a higher result in displacement than the other processes.



Figure 70. Bar chart showing Tensile strength for weld test coupon samples

4.4.3 Summary for B-pillars and Weld Test Coupons (WTC)

All samples from B-pillars failed in the softer 500 material, except one sample from the reference STD-welding process (No FW & Partial Ablation) which was considered to fail in the weld. The STD-welding process (No FW & Partial ablation) and WC-welding process (No FW & No Ablation) in the WTC samples failed in the HAZ. The FW-welding process (FW & No ablation) was considered to fail in the parent material. That all samples except one failed in the parent material on the B-pillar samples, could indicate that the weld seam is mechanically stronger than the parent material, whatever welding process used. However, this is not completely supported by the results from the WTC samples, where six out of nine samples failed in the HAZ. On the other hand, all samples tested showed strengths in region of 500 to 600 MPa which is in the same region as the properties of the softer 500 material. The dimensions on all samples used for tensile testing in this thesis was not optimal, the orientation of the weld seam to the pulling direction on the B-pillar samples was not 90° and varied quite significantly among the samples. The weld seam orientation to the pulling direction on the WTC samples were on the other hand always 90°, and the dimensions were slightly better, but not optimal. Furthermore, the condition on the clamping jaws in the tensile testing equipment may have affected the results. With the background of all these small drawbacks affecting the results it becomes difficult to comment on minor differences, but what could be said is that the results showed no significant differences among the samples. The FW-welding process (FW & No ablation) showed no tendency to perform worse compared to the other processes in the test, rather the opposite.

5 Discussion

In this chapter the research questions and the results are being discussed. Just below are some abbreviations and acronyms used in this and the following chapter, explained.

<i>STD & STD2</i>	<i>Partial ablation & No filler wire</i>	<i>WTC</i>	<i>Weld Test Coupon</i>
<i>FW</i>	<i>No ablation & filler wire</i>	<i>HAZ</i>	<i>Heat Affected Zone</i>
<i>WC</i>	<i>No ablation & No filler wire</i>	<i>SME</i>	<i>Subject Matter Expert</i>
<i>SC</i>	<i>Partial ablation & filler wire</i>	<i>IMC</i>	<i>Inter Metallic Compound</i>

A relatively extensive theoretical background search was carried out in this thesis, not only to build up a summarizing report of the major processes affecting the final component to Volvo Cars but also to give a better understanding and overview of the complete manufacturing process. The literature survey gave indications of that the most promising of the more novel techniques within tailored blanks are Tailor Heat Treated Blanks.

The majority of the studies and research found on the area concerning tailor laser welded Al-Si coated blanks did not include any research on joining the material combination investigated in this thesis. However, the studies have mainly been investigating the laser welding of Al-Si coated 22MnB5 steel, similar to the 1500 material. In many of the cases only one material has been used, and not a combination. The studies have showed that the Al-Si coating has a negative effect on the mechanical properties of the weld if the coating is not removed prior to welding, when 22MnB5 or similar steel grades are joined together. It can also be worth noting that one of the most known researches carried out on that specific area, is performed by persons with close connections to the company holding the patent on partial ablation. No research has been found on replacing or exchanging the laser ablation to filler wire in the welding process, with the intention of diluting and mitigate the effects of having the coating in the fusion zone to achieve similar properties as the parent material.

The results from the drop weight test showed no indications of cracks occurring due to failure in the weld or the HAZ on any of the welding processes tested. The deformation behaviour and the cracks that did occur, most likely did so due to shearing and tensile stresses, and the similar appearance made it difficult to comment on differences. Also, the minor changes that became necessary to perform when changing between welding processes, due to different models on components, could have caused the minor differences. On the other hand, these differences did not appear near the weld seam. The setup and execution of this test was performed according to calculations performed by the CAE engineers. In retrospect, it can of course be questioned if this was the most optimal way of performing the test since no defects could be seen on the welds. Maybe a different setup and execution could have stressed the weld seams more?

As expected the hardness profiling showed that the hardness shifted from the 500 material over the weld cross section to the 1500 material, from ~200 to ~500 HV1, on all samples tested. The WC-welding process showed minor indications of shifting to ~500 HV1 later than the others. However, the starting position and distances between the indents varied among all samples, and since the equipment used was completely manual, it is difficult to comment on the results. A more useful method could have been to perform the hardness profiling with a hardness testing machine equipped with a graded scale table. Then a more accurate profiling could have been performed and a comparison between samples would most likely been possible.

The macro examination of the microstructure in weld cross section showed that more segregated areas of ferrite was present in the FW-welding process than in the STD-welding process. This was expected, since the FW process is only diluting the coating and it is not removed as in the STD-welding process. The WC-welding process showed a large and almost chaotic distribution of segregated ferrite and possible IMCs in the fusion zone. It was also clearly seen that both the STD-welding and WC-welding process suffered from having a weld undercut which the FW-welding process did not. The weld undercut would act as a stress raiser during mechanical impact. However, this is also true for the hard to soft transition between possible IMCs and ferrite or martensite and ferrite. The results showed that all processes had their pros and cons, but the WC-welding process tended to have more cons than pros. Surprisingly, the SC-welding process also showed a weld undercut which was not expected since the purpose of adding a filler wire to this process was to avoid that.

All samples in the tensile testing showed tensile strengths in the same region as the weaker 500 material. This could indicate that the weld is good enough, on the other hand, all samples from the WTC specimens for both the STD-welding and WC-welding process failed in the HAZ, which did not happen for the FW-welding process. The most surprising result was that the WC-welding process showed equal or slightly higher tensile strength than the other processes, which could indicate that no necessary precautions are needed when joining Al-Si coated blanks in the combination of a 500 and 1500 material. Nonetheless, the samples did fail in the HAZ, due to either the severe segregation or the weld undercut, or both. One out of two on the B-pillar samples, and three out of three on WTC samples in the STD-welding process, were considered to fail in the HAZ. The different behaviour between the same welding processes is difficult to comment on, not only because of that the number of samples tested were few, but also the complications encountered – the differences between the orientation of the weld line to the pulling direction, and the dimensions of the samples – during testing. It could also indicate that the weld undercut is the major reason to failure, or that the WTC samples should have been prepared and made in a different way.

Whether the verification of the joint after welding is sufficient, has been a difficult task to address during this work. The reasons behind this are many, but the major one is that there was no access to perform any experimental work on an Erichsen testing machine. Furthermore, to follow up such an experiment would most likely lead to a need of hot forming those details, which was either not possible. Nonetheless, there

have not been any indications of that the verification in the form of an Erichsen test should not be enough. No difficulties have been reported on hot forming issues regarding defect welds on the present process used (STD). This points towards that the defect welds are sorted out by the Erichsen test. The most recent results reported by Wisco showed that the WC-welding process had slightly lower formability index than the FW-welding process, but only a few samples were tested and more work is needed here to define the limits of what an approved formability index could be. One could also investigate what the repeatability of such a test is.

According to Wisco Tailored Blanks, the addition of their filler wire in the laser welding process – the FW-welding process – should completely remove the risk of forming IMCs. Yet the SEM/EDX analysis carried out on the cross section of the fusion zone on the FW process showed relatively high values of aluminium content in the whitebands (segregated areas of ferrite and possible IMCs). However, the results should be taken with ease since only one sample was analysed and much more work is needed to come up with reliable conclusions. Still, speculations and questions arise from these results. Would the aluminium content be higher if the filler wire is not used (WC-welding process)? Is the filler wire improving the Al distribution? Can IMCs form in the FW-welding process? Are IMCs even formed in the WC-welding process on the material combination studied in this work?

Access to material together with the possibility to carry out experimental work has been limited during this thesis. The amount of samples for every welding process have been relatively low and the dimensions have not been optimal. Together, these circumstances may have affected the results. On the other hand, when comparing the results produced in this thesis to the previous results produced by both Volvo Cars and Wisco Tailored blanks, everything points in the direction that the FW-welding process performs equally or better than the STD-welding process in all mechanical testing performed. The FW-welding process does not suffer from any weld undercut, but it still shows relatively large areas of whitebands (segregated areas of ferrite and possible IMCs) present in the fusion zone, which on the other hand does not seem to affect the mechanical properties. The result could indicate that the weld undercut is a more severe defect than the presence of whitebands (segregated areas of ferrite and possible IMCs) in the fusion zone.

A change from the present STD-welding to the FW-welding process will affect the manufacturing process for the current components, and the assembly of the body in white. The FW-welding process causes a weld bead which will affect the hot forming process and the mating surfaces in the assembly. So-called carry-back are therefore difficult and an implementation has to be taken into consideration in the early design stage. Adding a filler wire to the laser welding process adds complexity and complications to the robustness of the process. This is supported both in literature and by the SME in laser welding at Volvo Cars. On the other hand, it can also add possibilities to the process like affecting the chemical composition and completely removing the risk of creating a weld undercut.

The addition of filler wire cannot be implemented in a general standard. The usage of filler wire seems to work on the material combination investigated in this thesis, however that does not mean that it would work on other combinations. This will have to be investigated further.

I would like to finish off this discussion by mentioning the tailored blanks technique THTB once more. The information found on this sounds very promising for producing and improving the desired properties in the current components. An implementation of the technique in the already existing hot forming process could be relatively trouble-free since the techniques are similar.

6 Conclusion

The STD-welding process was suggested to be replaced with the FW-welding process in the manufacturing of tailor welded blanks used for hot formed components. Four questions regarding the consequences this could have on the component and the manufacturing process were formulated during the initiation of this work. Some of the questions were relatively broad, maybe too broad, but the intention was to capture the complexity of the subject. The questions that this work were not able to conclude on have been brought up in the discussion, or will be in the recommendation for future work. The conclusions that can be drawn from this work will follow below.

- The FW-welding process performs in general equal or better in all mechanical testing performed in this work and in previous work performed by Wisco Tailored Blanks and Volvo Cars.
- The filler wire used by Tailor Welded Blanks in their FW-welding process does not completely remove the risk of forming segregated areas of ferrite and possible IMCs (whitebands) in the fusion zone of the weld. Furthermore, the results from the tensile test could indicate that a weld undercut is a more severe defect than segregated areas of ferrite and possible IMCs in the fusion zone of the weld.
- A tensile test, together with a hardness profile on the cross section of the weld, would be a suitable test to verify the mechanical properties of the weld seam after hot forming. Since the material combination investigated in this thesis consists of a 500 and 1500 material, the mechanical properties of the weld properties only have to be equal or slightly better than the weaker 500 material. If the sample fails in the weaker 500 material, the weld properties could be considered as good enough. A hardness profile of the cross section could also give an indication of the mechanical properties, maybe not as good as a tensile test. However, it is a low-cost alternative and a simple test to perform, and if done accurately and consistent it can lead to useful results.
- It was seen in the tensile testing that the WC-welding process performed equal in tensile strength to the other welding processes investigated. Further work is however needed to establish how this process performs compared to the others.
- All welding processes investigated except the FW-welding process suffered from having a weld undercut or a weld surface concavity. A weld undercut is a known stress raiser and such a defect is completely avoided in the FW welding process.
- The FW-welding process will generate a weld bead with a height ranging from 0 to 15% of the nominal blank thickness above the flat surface on the parent materials. A weld bead with a possible height of 15% of the nominal thickness will affect the hot forming process, especially the design of the forming tool, and efforts will be necessary to compensate for such a geometry deviation. The weld bead also affects the mating surfaces between the components investigated and the components which they are to be assembled with. The possible mating surfaces needs to be taken into consideration in the early

design stage of the car bodies concerned by the current components. An implementation of the FW-welding process in the current manufacturing, a so-called carryback, would therefore be impossible.

- Adding a filler wire to the laser welding process adds complexity and complications to an already complex welding process. The robustness of the manufacturing process is of a major concern if high quality components are to be manufactured, and the addition of filler wire will have a negative impact on the robustness of such a process.
- Volvo Cars had a desire to add and allow the usage of filler wire in their standard for laser welded tailored blanks. The basic idea was that the welding process could be a sort of black box, meaning that the manufacturer could weld it however they preferred, as long as the properties of the weld could be verified with a specific test. This is however not possible – allowing the manufacturer to add filler wire on any material combination could have detrimental effects not only on the TWB but also the entire manufacturing chain of the car body. This thesis has only investigated the material combination of a 500 together with a 1500 material, and the results presented are only valid for such a combination. This material combination is a special case and should also be regarded as such.

7 Recommendations for actions and future work

A weld will always contain defects, and even if it is decided to proceed with investigations regarding the welding process on TWBs it could also be considered to replace the technology with one that does not include welding. Tailor Heat Treated Blanks THTB is a tailored blank technique which does not include a welding operation and the technique offers good potential in achieving the desired properties in the current components.

If further investigations are to be conducted regarding the welding process on TWBs, some ideas on direction follows below.

Access to material has been a limitation during this thesis, only a few samples have been tested for every welding process examined. Further work is needed, with investigations of more samples.

Since the FW-welding process can generate a weld bead with a height of up to 15% of the nominal blank thickness above the flat surface on the parent materials, this would affect the mating surfaces. It could be beneficial to investigate how high the weld bead height can be while still achieving a good enough mating surface. This specific height could then be used as a requirement on the weld seam geometry. No consideration would then need to be taken to the mating surfaces in the early design stage of the car body.

Wisco Tailored blanks can only achieve a weld bead minimum height of 15% of the nominal blank thickness, which is most likely originating from their tolerances on the gap between the blanks during welding and the wire feeding process. These tolerances directly affect the mechanical properties of the weld. For example, if the gap between the blank is close to zero, and the amount of filler wire in the weld is at the lowest acceptable, it means that the amount of coating in the weld would be at its maximum. Hence, the mechanical properties of the weld would be negatively affected. Is such a weld good enough? This has to be taken into consideration regarding the FW-welding process.

It was seen in the tensile testing that the WC-welding process performed equal or higher in tensile strength than the other welding processes investigated. Questions arouse around this process and further work is needed to establish how this process performs compared to the STD- and FW-welding process. What properties concerning stress vs strain are necessary to achieve a good enough component? (neither strain nor different strain rates were analysed during this research). Furthermore, did samples fail in the HAZ due to the weld undercut and concavity, or was it because of the segregated areas of ferrite and possible IMCs? Can IMCs form in the material combination of Al-Si coated 500 and 1500 materials? How would the WC-welding process perform in mechanical testing if the weld undercut and weld concavity is removed? If IMCs are formed, are they affecting the mechanical properties of the weld seam?

If the welding process is to be changed, it would be wise to make use of that opportunity to raise the requirements on the welding process and the continuous quality control of it, if considered necessary.

8 References

- [1] "Press Material - Volvo Car Group." [Online]. Available: <https://www.media.volvocars.com/global/en-gb/media/photos/list>. [Accessed: 15-Feb-2018].
- [2] A. Pic, D. Duque Múnera, and F. Pinard, "Press hardened steel based laser welded blanks: The ultimate tool for crashworthiness," *Rev. Métallurgie*, vol. 105, no. 1, pp. 50–59, 2008.
- [3] H. Huh, J. H. Song, K. P. Kim, and H. S. Kim, "Crashworthiness assessment of auto-body members considering the fabrication histories," *AIP Conf. Proc.*, vol. 778 A, pp. 167–172, 2003.
- [4] M. Merklein, M. Johannes, M. Lechner, and A. Kuppert, "A review on tailored blanks - Production, applications and evaluation," *J. Mater. Process. Technol.*, vol. 214, no. 2, pp. 151–164, 2014.
- [5] Š. M. Babić Ž., "Application of Tailored Blanks in the Automotive Industry," *J. Technol. Plast.*, vol. 27, no. 1–2, pp. 61–71, 2002.
- [6] "Gestamp." [Online]. Available: <http://www.gestamp.com/what-we-do/technologies/welding/laser-welded-blanks>. [Accessed: 15-Feb-2018].
- [7] M. Spöttl and H. Mohrbacher, "Laser-based manufacturing concepts for efficient production of tailor welded sheet metals," *Adv. Manuf.*, vol. 2, no. 3, pp. 193–202, 2014.
- [8] M. Eisenmenger and D. Szymanski, "Tailor welding coils with the fiber-delivered laser," 2012. [Online]. Available: <https://www.industrial-lasers.com/articles/print/volume-27/issue-06/features/tailor-welding-coils-with-the-fiber-delivered-laser.html>. [Accessed: 14-Feb-2018].
- [9] "ThyssenKrupp Patchwork Blanks. ThyssenKrupp Tailored Blanks."
- [10] R. George, A. Bardelcik, and M. J. Worswick, "Hot forming of boron steels using heated and cooled tooling for tailored properties," *J. Mater. Process. Technol.*, vol. 212, no. 11, pp. 2386–2399, 2012.
- [11] O. Kragt, C. Koroschetz, L.-O. Jönsson, J. Eman, and E. Sandlund, "Advanced manufacturing of locally graded components for lightweight car body design," *Adv. High Strength Steel Press Hardening*, vol. 3, pp. 301–313, 2016.
- [12] T. Altan, "Hot-stamping boron-alloyed steels for automotive parts - Part II," 2007. [Online]. Available: <https://www.thefabricator.com/article/stamping/hot-stamping-boron-alloyed-steels-for-automotive-parts---part-ii>. [Accessed: 14-Feb-2018].
- [13] K. Hjelmtorp, "Resistance spot welding of galvanized steel-toread," 2017.
- [14] M. B. Djurdjević, S. Manasijević, Z. Odanović, and N. Dolić, "Calculation of liquidus temperature for aluminum and magnesium alloys applying method of equivalency," *Adv. Mater. Sci. Eng.*, vol. 2013, 2013.
- [15] "ArcelorMittal Automotive." [Online]. Available: <http://automotive.arcelormittal.com/europe/products/EN>. [Accessed: 14-Feb-2018].
- [16] C. Henager, "Hydrogen Permeation Barrier Coatings," *Mater. Hydrog. Econ.*, no. February, pp. 181–190, 2007.
- [17] R. Vierstraete, W. Ehling, F. Pinard, L. Cretteur, A. Pic, and Q. Yin, "Laser ablation for hardening laser welded steel blanks - Industrial Laser Solutions," 2010. [Online]. Available: <https://www.industrial-lasers.com/articles/2010/01/laser-ablation-for.html>. [Accessed: 14-Feb-2018].
- [18] O. L. R. Ighodaro, E. Biro, and Y. N. Zhou, "Study and Applications of Dynamic Resistance Profiles During Resistance Spot Welding of Coated Hot-Stamping Steels," *Metall. Mater. Trans. A Phys. Metall. Mater. Sci.*, vol. 48, no. 2, pp. 745–758, 2017.
- [19] M. Windmann, A. Röttger, H. Kügler, W. Theisen, and F. Vollertsen, "Laser beam welding of aluminum to Al-base coated high-strength steel 22MnB5," *J. Mater. Process. Technol.*, vol. 217, pp. 88–95, 2015.
- [20] J. Li, "The Effect of Weld Design on the Formability of Laser Tailor Welded Blanks," p. MASC Thesis, 2010.
- [21] J. C. Lippold, *Welding Metallurgy and Weldability*. 2014.
- [22] J. Svenungsson, I. Choquet, and A. F. H. Kaplan, "Laser Welding Process - A Review of Keyhole Welding Modelling," *Phys. Procedia*, vol. 78, no. August, pp. 182–191, 2015.

- [23] D. Larcombe, "Fiber versus CO2 laser cutting," 2013. [Online]. Available: <https://www.industrial-lasers.com/articles/2013/11/fiber-versus-co2-laser-cutting.html>. [Accessed: 14-Feb-2018].
- [24] K. Fahlström, "Laser welding of boron steels for light-weight vehicle applications," no. 1, 2015.
- [25] "Laser Welding Fundamentals."
- [26] J. Eastman, "Conduction Mode vs. Keyhole Mode Laser Welding," 2015. [Online]. Available: <https://ewi.org/conduction-mode-vs-keyhole-mode-laser-welding/>. [Accessed: 14-Feb-2018].
- [27] A. Kaplan, "Metallurgy and Imperfections of Welding and Hardening," in *The Theory of Laser Materials Processing: Heat and Mass Transfer in Modern Technology*, J. Dowden and W. Schulz, Eds. Cham: Springer International Publishing, 2017, pp. 89–112 & 241–261.
- [28] "Sheet Metal Cutting (Shearing)." [Online]. Available: <http://www.custompartnet.com/wu/sheet-metal-shearing>. [Accessed: 14-Feb-2018].
- [29] "Hot Cracking - Definition from Corrosionpedia." [Online]. Available: <https://www.corrosionpedia.com/definition/634/hot-cracking>. [Accessed: 22-Apr-2018].
- [30] H. K. D. H. Bhadeshia, "Formability." [Online]. Available: <http://www.phase-trans.msm.cam.ac.uk/2007/LDH.html>. [Accessed: 19-Feb-2018].
- [31] W. C. Emmens, *Formability: A review of parameters and processes that control, limit or enhance the formability of sheet metal*, no. 9783642219030. 2011.
- [32] H. Karbasian and A. E. Tekkaya, "A review on hot stamping," *J. Mater. Process. Technol.*, vol. 210, no. 15, pp. 2103–2118, 2010.
- [33] K. Mori *et al.*, "Hot stamping of ultra-high strength steel parts," vol. 66, pp. 755–777, 2017.
- [34] M. Merklein, M. Wieland, M. Lechner, S. Bruschi, and A. Ghiotti, "Hot stamping of boron steel sheets with tailored properties: A review," *J. Mater. Process. Technol.*, vol. 228, pp. 11–24, 2016.
- [35] "MBW thyssenkrupp," 2016.
- [36] "Steels for hot stamping - Usibor® and Ductibor."
- [37] O. Hedegård and M. Åslund, "Tempering of hot-formed steel using induction heating," no. 54, 2011.
- [38] "Boron in Steel: Part One," 2007. [Online]. Available: <http://www.totalmateria.com/page.aspx?ID=CheckArticle&site=kts&NM=212>. [Accessed: 14-Feb-2018].
- [39] "Boron in Steel: Part Two," 2007. [Online]. Available: <http://www.totalmateria.com/page.aspx?ID=CheckArticle&LN=SV&site=KTS&NM=214>. [Accessed: 14-Feb-2018].
- [40] "Advanced Structural Steels: Part Two," 2009. [Online]. Available: <http://www.totalmateria.com/page.aspx?ID=CheckArticle&LN=SV&site=KTS&NM=256>. [Accessed: 14-Feb-2018].
- [41] K. Eriksson and R. Johansson, "Investigation of Ductibor 500P AS150 manufactured by VAMA," *Intern. Rep.*, 2016.
- [42] "Hot forming." [Online]. Available: <https://www.autoform.com/en/glossary/hot-forming/>. [Accessed: 14-Feb-2018].
- [43] M. Kang, C. Kim, and S. . Bae, "Laser tailor –welded blanks for hot-press-forming steel with arc pre-treatment," *Int. J. ...*, vol. 13, no. 2, pp. 293–300, 2014.
- [44] C. Kim, J. Choi, M. Kang, and Y. Park, "A study on the CO2 laser welding characteristics of high strength steel up to 1500 MPa for automotive application," *J. Achiev. ...*, vol. 39, no. 1, pp. 79–86, 2010.
- [45] Z. Sun and A. S. Salminen, "Current status of laser welding with wire feed," *Mater. Manuf. Process.*, vol. 12, no. 5, pp. 759–777, 1997.
- [46] U. Dilthey, D. Fuest, and W. Scheller, "Laser welding with filler wire," *Opt. quantum Electron.*, vol. 27, no. 12, pp. 1181–1191, 1995.
- [47] "Wire feed systems for laser welding," 2004. [Online]. Available: <https://www.industrial-lasers.com/articles/print/volume-19/issue-9/features/wire-feed-systems-for-laser-welding.html>. [Accessed: 15-Feb-2018].

- [48] M. Banasik, J. Dworak, and S. Stano, "Laser welding with filler material in the form of a wire," *Weld. Int.*, vol. 26, no. 7, pp. 516–520, 2012.

Acknowledgement of the sources

Figure 15. J. C. Lippold, *Welding Metallurgy and Weldability*. 2014. With permission of John Wiley & Sons

Figure 16. J. C. Lippold, *Welding Metallurgy and Weldability*. 2014. With permission of John Wiley & Sons

Figure 21. W. C. Emmens, *Formability: A review of parameters and processes that control, limit or enhance the formability of sheet metal*, no. 9783642219030. 2011. With permission of Springer

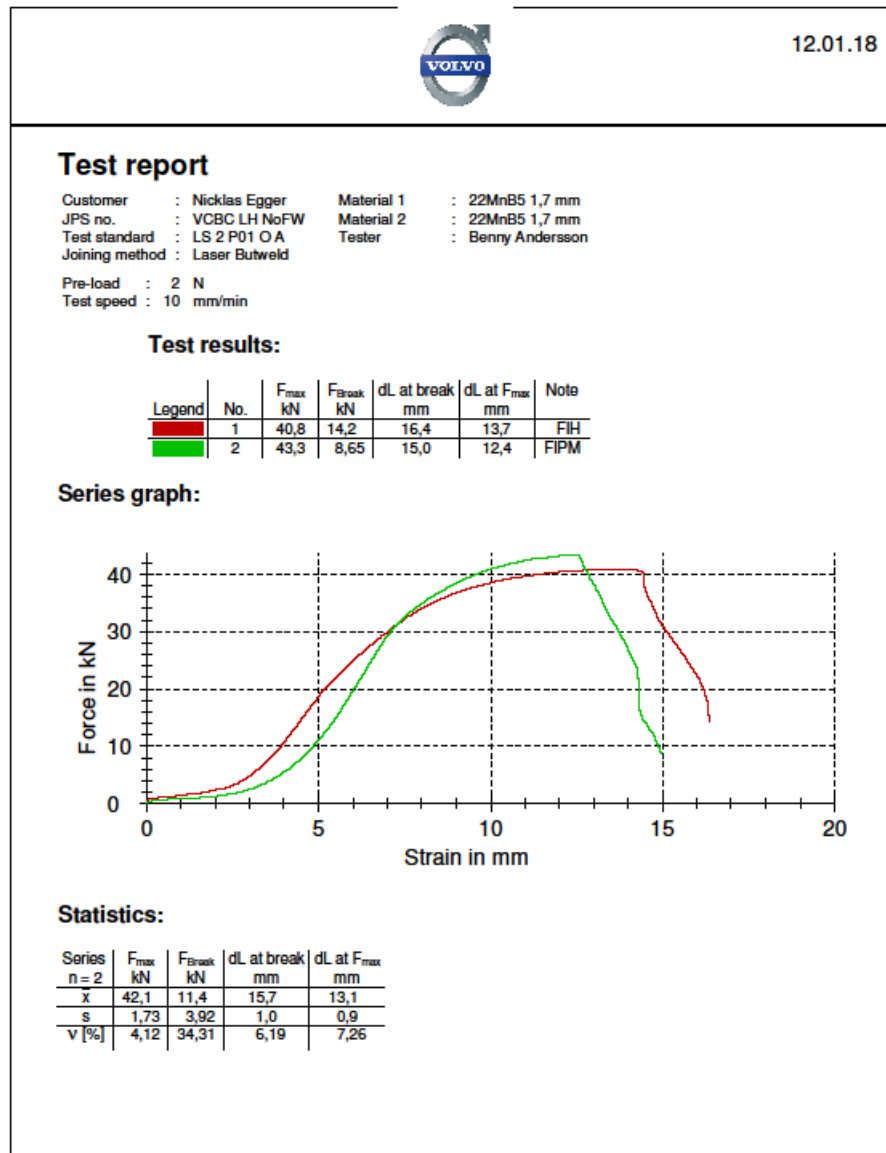
Figure 30. A. Kaplan, "Metallurgy and Imperfections of Welding and Hardening," in *The Theory of Laser Materials Processing: Heat and Mass Transfer in Modern Technology*, J. Dowden and W. Schulz, Eds. Cham: Springer International Publishing, 2017, pp. 89–112 & 241–261. With permission of Springer

Appendices

Tensile test

B-Pillars

STD-Process





12.01.18

Test report

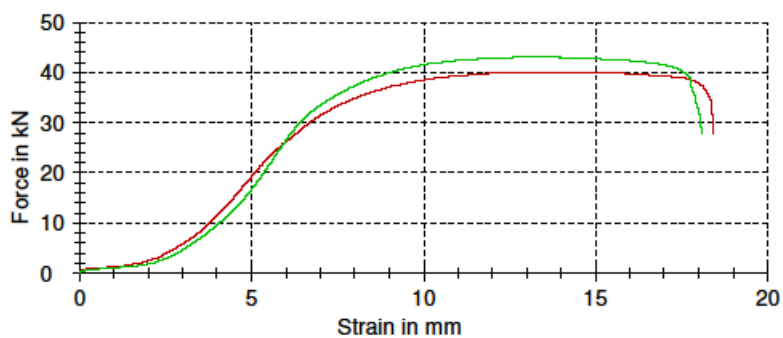
Customer : Nicklas Egger Material 1 : 22MnB5 1,7 mm
 JPS no. : VCBC RH FW Material 2 : 22MnB5 1,7 mm
 Test standard : LS 2 P01 O A Tester : Benny Andersson
 Joining method : Laser Butweld

Pre-load : 2 N
 Test speed : 10 mm/min

Test results:

Legend	No.	F _{max} kN	F _{break} kN	dL at break mm	dL at F _{max} mm	Note
	1	40,1	27,7	18,4	13,8	FIPM
	2	43,0	27,7	18,1	13,3	FIPM

Series graph:



Statistics:

Series	F _{max} kN	F _{break} kN	dL at break mm	dL at F _{max} mm
n = 2				
\bar{x}	41,5	27,7	18,2	13,6
s	2,05	0,0407	0,2	0,3
v [%]	4,93	0,15	1,25	2,55



Test report

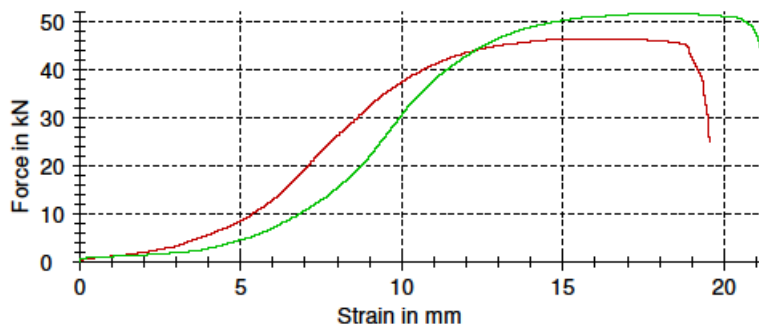
Customer : Nicklas Egger Material 1 : 22MnB5 1,7 mm
 JPS no. : K541No5 Material 2 : 22MnB5 1,7 mm
 Test standard : LS 2 P01 O A Tester : Benny Andersson
 Joining method : Laser Butweld

Pre-load : 2 N
 Test speed : 10 mm/min

Test results:

Legend	No.	F _{max} kN	F _{break} kN	dL at break mm	dL at F _{max} mm	Note
	1	46,5	25,1	19,5	16,1	FIPM
	2	51,7	43,3	21,1	18,1	FIPM

Series graph:



Statistics:

Series	F _{max} kN	F _{break} kN	dL at break mm	dL at F _{max} mm
n = 2				
\bar{x}	49,1	34,2	20,3	17,1
s	3,70	12,9	1,1	1,4
v [%]	7,53	37,65	5,52	8,32



Test report

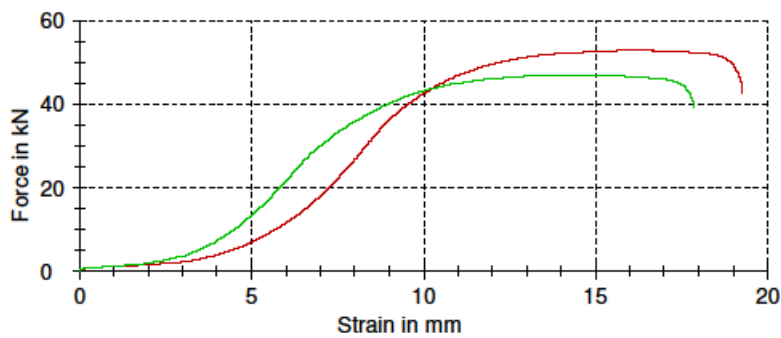
Customer : Nicklas Egger Material 1 : 22MnB5 1,7 mm
 JPS no. : K541FW5 Material 2 : 22MnB5 1,7 mm
 Test standard : LS 2 P01 O A Tester : Benny Andersson
 Joining method : Laser Buttweld

Pre-load : 2 N
 Test speed : 10 mm/min

Test results:

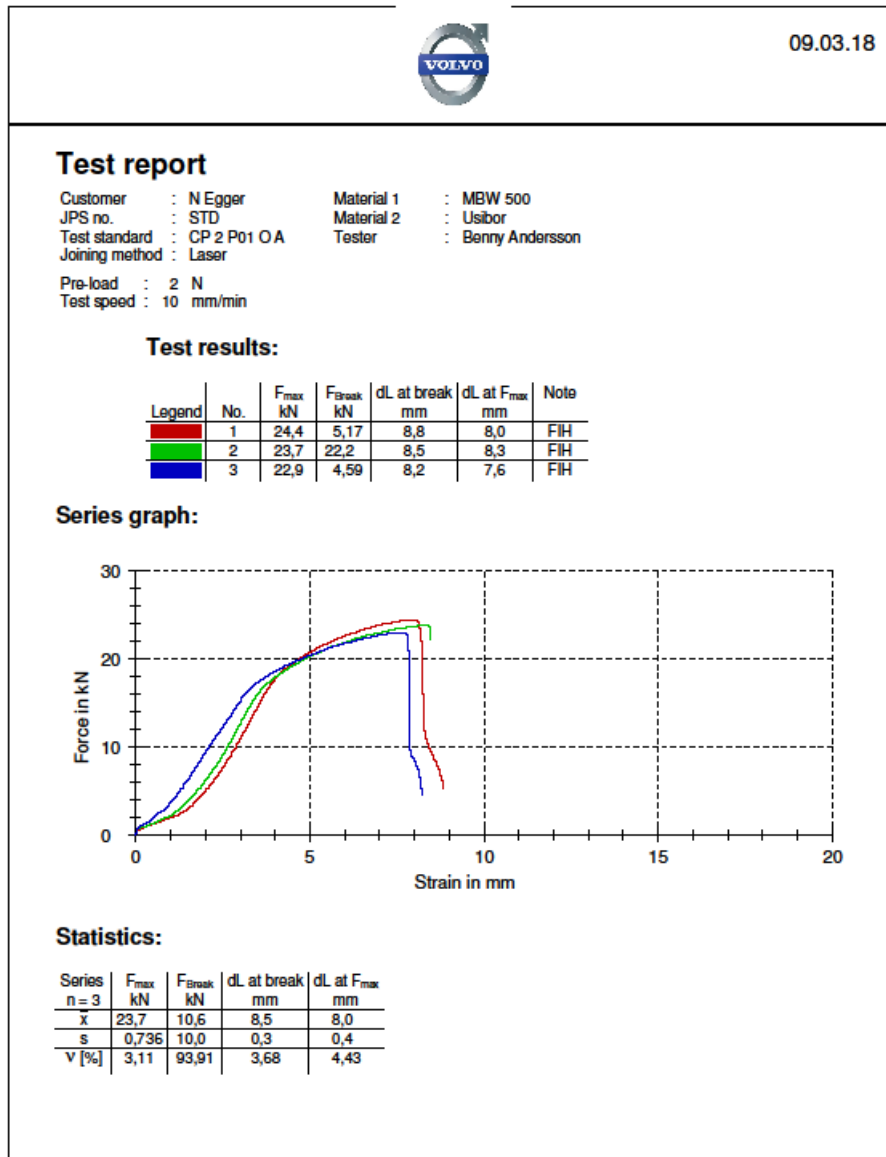
Legend	No.	F _{max} kN	F _{break} kN	dL at break mm	dL at F _{max} mm	Note
	1	52,8	42,6	19,3	16,4	FIPM
	2	46,8	39,2	17,9	14,4	FIPM

Series graph:



Statistics:

Series	F _{max} kN	F _{break} kN	dL at break mm	dL at F _{max} mm
n = 2				
\bar{x}	49,8	40,9	18,6	15,4
s	4,22	2,36	1,0	1,4
v [%]	8,47	5,77	5,28	8,99





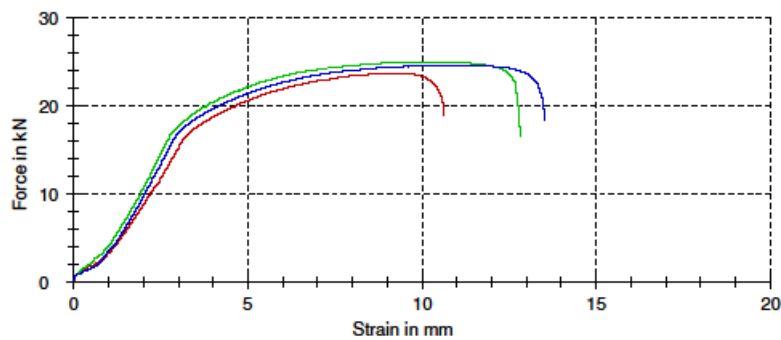
Test report

Customer : N Egger Material 1 : MBW 500
 JPS no. : FW Material 2 : Usibor
 Test standard : CP 2 P01 O A Tester : Benny Andersson
 Joining method : Laser
 Pre-load : 2 N
 Test speed : 10 mm/min

Test results:

Legend	No.	F _{max} kN	F _{Break} kN	dL at break mm	dL at F _{max} mm	Note
Red	1	23,6	18,8	10,6	9,2	FIPM
Green	2	24,9	16,5	12,8	10,4	FIPM
Blue	3	24,6	18,2	13,5	10,9	FIPM

Series graph:



Statistics:

Series	F _{max} kN	F _{Break} kN	dL at break mm	dL at F _{max} mm
n=3				
\bar{x}	24,4	17,9	12,3	10,2
s	0,654	1,18	1,5	0,9
V [%]	2,68	6,63	12,27	8,48



09.03.18

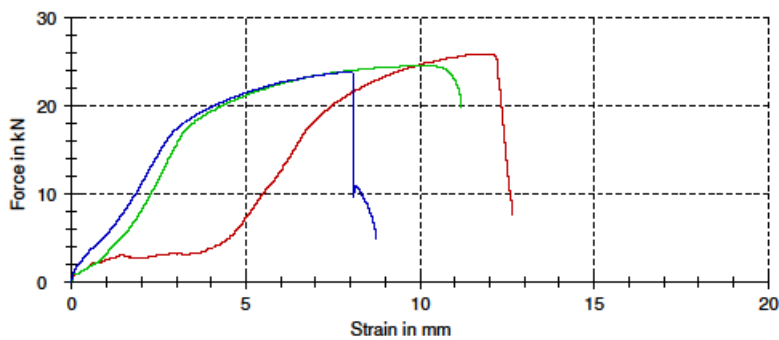
Test report

Customer : N Egger Material 1 : MBW 500
 JPS no. : WC Material 2 : Usibor
 Test standard : CP 2 P01 O A Tester : Benny Andersson
 Joining method : Laser
 Pre-load : 2 N
 Test speed : 10 mm/min

Test results:

Legend	No.	F _{max} kN	F _{Break} kN	dL at break mm	dL at F _{max} mm	Note
Red	1	25,9	7,64	12,6	11,8	FIH
Green	2	24,5	19,9	11,2	10,1	FIH
Blue	3	23,8	4,97	8,7	8,1	FIH

Series graph:



Statistics:

Series	F _{max} kN	F _{Break} kN	dL at break mm	dL at F _{max} mm
n=3				
\bar{x}	24,8	10,8	10,9	10,0
s	1,04	7,97	2,0	1,9
V [%]	4,20	73,49	18,16	18,80